as zero. If then the boundary conditions at the upstream and downstream ends are given by stage-time relationship, the initial stage may be given by linearly interpolating the stages at both boundaries. The velocity, in this case, may be again taken as zero. The setting of initial conditions is scarcely any problem, because the effect of initial conditions disappear soon after the start of simulation and is followed by hydraulic behaviour which is governed by boundary conditions.

IV. BOUNDARY CONDITIONS

The boundary conditions require special attention, and two types of boundary conditions have been used here; (1) discharge-time relationship and (2) stage-time relationship. If pumps are located at the boundary point, the boundary conditions must be given by the discharge-time relationship.

1. Discharge-Time Relationship as Boundary Condition

When the discharge-time relationship at the upstream and downstream ends are employed, the inflow and outflow discharge at both ends are treated by q in Eq. (2). The procedure for setting these boundary conditions is illustrated in Fig. 8. The boundary in the figure is at a distance grid of i=2 (or i=d). The equation of continuity at the boundary will then be over i=1 through i=3 (or i=c through i=e) with i=2 (or i=d) at the center. The discharges through i=1 (or i=e) in Eq. (14) are taken to be zero. By integrating the equation of continuity over i=2 through i=d, the water depth is thus obtained. The equation of

motion, on the other hand, is solved over i=3 through i=c. If, in this case, it is desirable to consider the velocity head at i=1 (or i=e), the velocity at i=3 (or i=c) is shifted to i=1 (or i=e).

2. Stage-Time Relationship as Boundary Condition

The situation in which the inflow and outflow discharge at the boundaries are not known, but the stage is given instead, is now considered. The procedure for setting these boundary conditions is illustrated in Fig. 9. First, the boundary condition at the downstream end, is explained. The boundary condition is given at i=2 and the equation of continuity is started to be solved at i=3. In this case, the velocity at the point of n=4 and i=1 is shifted from that of n=4 and i=3. Setting the boundary condition at the upstream end is also made in the similar way. That is, the boundary condition is given at i=e; and the equation of continuity is solved up to i=c. Solution of the equation of motion is then made up to i=d. The velocity at the point of n=4 and i=f is shifted from that of n=4 and i=d. The water depths at i=2 and i=e, with no influence from hydraulic behaviour in the open channel, are thus given as the boundary conditions. Conversely, there occurs hydraulic behaviour which satisfies the given boundary conditions.

3. Practical Application

By combining the two procedures described above, the practical problems can be simulated. For example, in the case of the periodic

change in water level due to the tide at the estuary and the inflow hydrograph at the upstream end, two different kinds of boundary conditions may be set, which are the stage-time relationship at the downstream boundary and the discharge-time relationship at the upstream. If pumps are installed at the upstream and downstream ends, the value of q in Eq. (2) is given from the capacity of the pumps, and discharge-time relationship are employed both at the upstream and downstream boundaries. It is quite difficult to measure the velocity compared with measurement of the stage. Measurement of the stage at the boundaries may thus serve the desired purpose.

V. HYDRAULIC BEHAVIOUR IN OPEN CHANNEL NETWORK[2)]

The waterways in irrigation and drainage systems often form a complex open channel network. To distribute the irrigation water without wasting it and to obtain efficient drainage management, it is necessary to simulate hydraulic behaviour at arbitrary points and times in a mathematical model, and thereby to obtain a rational design and management solution of irrigation and drainage systems.

An explanation of this problem is given with reference to the open channel network in Fig. 10. The flow-chart of the mathematical model simulation procedure is shown in Fig. 11. In computer programming wide freedom is given to the geometric, boundary and lateral inflow conditions in the open channel network. In this case, however, pumps for outflow are located at point 2. The operation of pumps is directed according to the discharge at point 3; that is, the number of pumps in-

operation is regulated by the need. Inflow into the network occurs at points 28 and 64, as shown in Fig. 12. The operational conditions for this mathematical model simulation are as follows,

(1) Δx=1,000 m,

(2) Δt=60 sec,

(3) Channel is of rectangular shape with 30 m in width and a flat bottom slope,

(4) n=0.025,

(5) Initial water depth = 3.0 m, and initial velocity = 0 m/sec, and

(6) Discharge capacity of pumps; 30 m^3/sec/pump x 5 pumps.

The results of the simulation tests are shown partly in Fig. 13, which are the number of pumps in operation, and the stage and discharge at point 2. Operation of pumps is started when the stage at point 2 reaches 4.0 m. and the outflow discharge by pumps shows 150 m^3/sec in peak. Then, with decrease of the discharge at point 3, the number of pumps in operation is reduced gradually to converge finally to the stage of 3.0 m. Figs. 14, 15 and 16 show the hydraulic characteristics such as stage, velocity, and discharge, two, three and four hours later after the start of simulation, respectively.

VI. STAGE REGULATION FUNCTION OF LAKE

A lake with a broad surface in an irrigation and drainage system, works to mitigate the abrupt change in stage of the waterways, and also to regulate operations of facilities such as the pumps and gates.

To discuss this kind of problem, the scheme in Fig. 17 is offered here. This system has the pumps with a maximum capacity of 60 m^3/sec at the downstream end or at point 2. The lake is located at point 10 at the midway of the system; its surface area is 1,810,000 m^2. The plan is now in progress of reclaiming land from the lake. It is, therefore, requested to estimate the eventual relationship between the lake area retained after reclamation and the maximum water stage during floods. The operational conditions used for this simulation are as follows.

(1) Δx = 400 m,

(2) Δt = 30 sec, and

(3) n = 0.03

The results of the simulation tests are summarized and are shown in Fig. 18. Incorporating the lake and waterway embankment reinforcement project with the above study, the area of the lake to be reclaimed may thus be determined.

VII. SALINITY INTRUSION IN ESTUARY DUE TO DIFFUSION[1)]

When the streamflow in the estuary is to be utilized, it is necessary to investigate the salinity distribution there. The mathematical model simulation tests for salinity diffusion is classified into the following two procedures: One is the case where the hydraulic behaviour governing salinity diffusion is already known as an unsteady flow; and the other, is the case that the hydraulic behaviour is also to be simulated in a mathematical model. Hydraulic behaviour is not so affected by salinity diffusion itself that in the former case the unsteady salinity diffusion

needs only to be treated. In most cases, however, the hydraulic behaviour is not known definitely. Therefore, it is required that both hydraulic behaviour and the salinity diffusion are simultaneously simulated under given boundary conditions.

As an example of this a simulation of intense mixing salinity diffusion and hydraulic behaviour is described below. The fundamental equations used here are the equation of continuity (2); and the equation of motion with the density term due to salinity, as follows,

$$\frac{1}{g}\left(\frac{\partial v}{\partial t}\right) + \frac{1}{g}\frac{\partial}{\partial x}\left(\frac{v^2}{2}\right) + i + \frac{1}{\rho}\frac{\partial}{\partial x}(\rho h) + \frac{n^2|v|v}{h^{4/3}} = 0 \qquad (15)$$

And the intense mixing salinity diffusion equation is

$$\frac{\partial(AS)}{\partial t} + \frac{\partial(AVS)}{\partial x} = \epsilon\frac{\partial}{\partial x}\left(A\frac{\partial S}{\partial x}\right) \qquad (16)$$

where ρ is the density of the water, i the bottom slope, S the salinity concentration and ϵ the diffusion coefficient. Other symbols in the above equations have the same significance as in Eqs. (1) and (2).

The mathematical model for intense mixing diffusion is made up of difference expressions of the Eqs. (2), (15) and (16), as described in II. 4. The operational conditions used for simulation are as follows,

(1) Distance of the estuary concerned is 10 km.

(2) $\Delta x = 500$ m,

(3) $\Delta t = 30$ sec, and

(4) $n = 0.035$

The boundary conditions are given by a stage-time relationship for the unsteady flow and by the salinity concentration for an intense mixing diffusion both at the upstream and downstream ends. The accuracy of the simulation techniques used is indicated in Fig. 19. It is seen that, with a diffusion coefficient of 800, the salinity diffusion in the estuary can well be simulated. Fig. 20 shows the relation between base flow discharge, salinity concentration and distance from the river mouth. The salinity concentration at any point in this estuary can be estimated readily from the figure if the stages at the upstream and downstream ends and the salinity concentration at the downstream end are known.

VIII. UNSTEADY FLOW IN CLOSED CONDUIT NETWORK[3)]

In recent years, closed conduit systems have been used for irrigation purposes, and particularly for sprinkler irrigation, which is made up of a complex network. Due to either the increase, decrease, or stoppage of the water supply which occurs at randoms in space and time, hydraulic behaviour is unpredictable. Mathematical model simulation techniques are also applied in examining the follwoing items,

(1) Discharge distribution,
(2) Pressure distribution,
(3) Velocity distribution,
(4) Water hammer pressure due to valve operation,
(5) Surging

By appling Manning's law of frictional resistance and by treating the water as a compressible fluid, the fundamental equations of unsteady flow through a closed conduit are given as follows,

$$\frac{1}{g}\frac{\partial v}{\partial t} + \frac{v}{g}\frac{\partial v}{\partial x} + \frac{\partial H}{\partial x} + \frac{n^2 + |v|}{(D/4)^{4/3}}v = 0 \qquad (17)$$

$$\omega \frac{\partial H}{\partial t} + \frac{K}{A}\cdot\frac{\partial Q}{\partial x} - q = 0 \qquad (18)$$

Here, H is the pressure head, D the conduit diameter, w the weight of water per unit volume, K the coefficient expansion of water per unit volume, and A the cross-sectional area of a closed conduit.

The mathematical model for the closed conduit can be given by the central difference expressions of Eqs. (17) and (18), whose procedure is similar to that in II. 4. The convergence of the solution by simulation techniques is indicated in Fig. 21. In this case, the closed conduit is placed as flat, and the valve is opened to full capacity in 1.0 sec at the terminal end of the network. The results shown in Fig. 21 are the characteristics at 35 sec after the opening of the valve, which is almost a steady condition. The discharge distribution in the figure is similar to that given by the Hardy-Cross method.

The unsteady flow phenomena in another closed conduit network as analyzed by the mathematical model test is shown in Fig. 22. The altitude of the network is given in Fig. 23. In this mathematical model simulation the difference in distance is taken as 500 m and that in time 0.25 sec, and the valves 1 and 2 are opened to full capacity

simultaneously. The pressure head-time and discharge-time relationship at point 18 are shown on the left side of Fig. 24. In the second example, after opening both valves to full capacity and the hydraulic behaviour reaching almost the steady state, only valve 1 is fully closed. The results of this experiment are given on the right side of Fig. 24.

In the conventional method for estimating the water hammer pressure in a closed conduit system, it is difficult to incorporate the frictional resistance and the altitude of conduits in the fundamental equation. Furthermore, it is a complicated matter in treating the conduits of different diameters in analysis of a steady flow. By using the mathematical model simulation of an unsteady flow, however, hydraulic behaviour results in high accuracy at a reasonable cost.

IX. TWO-DIMENSIONAL UNSTEADY FLOW [1) 4)]

Mathematical model simulation techniques have been developed for a two-dimensional unsteady flow in a bay or lake. The procedures used are similar to that for a uni-directional flow, described in II.

The equations of motion and of continuity for two-dimensional unsteady flow are given as

$$\frac{1}{g}\left(\frac{\partial v}{\partial t}\right) + \frac{1}{g} v \frac{\partial v}{\partial x} + \frac{1}{g} u \frac{\partial v}{y} + i_x + \frac{\partial h}{\partial x} + \frac{n^2\sqrt{v^2+u^2}}{h^{4/3}} v = 0$$

$$\frac{1}{g}\left(\frac{\partial u}{\partial t}\right) + \frac{1}{g} v \frac{\partial u}{\partial x} + \frac{1}{g} u \frac{\partial u}{\partial y} + i_y + \frac{\partial h}{\partial y} + \frac{n^2\sqrt{v^2+u^2}}{h^{4/3}} u = 0 \qquad (19)$$

$$\frac{\partial h}{\partial t} + \frac{\partial Qx}{\partial x} + \frac{\partial Qy}{\partial y} = 0$$

Here, v and u are the velocity, i_x and i_y the bottom slopes and Q_x and Qy the discharges per unit width, in the x and y directions, respectively. The mathematical model is made up of central difference expressions of Eqs. (19) and (20). The grid system is such as in Fig. 25, and operational procedures are shown in Figs. 26 and 27, for the equations of motion and continuity, respectively.

This simulation technique was applied to the Mihara-Seto on the Inland Sea of Seto. In this case, the difference in distance was 200 m and that in time was 15 sec. The stage-time relationship due to the tides is given as the boundary conditions. Figures 28 and 29 show the spatial distribution of stage and of velocity, 9 hours after the start of simulation testing, respectively.

REFERENCES

1) M.Nakamura, and H.Shiraishi; Analysis of unsteady flow phenomena by mathematical model simulation, Bulletin of the National Research Institute of Agricultural Engineering No.9, Mar. 1971.

2) H.Shiraishi; Analysis of the unsteady flow in an open channel network, Technical Report of the National Research Institute of Agricultural Engineering No.6, Mar. 1972.

3) H.Shiraishi and K.Iwasaki; Analysis of the unsteady flow in a closed conduit system, Proceedings of General Meeting of the Japanese Society of Irrigation, Drainage and Reclamation Engineering, 1972.

4) H.Shiraishi; Analysis of the two dimensional unsteady flow over the complex geometry, Technical Report of the National Research Institute of Agricultural Engineering, No. F 7, Mar. 1972.

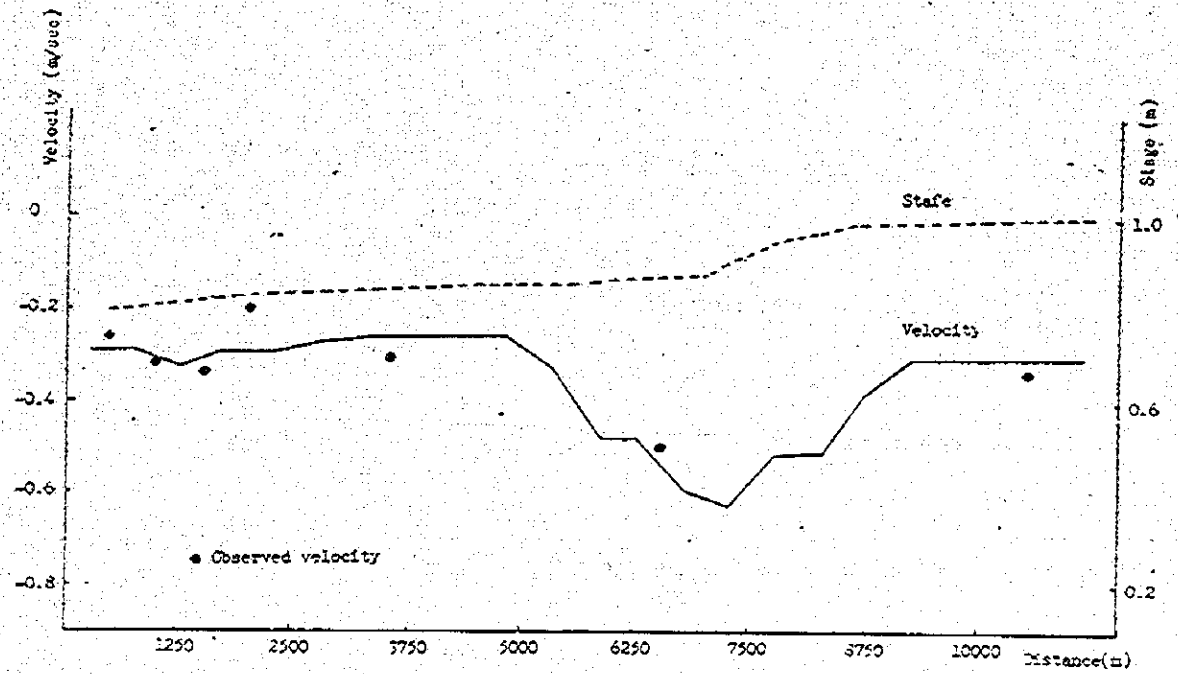

Fig. 1. Simulated and observed characteristics at the upstream from the Hitachigawa gate

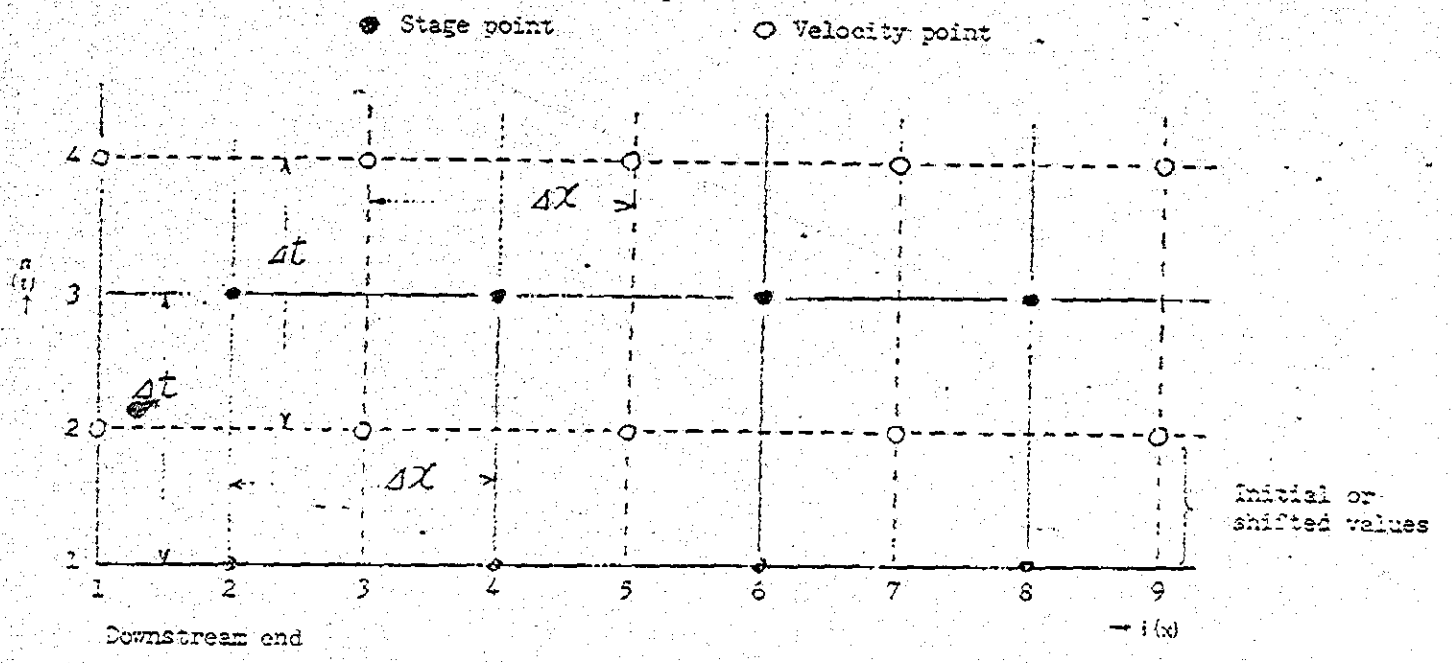

Fig. 2. Operational grid system

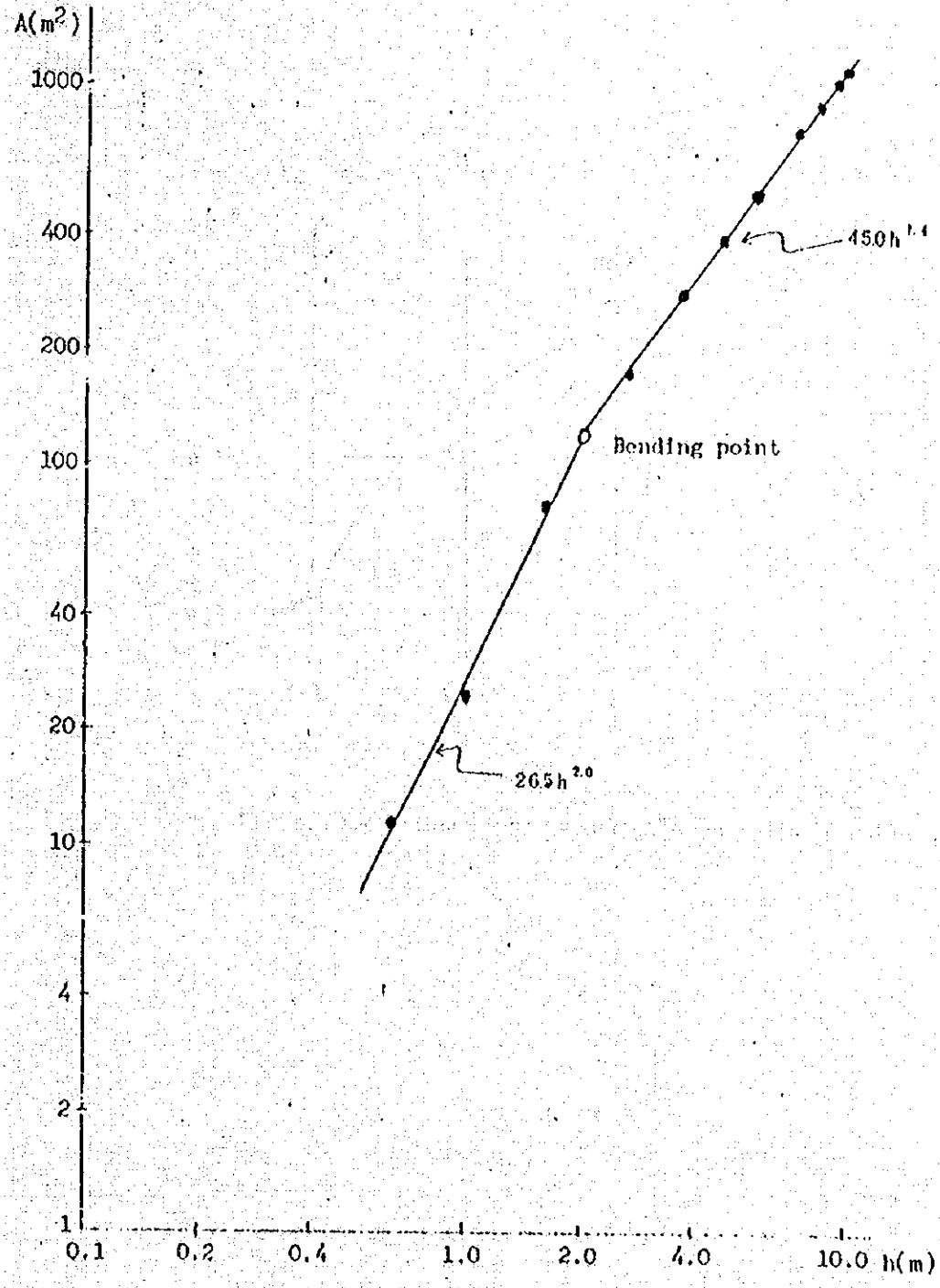

Fig. 3. Functional representation of the cross-sectional area at Osamunai on the Ishikari River

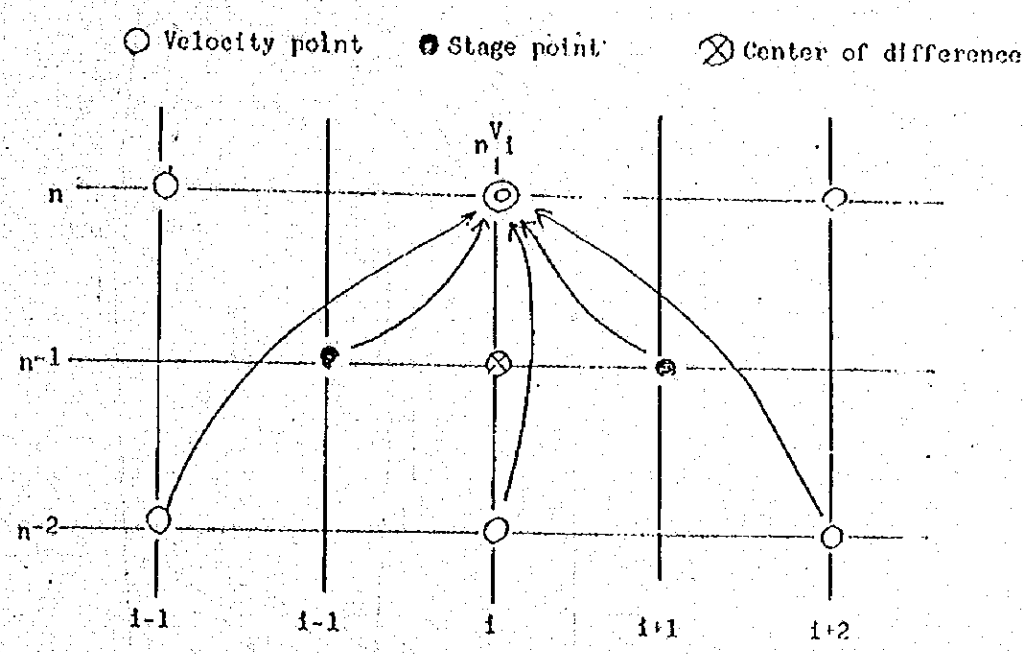

Fig. 4. Operational grid system of the equation of motion

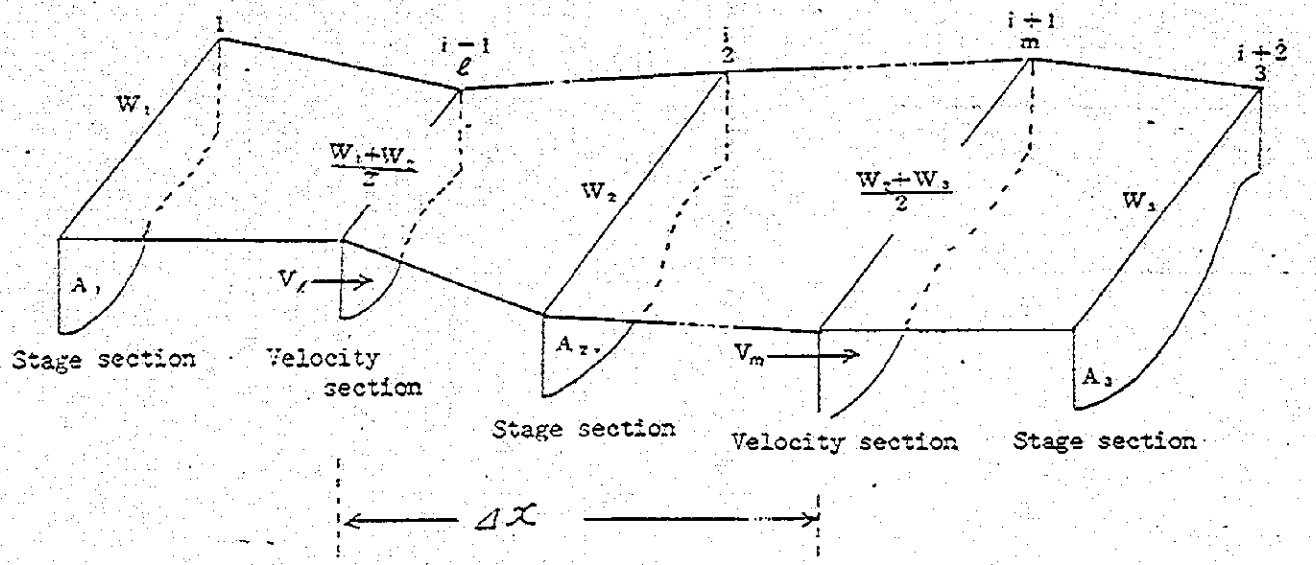

Fig. 5. Treatment of geometric conditions to solve the equation of continuity

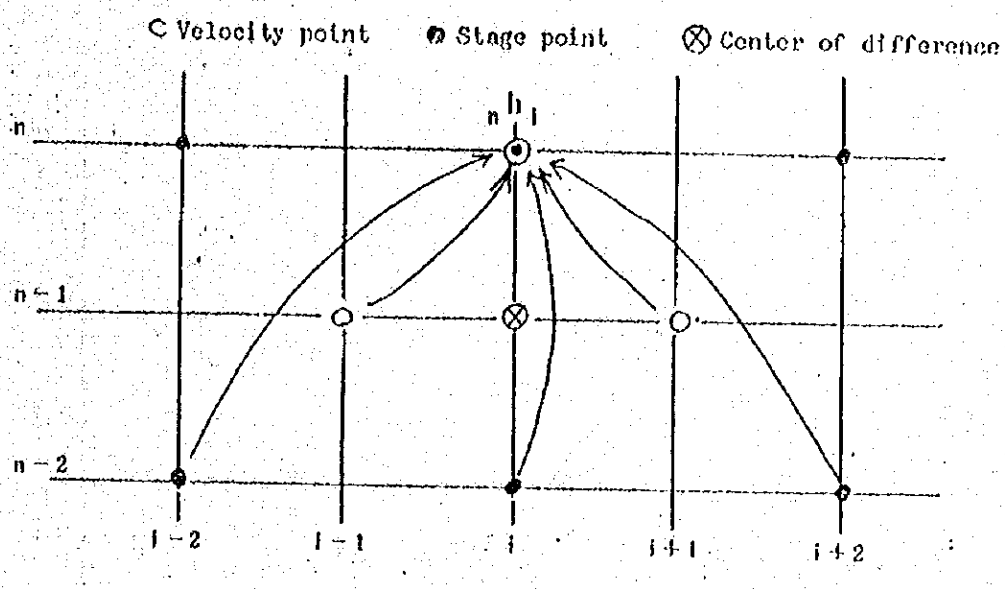

Fig. 6. Operational grid system of the equation of continuity

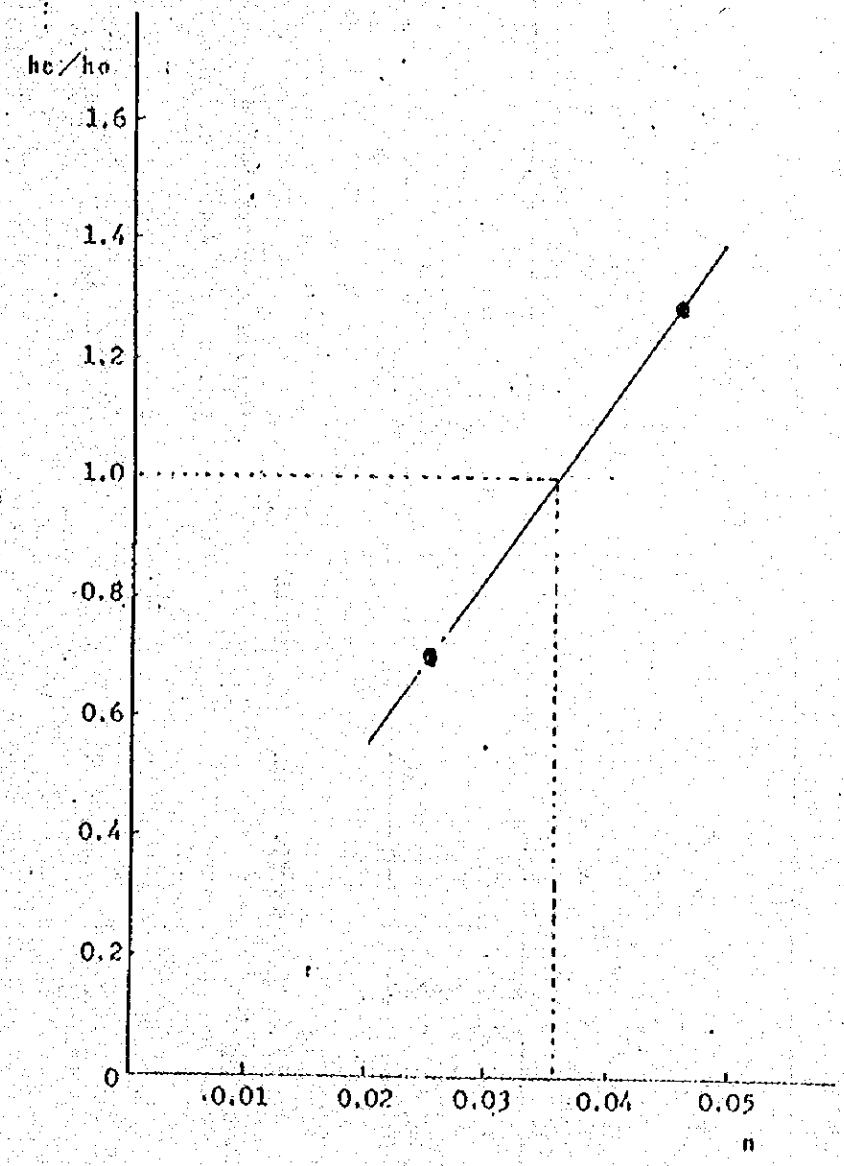

Fig. 7 Estimation of the roughness coefficient

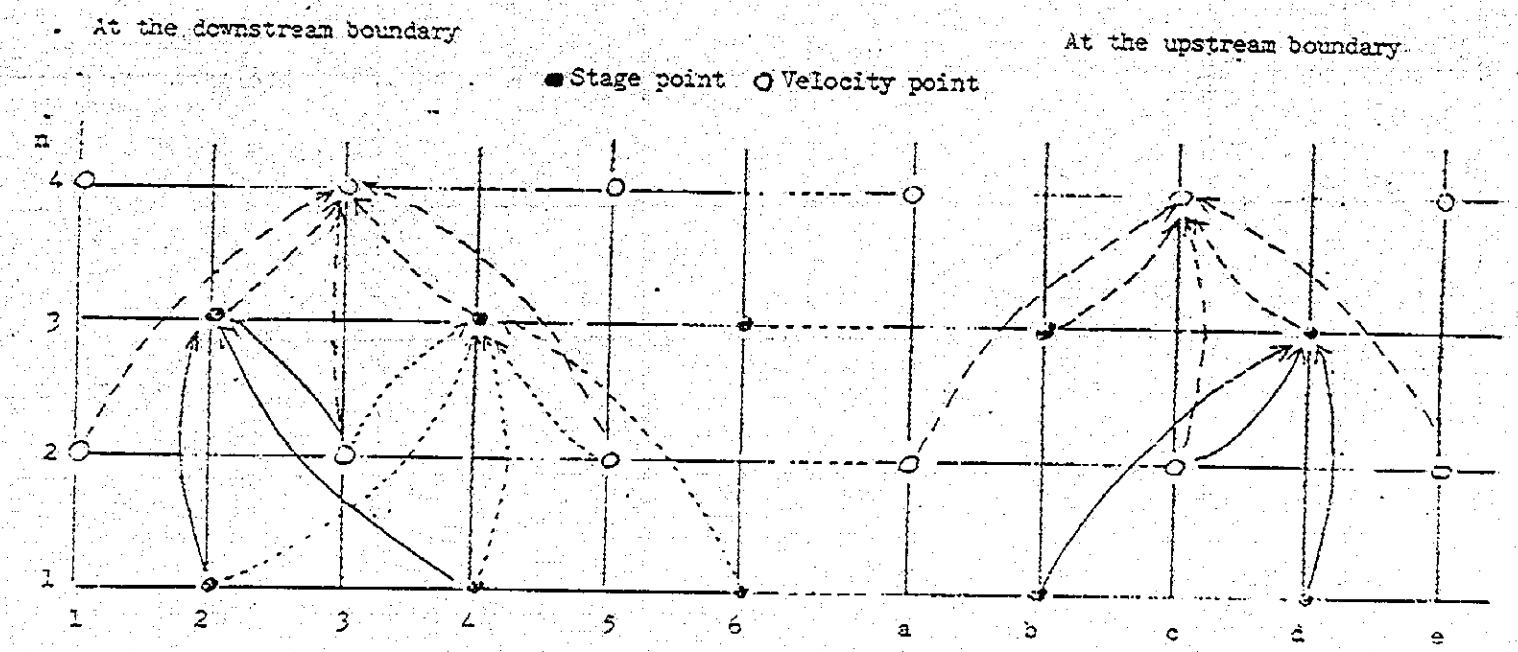

Fig. 8. Operational grid system for discharge-time relationship as boundary conditions

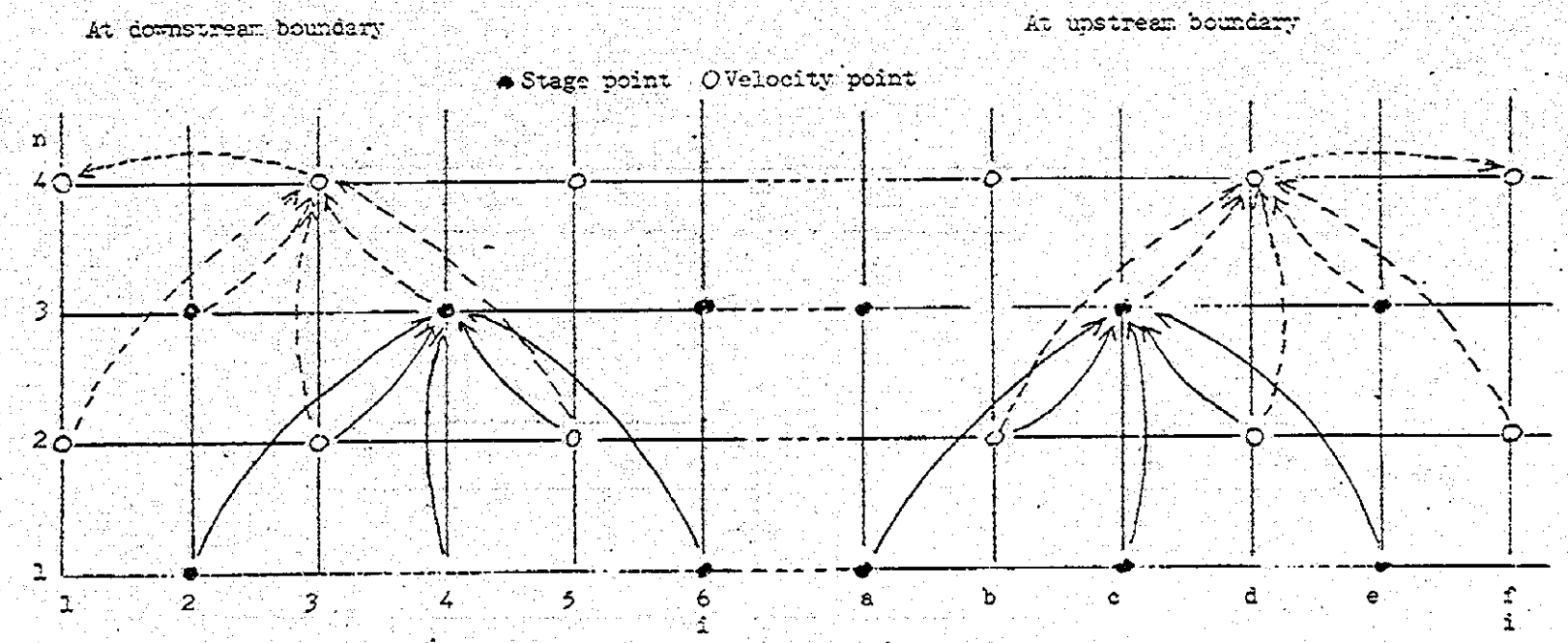

Fig. 9. Operational grid system for stage-time relationship as boundary conditions

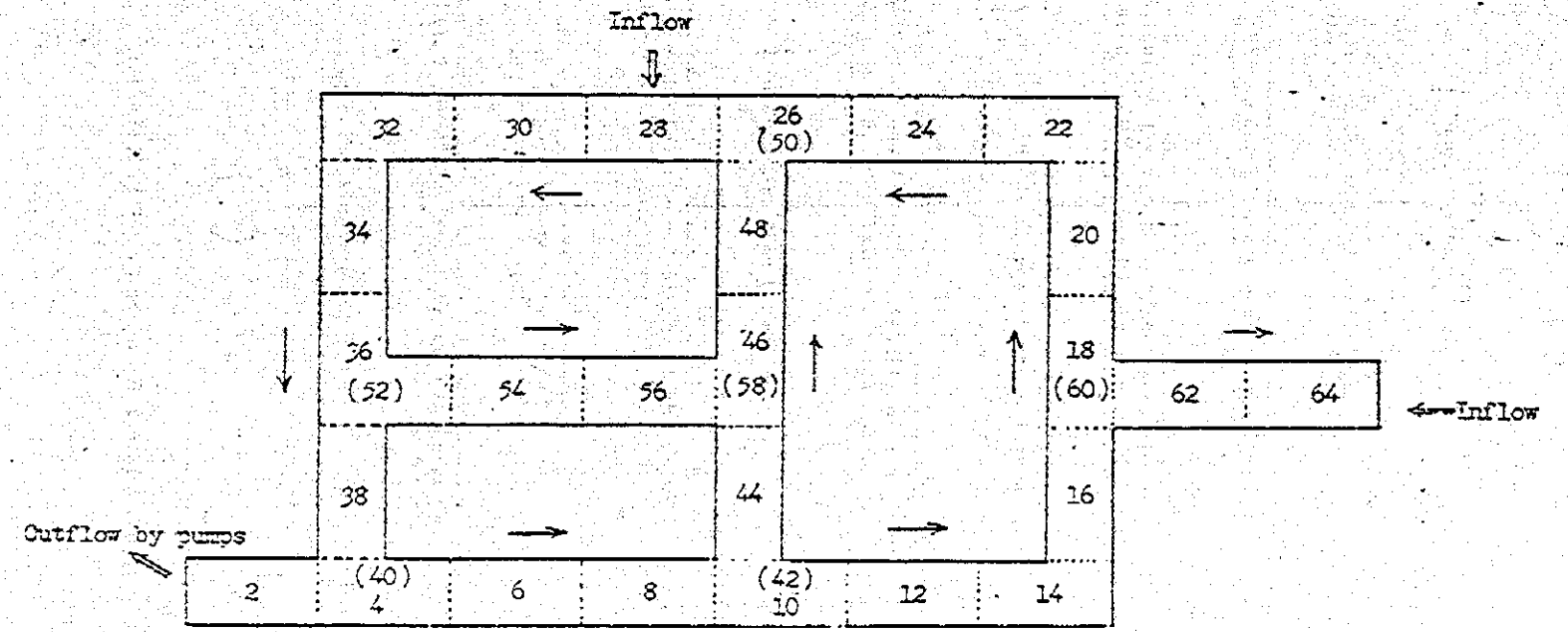

Fig. 10. Open channel network model

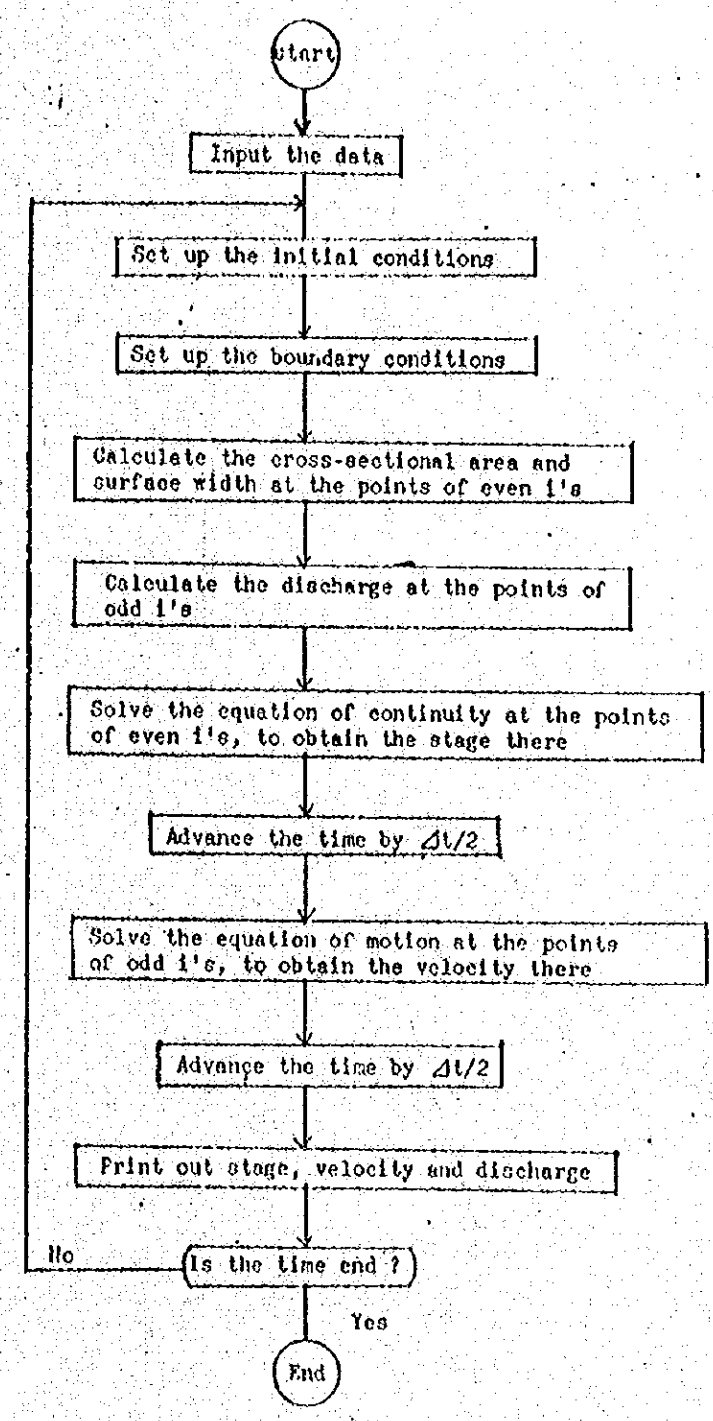

Fig. 11. Flow-chart of the mathematical model simulation

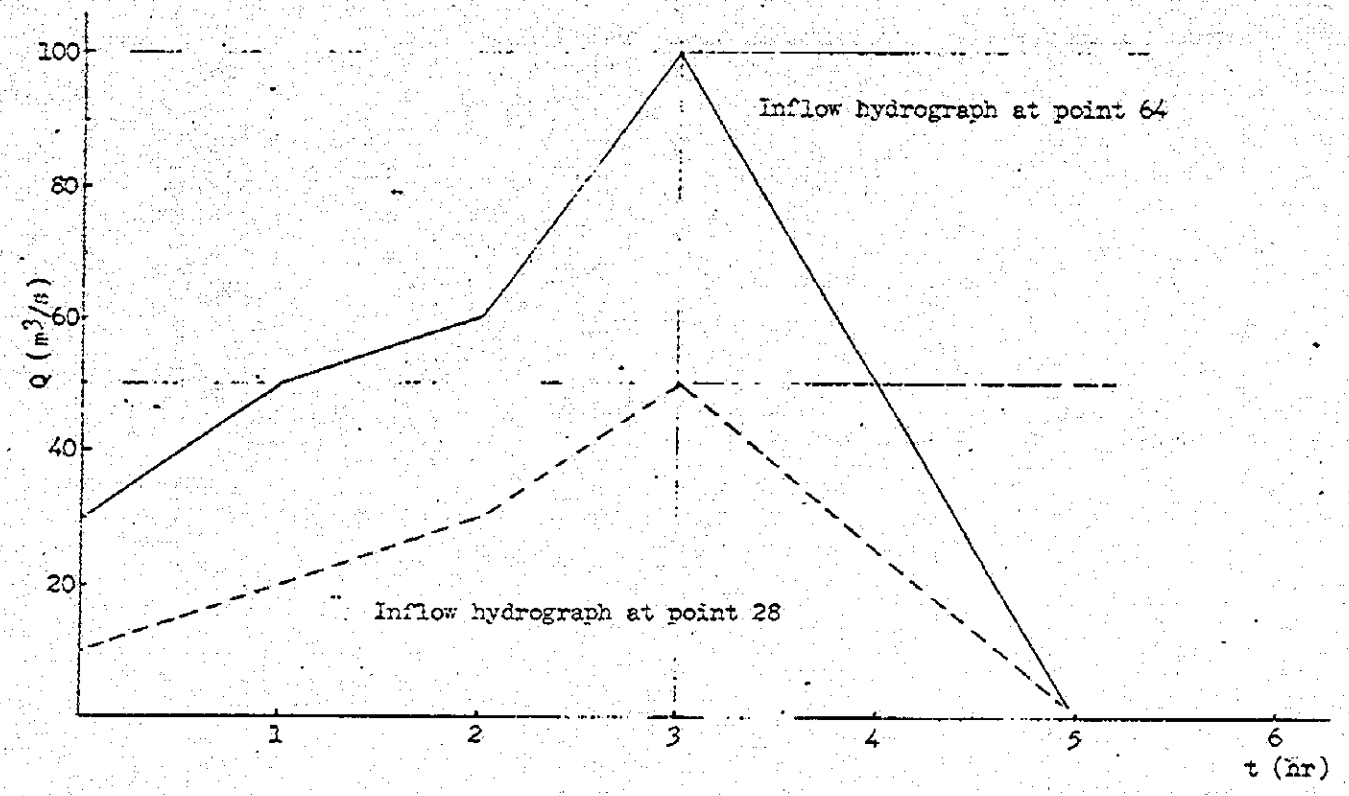

Fig. 12. Inflow hydrograph at points 64 and 28

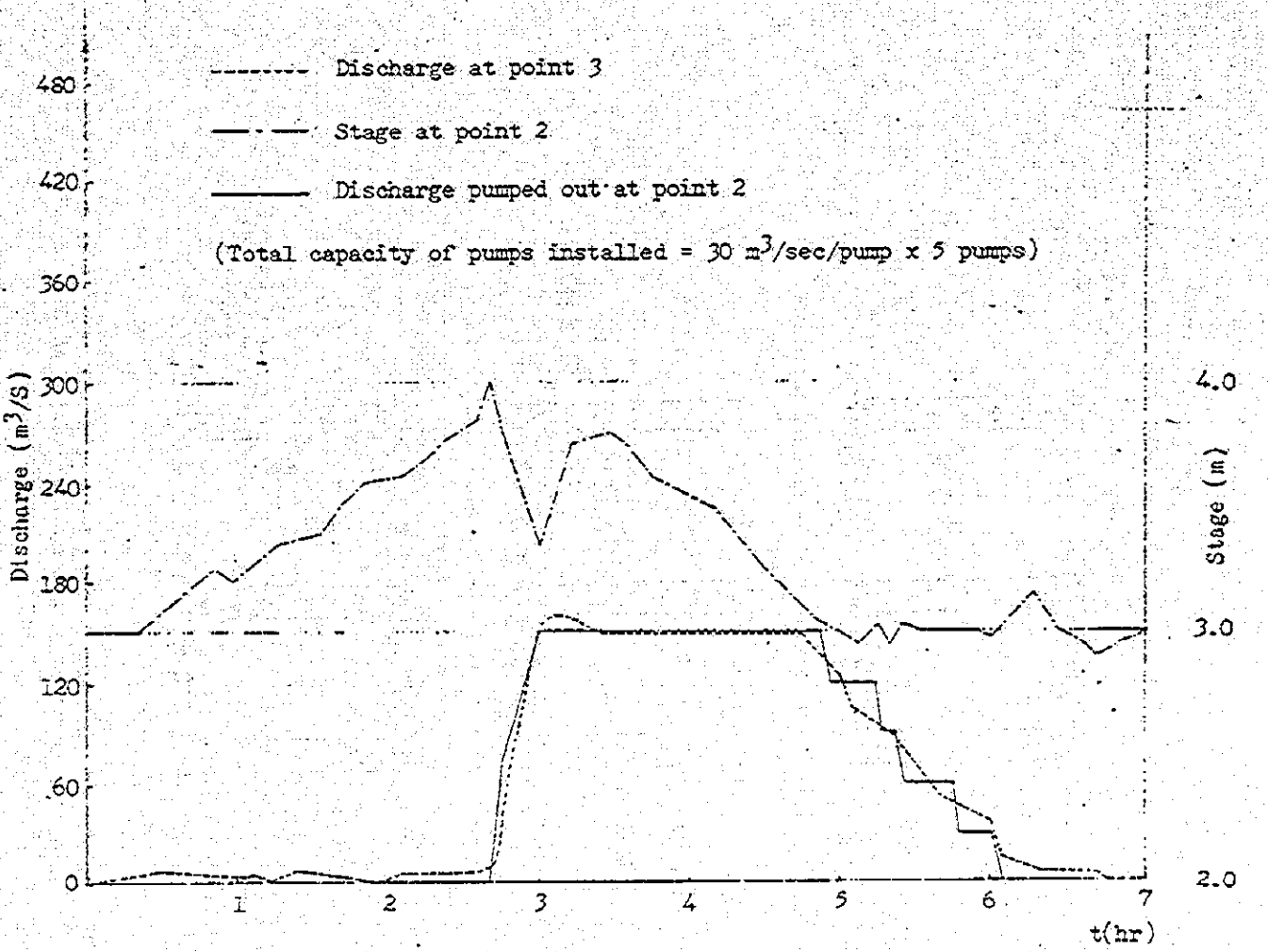

Fig. 13. Operation of the pumps

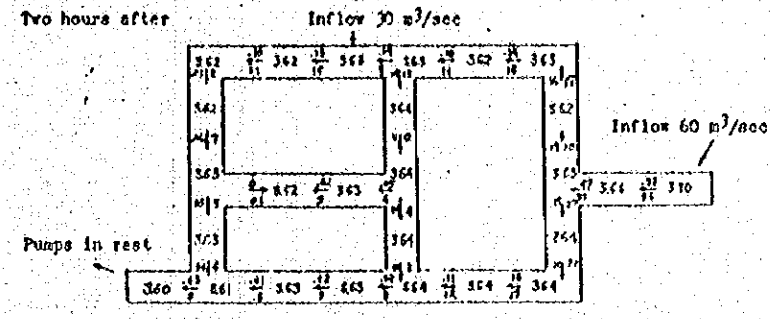

Fig. 14. Hydraulic behaviour in the open channel network (No. 1)

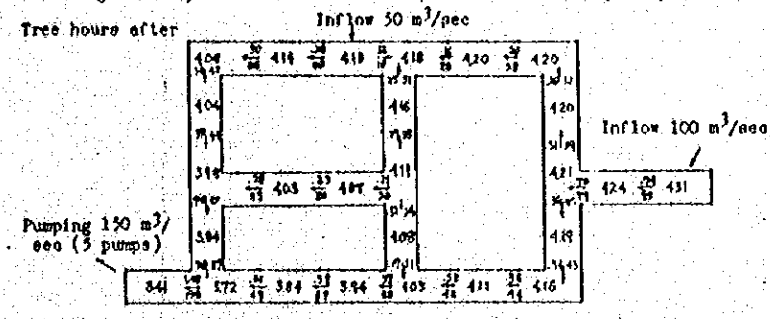

Fig. 15. Hydraulic behaviour in the open channel network (No. 2)

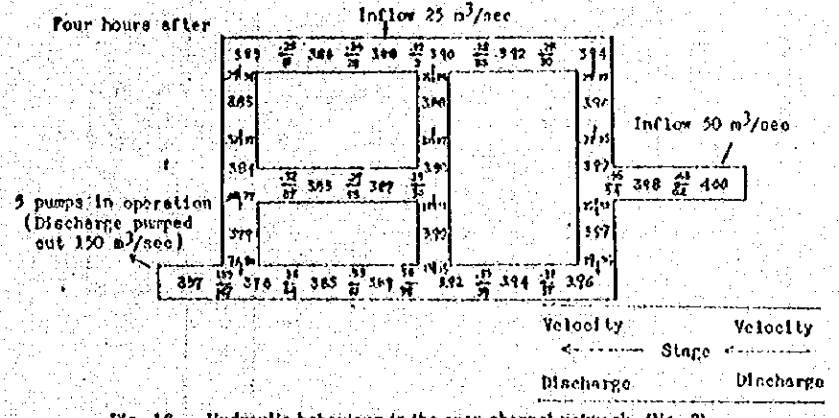

Fig. 16. Hydraulic behaviour in the open channel network (No. 3)

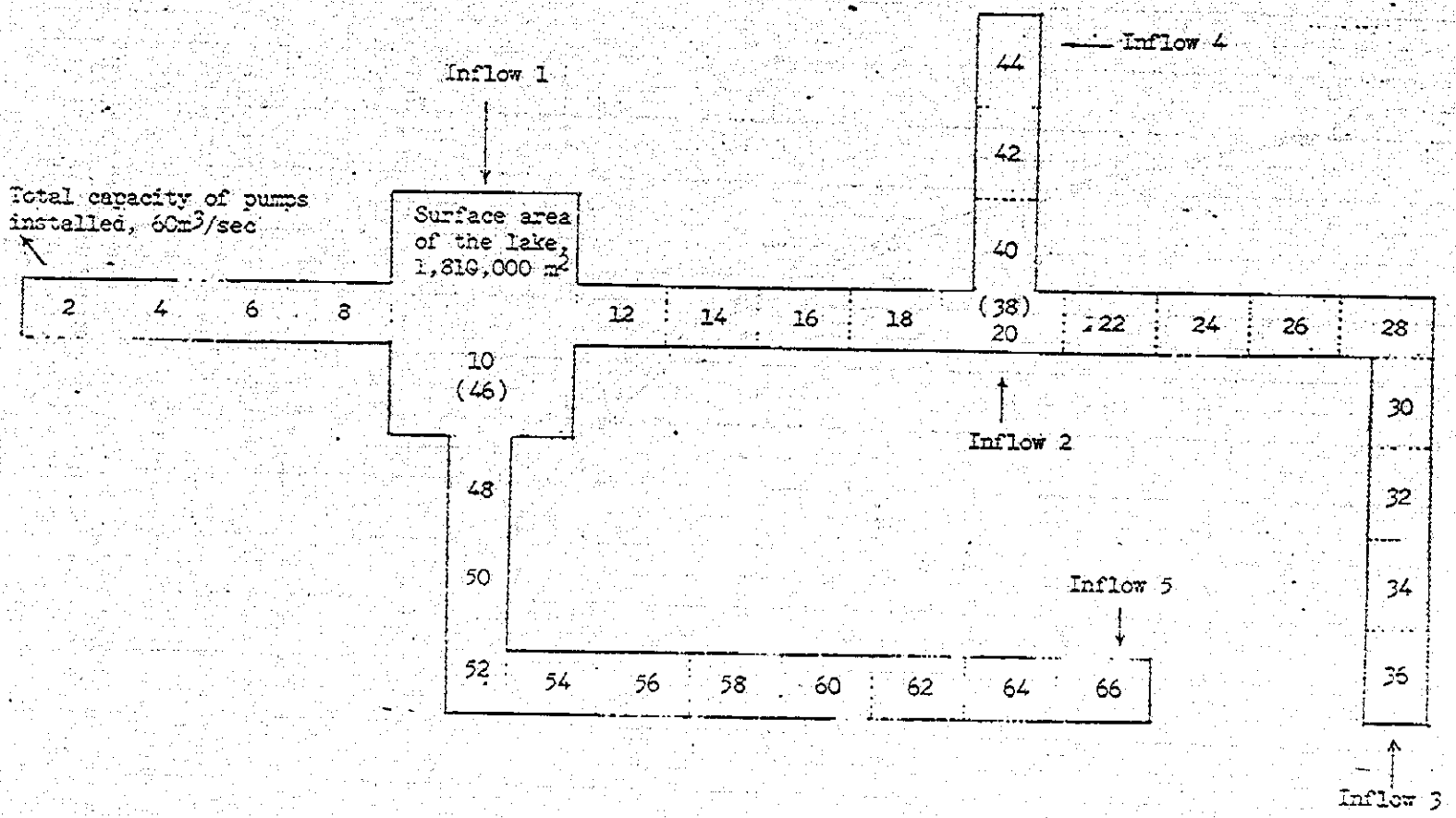

Fig. 17. Open channel with a broad storage in it

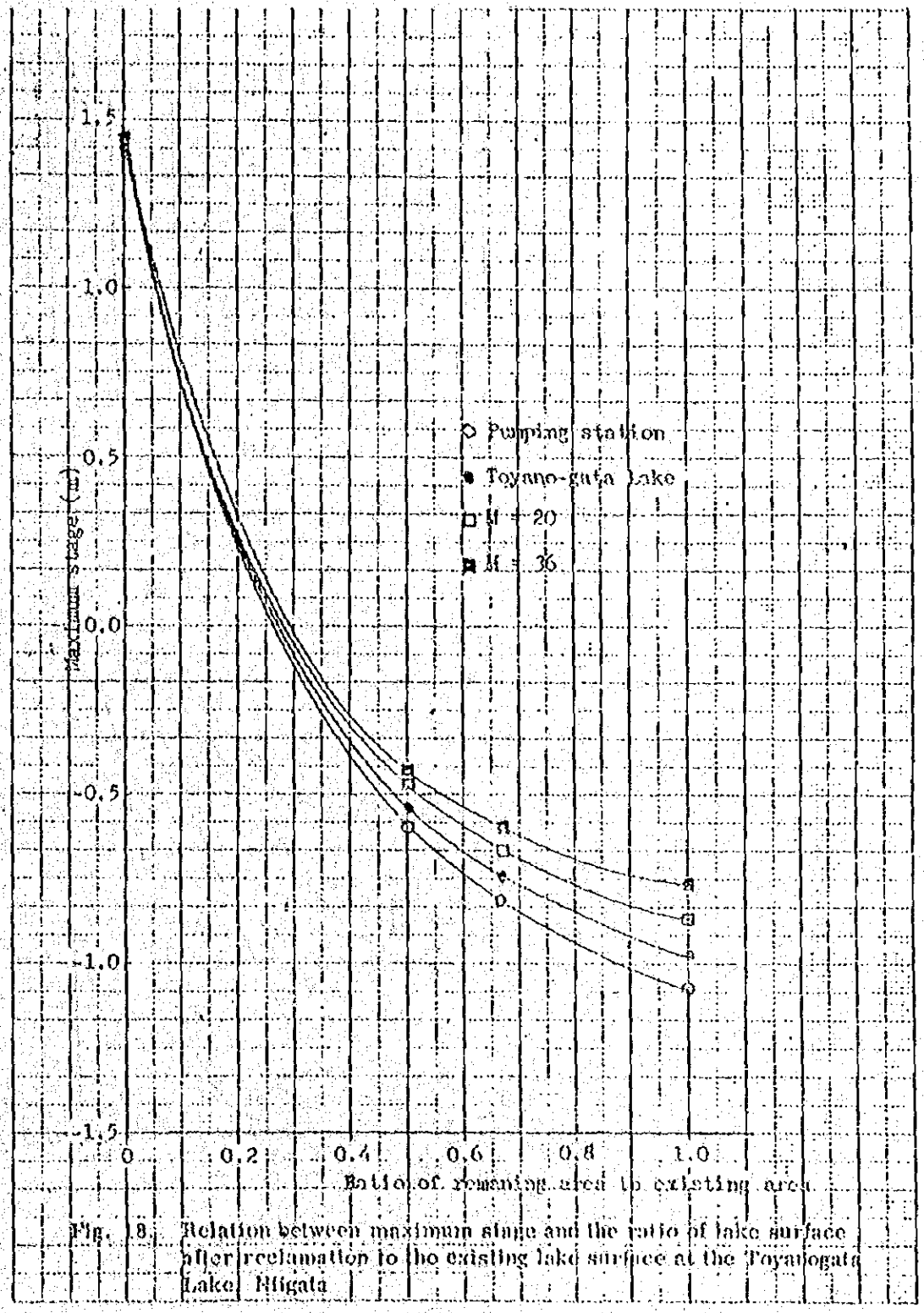

Fig. 18. Relation between maximum stage and the ratio of lake surface after reclamation to the existing lake surface at the Toyanogata Lake, Niigata

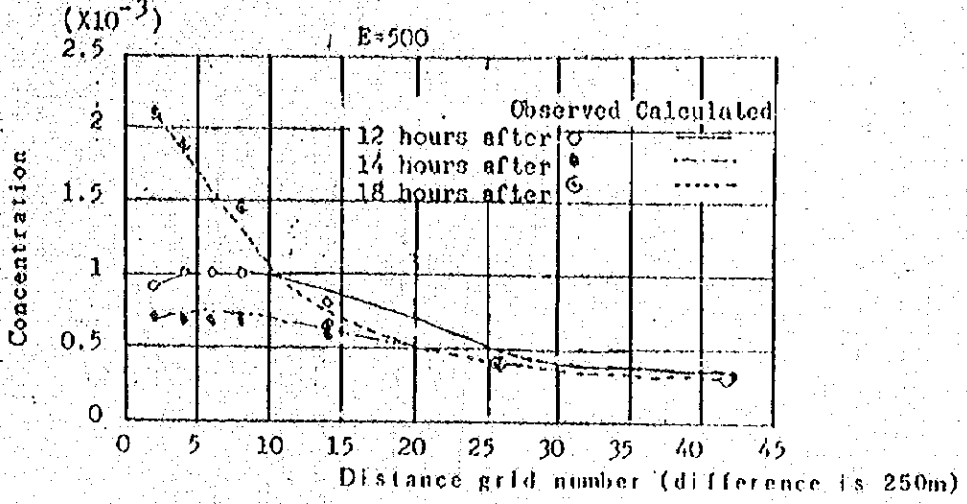

Fig. 19. Computed and observed salinity concentration in the estuary of the Hitachi-gawa River

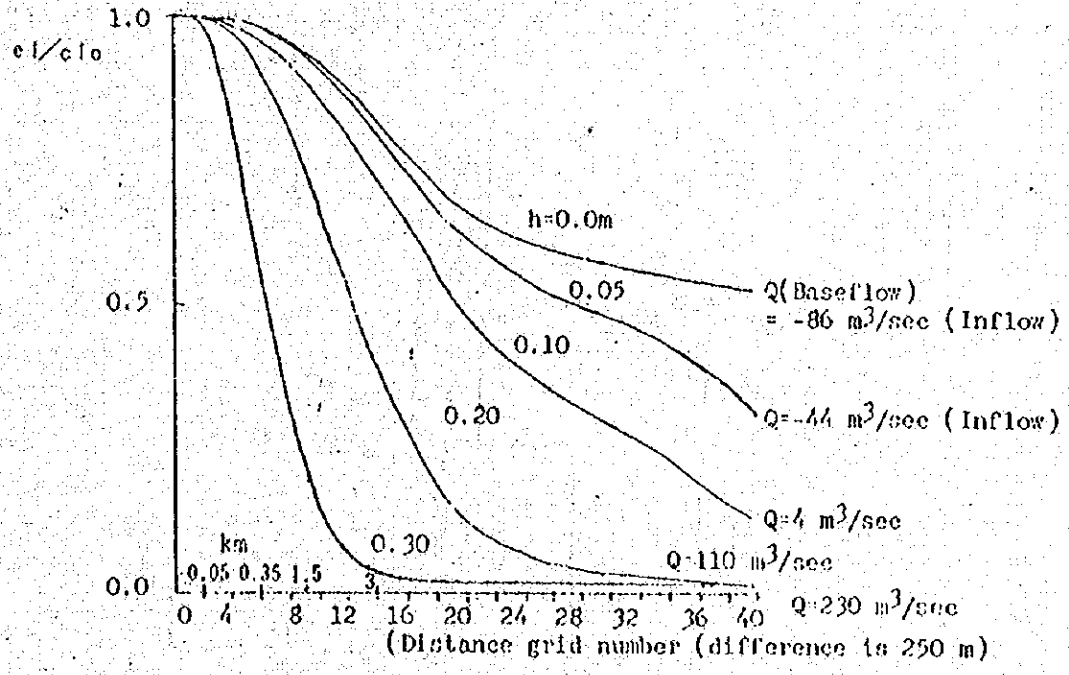

Fig. 20. Relation between the base flow discharge, salinity concentration and the distance from the rive mouth

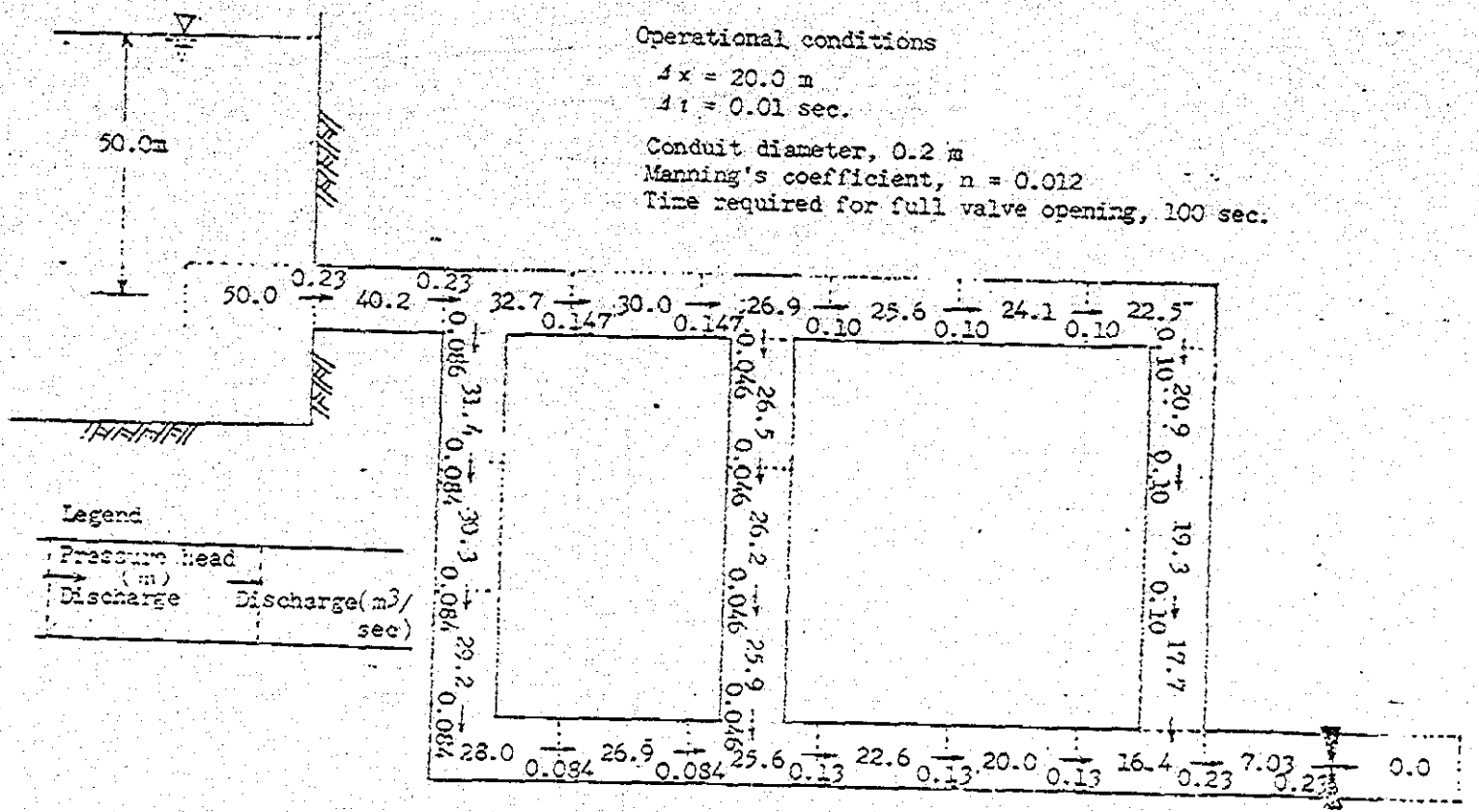

Fig. 21. Hydraulic behaviour in the closed conduits network (35 sec after start of the valve opening)

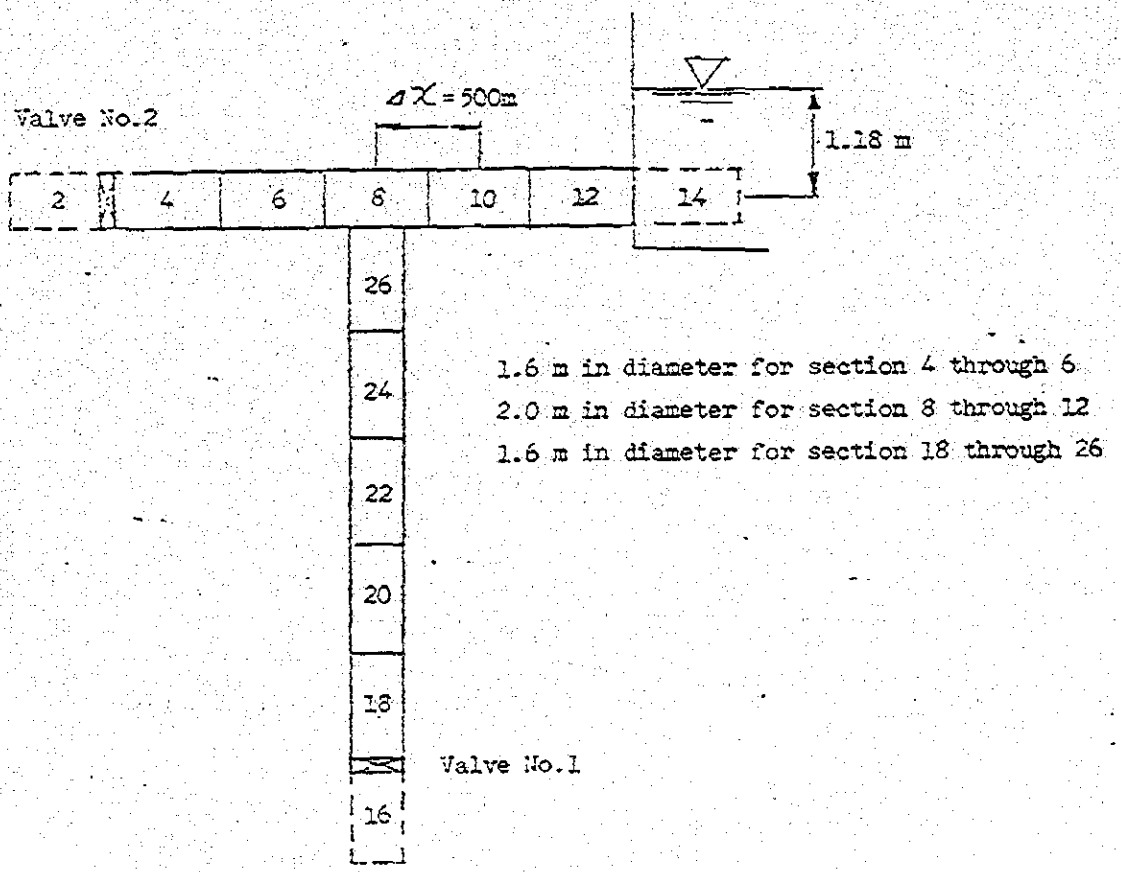

Fig. 22. Branching closed conduit

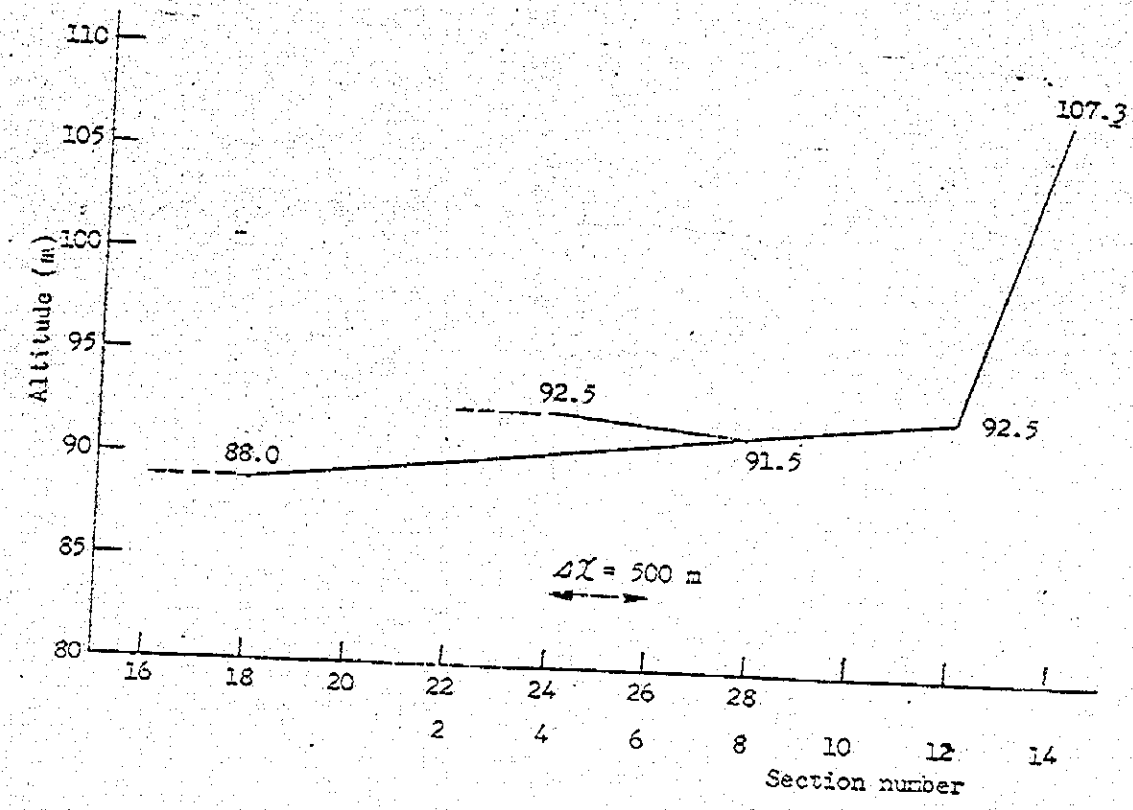

Fig. 23. Altitudes of the conduits

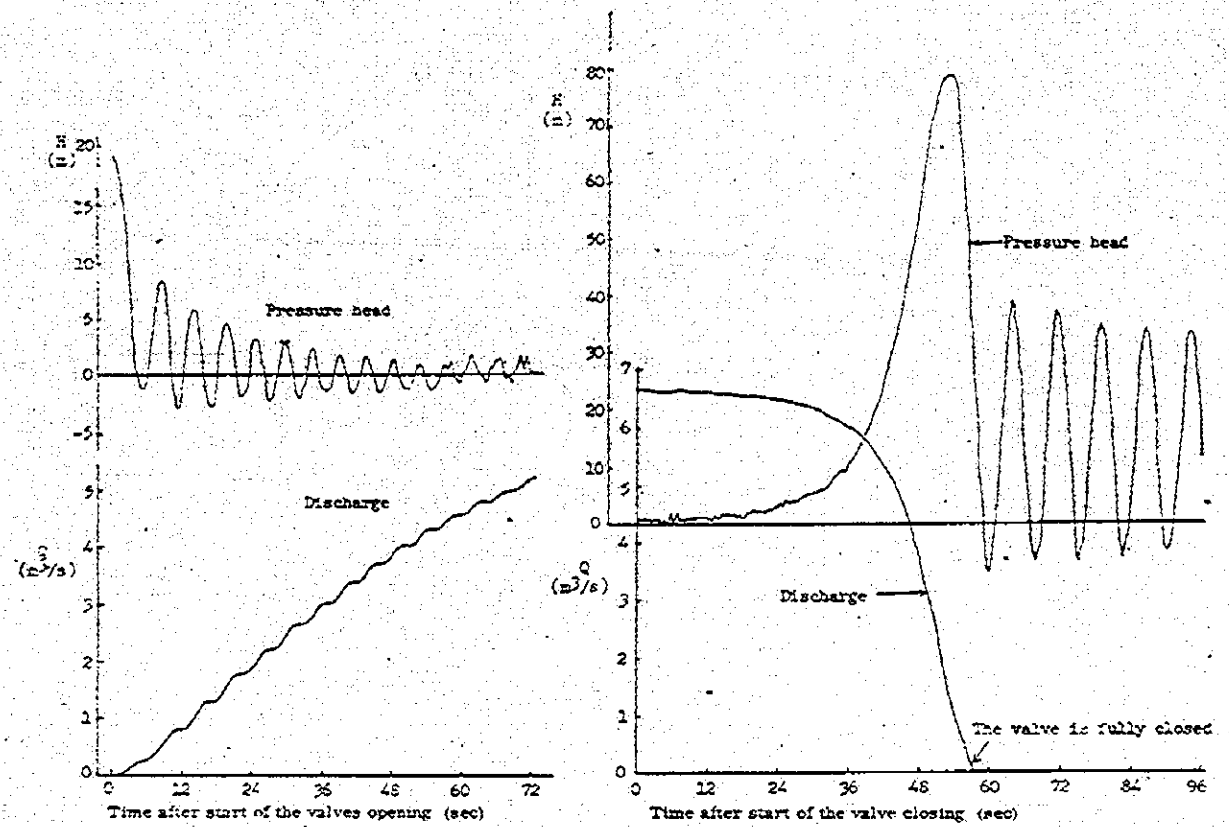

Fig. 24. Hydraulic characteristics of the closed conduit system

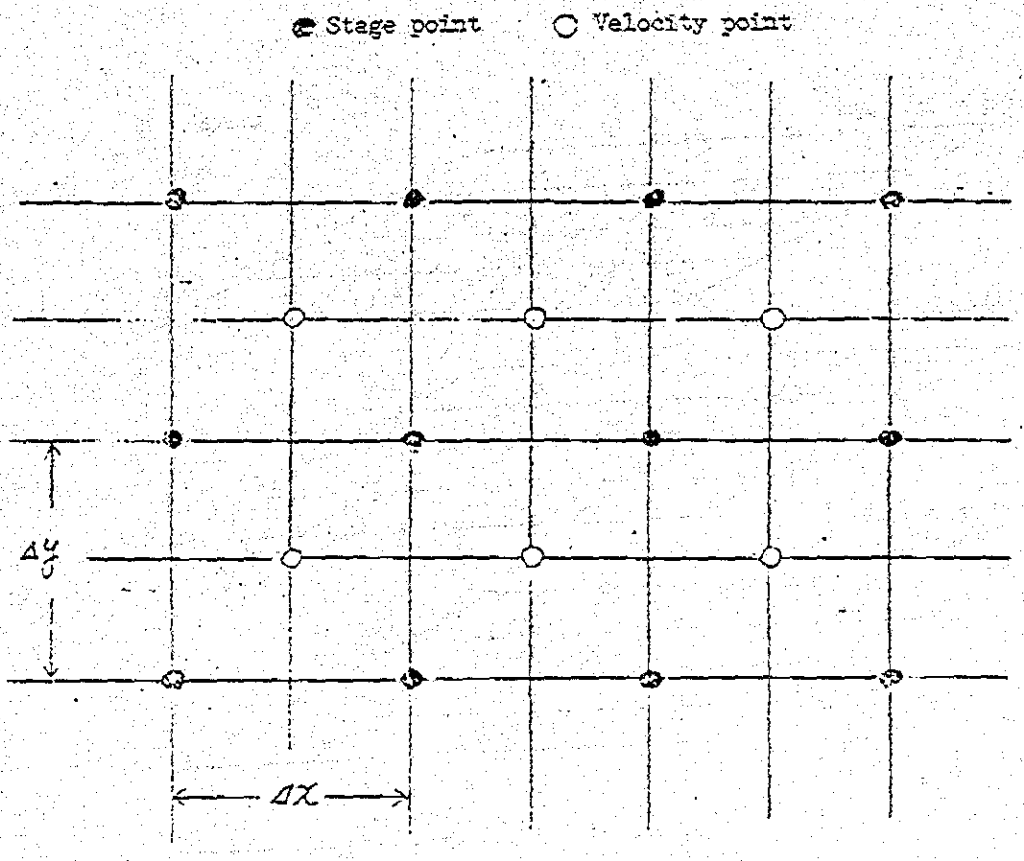

Fig. 25. Operational grid system of the two-dimensional unsteady flow

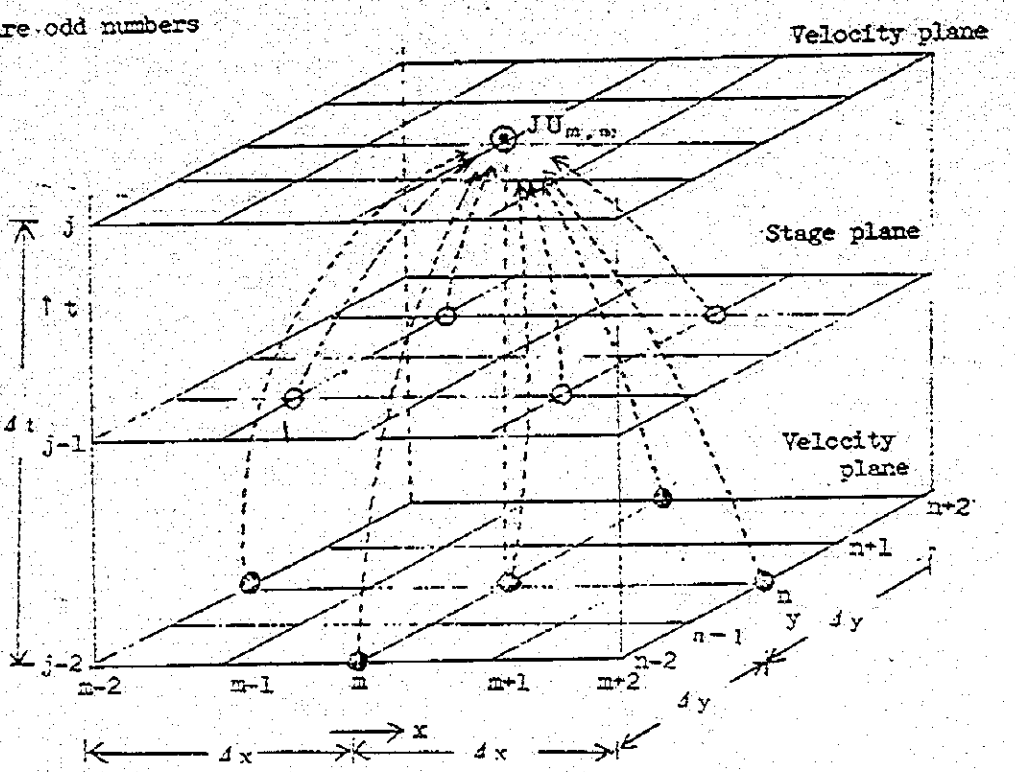

Fig. 26. Operational grid system of the equation of motion for the two-dimensional unsteady flow

m, n are even number

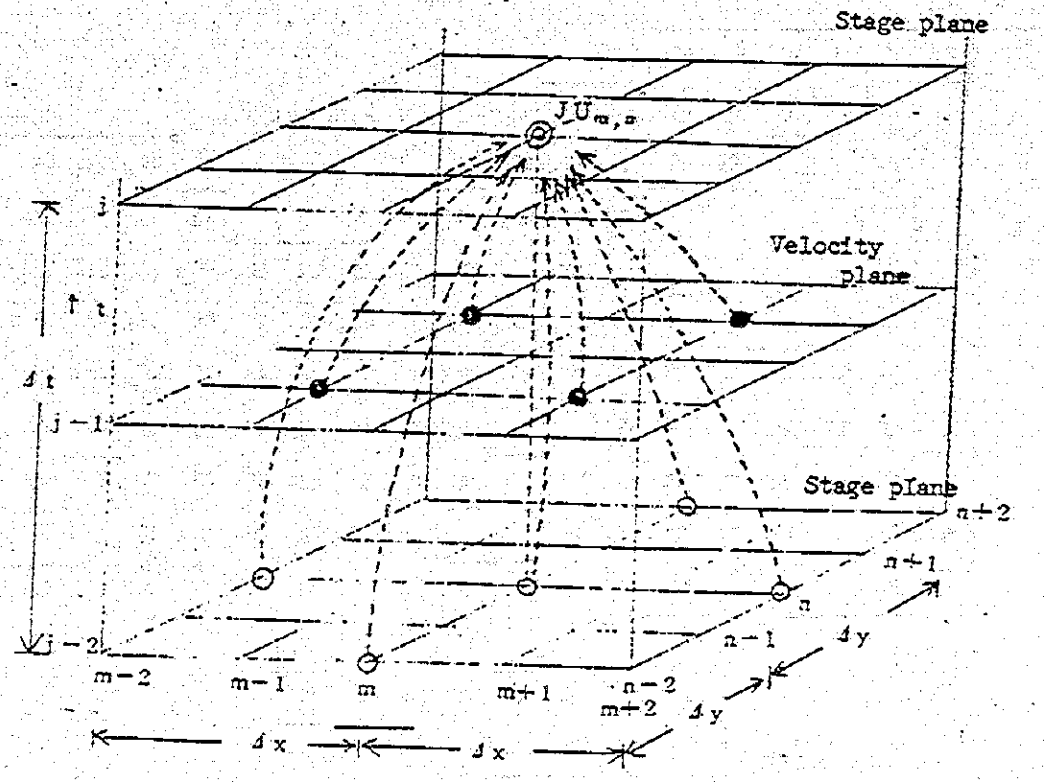

Fig. 27. Operational grid system of the motion for the two-dimensional unsteady flow

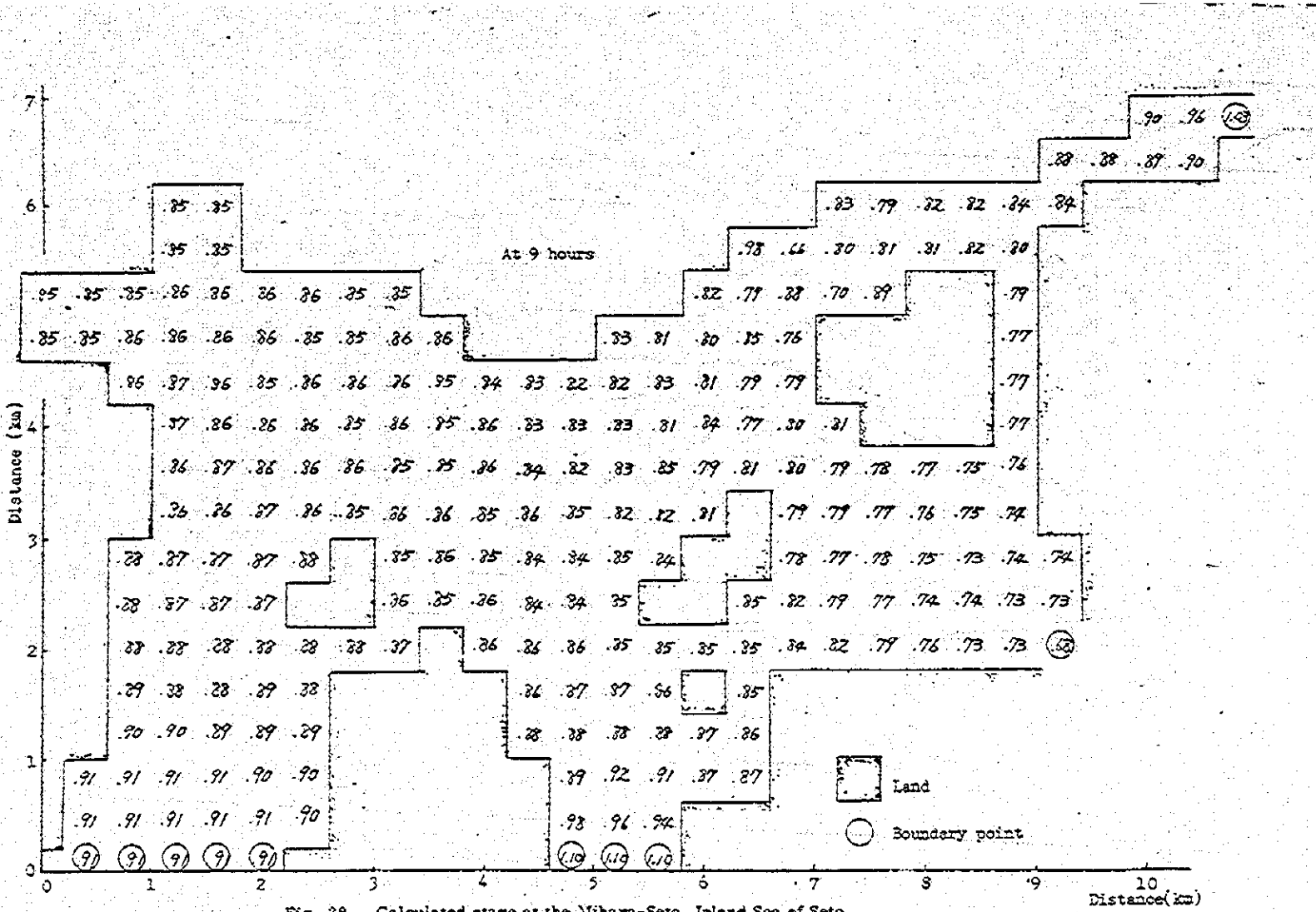

Fig. 28. Calculated stage at the Mihara-Seto, Inland Sea of Seto

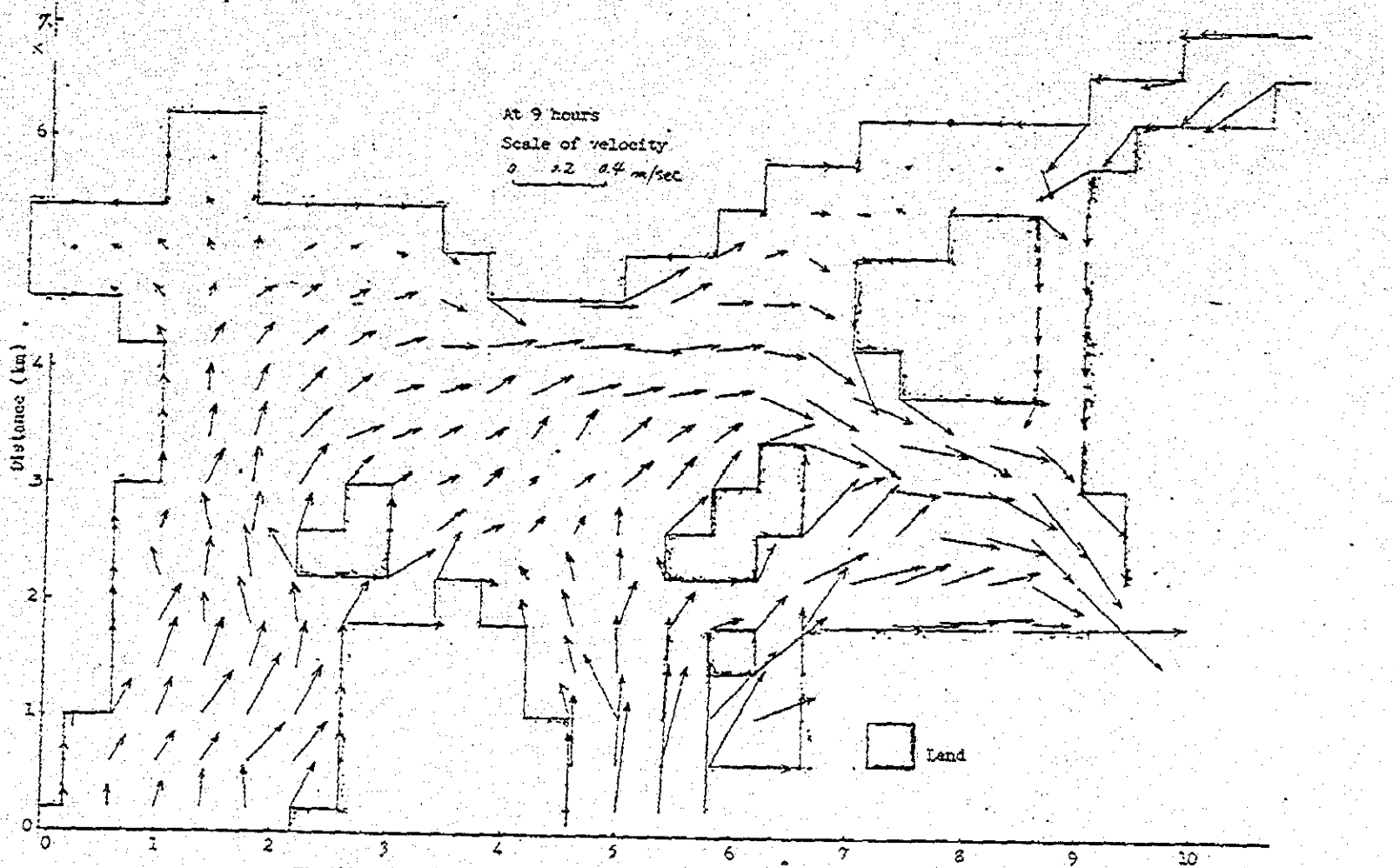

Fig. 29. Calculated velocity at the Mihara-Seto, Inland Sea of Seto

ANNEX C

ANNEX C

The computation result of Sg. Perai river flow on Perai Barrage gate operation

(1) Simulation of attempt gate operation on 17 May 1984

a) Tide table is used as downstream boundary condition in this case. Gates are not operated.

Inflow discharge QIN1=10 m³/sec
(QIN1 is constant with regard to time)

Fig. 1-1 Fluctuation of water level at downstream, Mesh 2 and upstream, Mesh 22 of the Barrage

Fig. 1-2 Fluctuation of water level at downstream of the Barrge, Mesh 20

b) Tide table is used as downstream boundary condition in this case. Gates are operated on 17 May.

Inflow discharge QIN1=10 m³/sec
(QIN1 is constant with regard to time)

Fig. 1-3 Fluctuation of water level at downstream of the Barrge Mesh 20

Fig. 1-4 Opening height of gates

Fig. 1-5 Peak of Fluctuation at down stream of the Barrage, Mesh 20

Fig. 1-6 Fluctuation of water level at downstream, Mesh 20 and upstream, Mesh 22 of the Barrage

Fig. 1-7 Fluctuation of water level at Mesh 18 and Mesh 24

c) Design tide is used as downstream boundary condition in this case. Gates are operated on 17 May.

Inflow discharge QIN1=10 m³/sec
(QIN1 is constant with regard to time)

Fig. 1-8 Fluctuation of water level at downstream of the Barrge, Mesh 20

Fig. 1-9 Opening height of gates

Fig. 1-10 Peak of Fluctuation at down stream of the Barrage Mesh 20

Fig. 1-11 Fluctuation of water level at downstream, Mesh 20 and upstream, Mesh 22 of the Barrage

Fig. 1-12 Fluctuation of water level at Mesh 18 and Mesh 24

d) Design tide is used as downstream boundary condition in this case. Gates are operated on 17 May.

Inflow discharge QIN1=100 m³/sec
(QIN1 is constant with regard to time)

Fig.1-13 Fluctuation of water level at downstream of the Barrge, Mesh 20

Fig.1-14 Opening height of gates

Fig.1-15 Peak of Fluctuation at down stream of the Barrage Mesh 20

Fig.1-16 Fluctuation of water level at downstream, Mesh 20 and upstream, Mesh 22 of the Barrage

Fig.1-17 Fluctuation of water level at Mesh 18 and Mesh 24

(2) Simulation of gate operation case-2
a) Gates are operated by judgement base on .up and downstre water level at the Barrage only. Design tide is used as downstream boundary condition in this case.

Inflow discharge QIN1=100 m³/sec
(QIN1 is constant with regard to time)

Fig.2-1 Fluctuation of water level at downstream, Mesh 20 and upstream, Mesh 22 of the Barrage

Fig.2-2 Fluctuation of water level at Mesh 18 and upstream, Mesh 24

Fig.2-3 Fluctuation of water level at Mesh 24, Mesh 34, Mesh 44 and Mesh 52

Fig.2-4 Discharge passed through gates

Fig.2-5 Opening height of gates

Fig.2-6 Discharge at Mesh 3 and Mesh 17

Fig.2-7 Discharge at Mesh 23 and Mesh 43

(3) Simulation of gate operation case-3

Gates are operated by judgement base on up and downstre water level at the Barrage, gates are started to close when tide is rising and its water level becomes 0.0 m.

Design tide is used as downstream boundary condition in this case.

a) inflow discharge QIN1=10 m³/sec
(QIN1 is constant with regard to time)

Fig.3-1 Fluctuation of water level at downstream, Mesh 20 and upstream, Mesh 22 of the Barrage

Fig.3-2 Fluctuation of water level at Mesh 18 and Mesh 24

Fig.3-3 Fluctuation of water level at Mesh 24, Mesh 34, Mesh 44 and Mesh 52

Fig.3-4 Discharge passed through gates

Fig.3-5 Opening height of gates

b) inflow discharge QIN1=50 m³/sec
(QIN1 is constant with regard to time)

Fig.3-6 Fluctuation of water level at downstream, Mesh 20 and upstream, Mesh 22 of the Barrage

Fig.3-7 Fluctuation of water level at Mesh 18 and Mesh 24

Fig.3-8 Fluctuation of water level at Mesh 24, Mesh 34, Mesh 44 and Mesh 52

Fig.3-9 Discharge passed through gates

Fig.3-10 Opening height of gates

Fig.3-11 Discharge at Mesh 23 and Mesh 43

c) inflow discharge QIN1=10 m³/sec
(QIN1 is constant with regard to time)

Fig.3-12 Fluctuation of water level at downstream, Mesh 20 and upstream, Mesh 22 of the Barrage

Fig.3-13 Discharge passed through gates

Fig.3-14 Opening height of gates

Fig.3-15 Discharge at Mesh 23 and Mesh 43

(4) Simulation of gate operation case-4

Gates are operated by judgement base on up and downstre water level at the Barrage, gates are started to open when water level at downstream of the Barrage becomes 0.0 m.

Design tide is used as downstream boundary condition in this case.

inflow discharge QIN1=10 m^3/sec
(QIN1 is constant with regard to time)

Fig.4-1 Fluctuation of water level at downstream, Mesh 20 and upstream, Mesh 22 of the Barrage

Fig.4-2 Fluctuation of water level at Mesh 18 and Mesh 24

Fig.4-3 Fluctuation of water level at Mesh 24, Mesh 34, Mesh 44 and Mesh 52

Fig.4-4 Discharge passed through gates

Fig.4-5 Opening height of gates

Fig.4-6 Discharge at Mesh 3, Mesh 17 and Mesh 53

Fig.4-7 Discharge at Mesh 23 and Mesh 43

(5) Simulation of gate operation case-5

Gate operation is the same as case-3, and one of gates is always opened.

Design tide is used as downstream boundary condition in this case.

inflow discharge QIN1=10 m^3/sec
(QIN1 is constant with regard to time)

Fig.5-1 Fluctuation of water level at downstream, Mesh 20 and upstream, Mesh 22 of the Barrage

Fig.5-2 Fluctuation of water level at Mesh 18 and Mesh 24

Fig.5-3 Fluctuation of water level at Mesh 24, Mesh 34, Mesh 44 and Mesh 52

Fig.5-4 Discharge passed through gates

Fig.5-5 Opening height of gates

Fig.5-6 Discharge at Mesh 23 and Mesh 43

(6) Simulation of gate operation on flood

Gate operation is the same as case-3

Design tide is used as downstream boundary condition in this case.

a) The calculation result on runoff of which conditon is return period T=1/40 year, N=0.7, R1max=100 mm is used as inflow dicsharge.
Peak of inflow discharge Qp=554 m³/sec

Fig.6-1 Fluctuation of water level at downstream, Mesh 20 and upstream, Mesh 22 of the Barrage

Fig.6-2 Fluctuation of water level at Mesh 18 and Mesh 24

Fig.6-3 Fluctuation of water level at Mesh 24, Mesh 34, Mesh 44 and Mesh 52

Fig.6-4 Discharge passed through gates

Fig.6-5 Opening height of gates

Fig.6-6 Discharge at Mesh 3, Mesh 17 and Mesh 53

Fig.6-7 Discharge at Mesh 23 and Mesh 43

b) The calculation result on runoff of which conditon is return period T=1/10 year, N=1.0, R1max=150 mm is used as inflow dicsharge.
Peak of inflow discharge Qp=121 m³/sec

Fig.6-8 Fluctuation of water level at downstream, Mesh 20 and upstream, Mesh 22 of the Barrage

Fig.6-9 Fluctuation of water level at Mesh 18 and Mesh 24

Fig.6-10 Fluctuation of water level at Mesh 24, Mesh 34, Mesh 44 and Mesh 52

Fig.6-11 Discharge passed through gates

Fig.6-12 Opening height of gates

Fig.6-13 Discharge at Mesh 3, Mesh 17 and Mesh 53

Fig.6-14 Discharge at Mesh 23 and Mesh 43

c) The calculation result on runoff of which conditon is return period T=1/20 year, N=0.7, R1max=150 mm is used as inflow dicsharge.
Peak of inflow discharge Qp=225 m³/sec

Fig.6-15 Fluctuation of water level at downstream, Mesh 20 and upstream, Mesh 22 of the Barrage

d) The calculation result on runoff of which conditon is return period T=1/40 year, N=1.0, R1max=150 mm is used as inflow dicsharge.
Peak of inflow discharge Qp=211 m³/sec

e) The calculation result on runoff of which conditon is return period T=1/20 year, N=1.0, R1max=150 mm is used as inflow dicsharge.
Peak of inflow discharge Qp=162 m³/sec

CASE-1

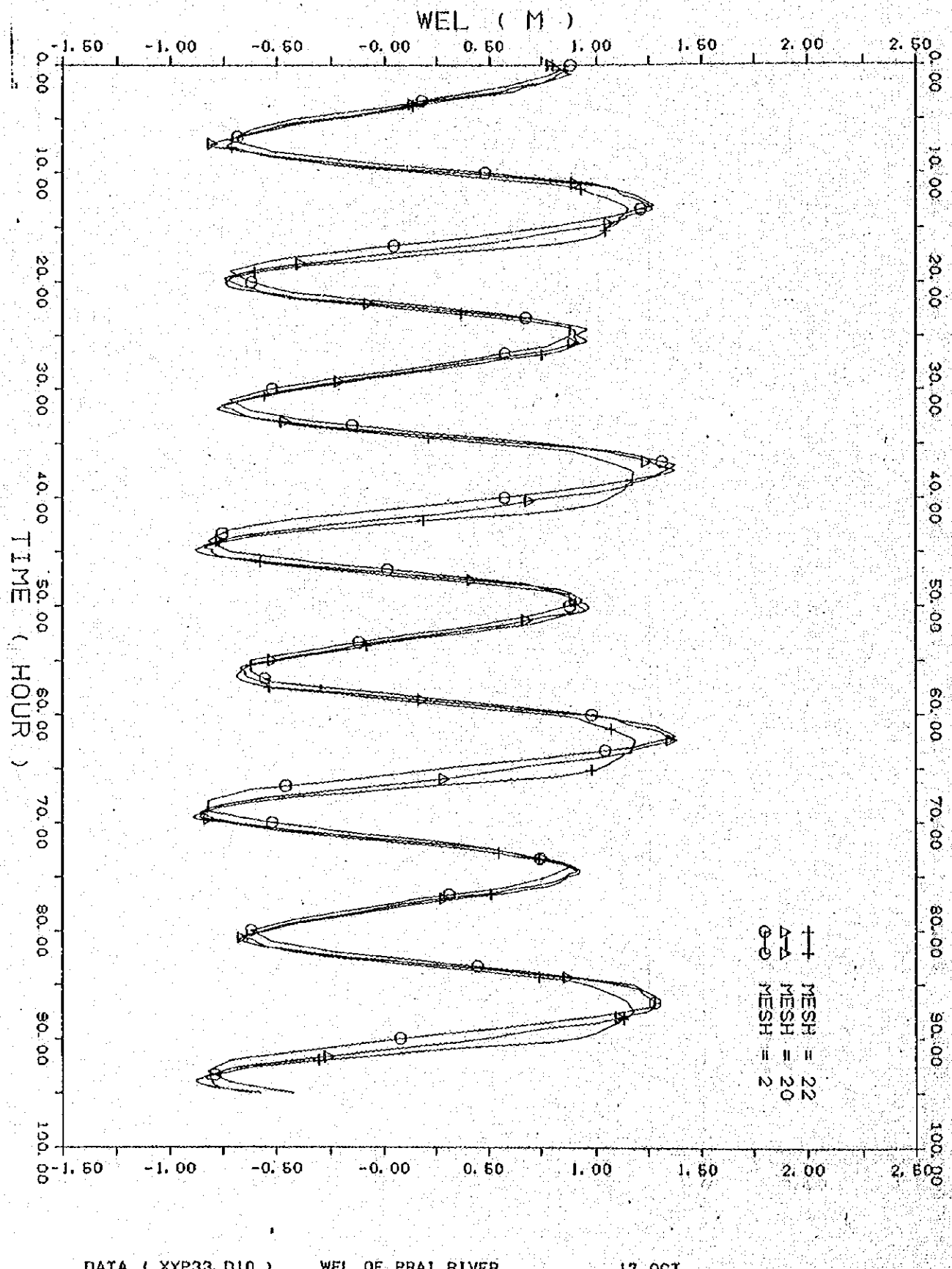

Fig.1-1 Fluctuation of water level at downstream, Mesh 20 and upstream, Mesh 22 of the Barrage

Fig.1-2 Fluctuation of water level at downstream of the Barrge, Mesh 20

Fig. 1-3 Fluctuation of water level at downstream of the Barrge Mesh 20

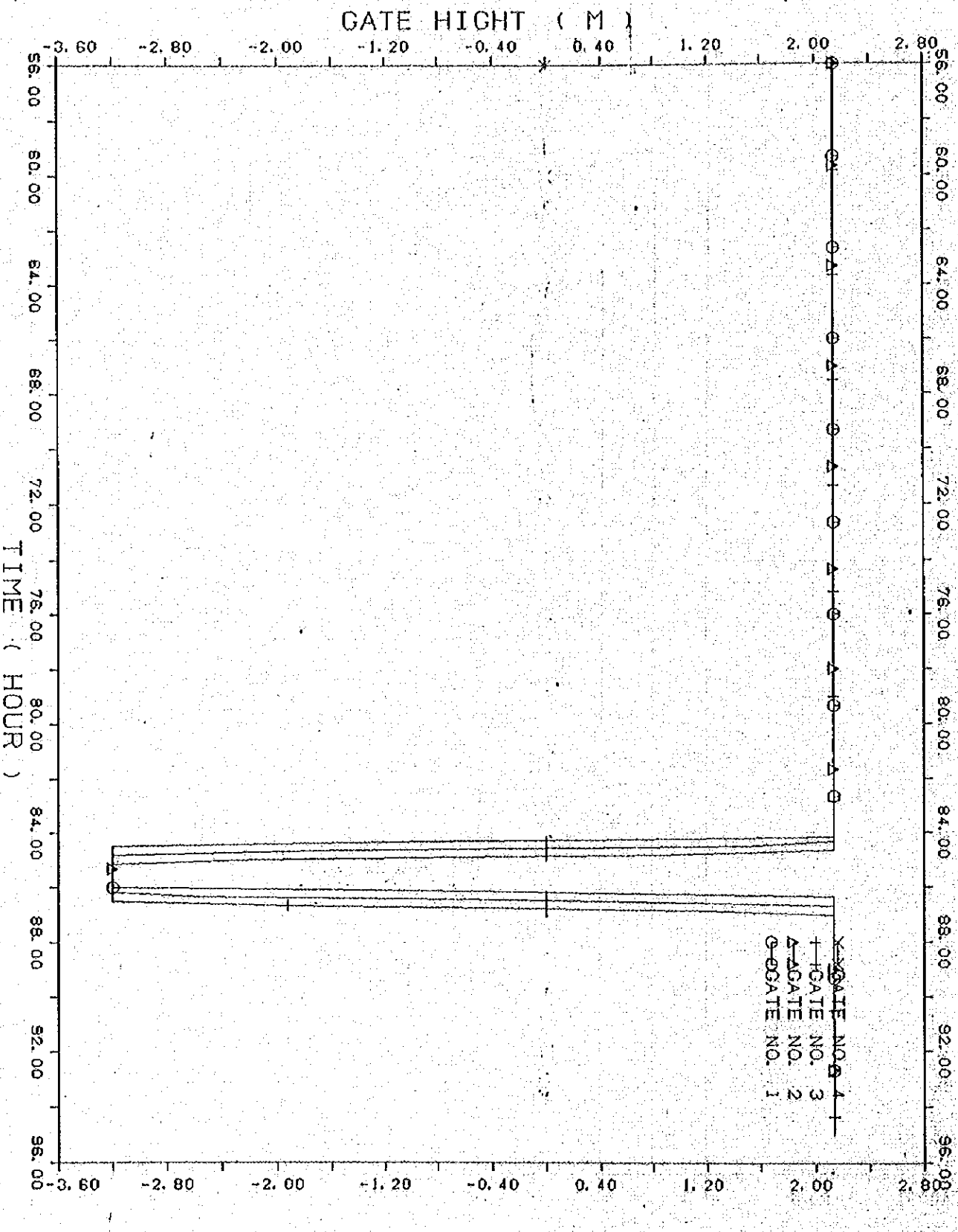

Fig. 1-4 Opening height of gates

DATA (XYP3.DAT)
DINI = 10.0 RN = 0.020 RNG = 0.030 17 OCT

PRAI * CASE B-3 * NOV. 05, '88 PRAID.DAT
DOWN STREAM BOUNDALY TIDE TABLE (14/3/84 - 17/3/84)
INUN. AREA 8KM (26-40) 0.M AT 0.8 M. 560.M AT 1.0 M

XYPLOT33 16/10/88

Fig.1-5 Peak of Fluctuation at down stream of the Barrage, Mesh 20

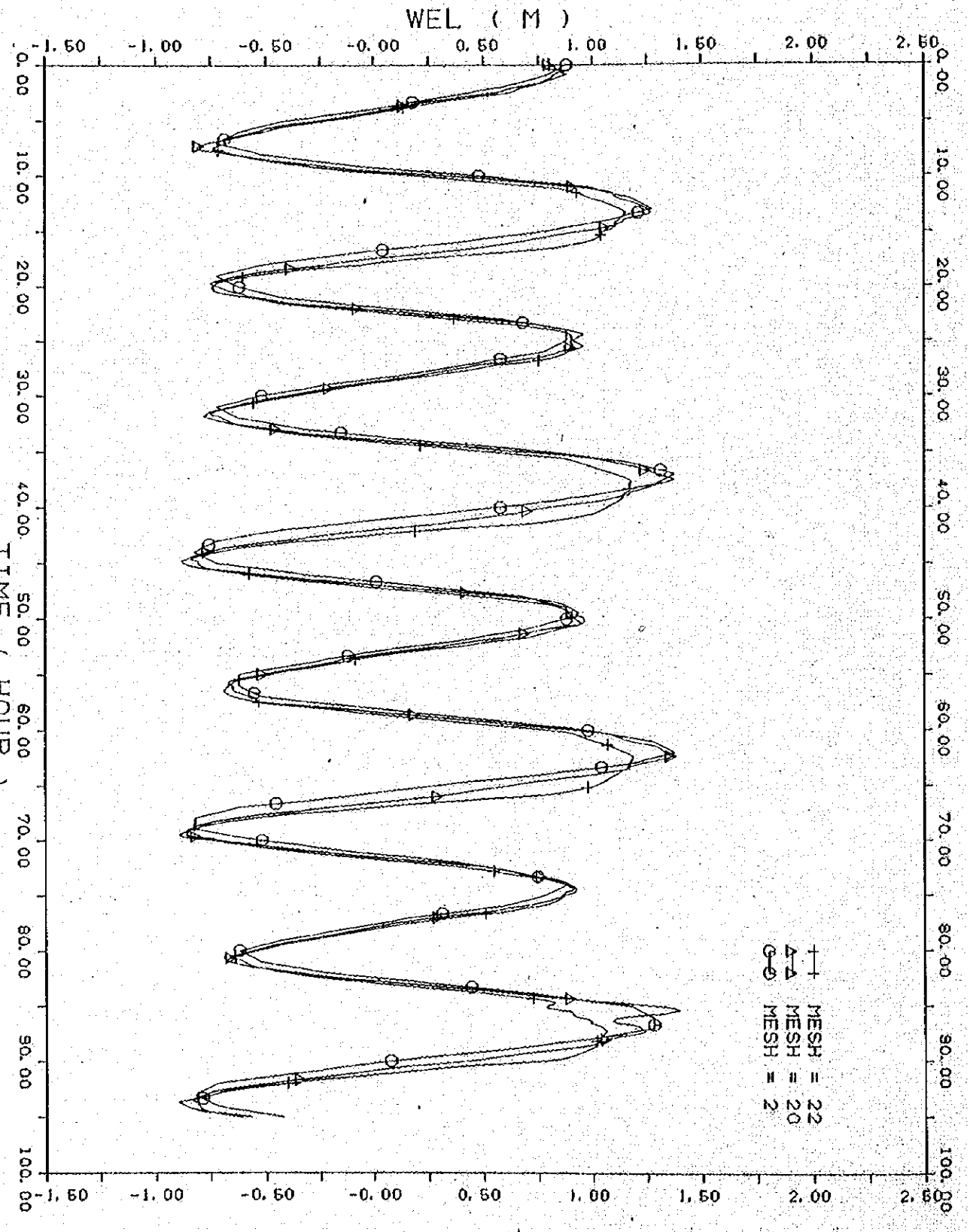

Fig. 1-6 Fluctuation of water level at downstream, Mesh 20 and upstream, Mesh 22 of the Barrage

DATA (XYP33.D10) WEL OF PRAI RIVER 17 OCT
QINI = 10.0 RN = 0.020 RNO = 0.030

PRAI * CASE B-3 * NOV. 05, '88 PRAID.D01
DOWN STREAM BOUNDALY TIDE TABLE (14/3/84 - 17/3/84)
INUN. AREA 8KM (26-40) 0.M AT 0.8 M. 550.M AT 1.0 M

XYPLOT33 15/10/88

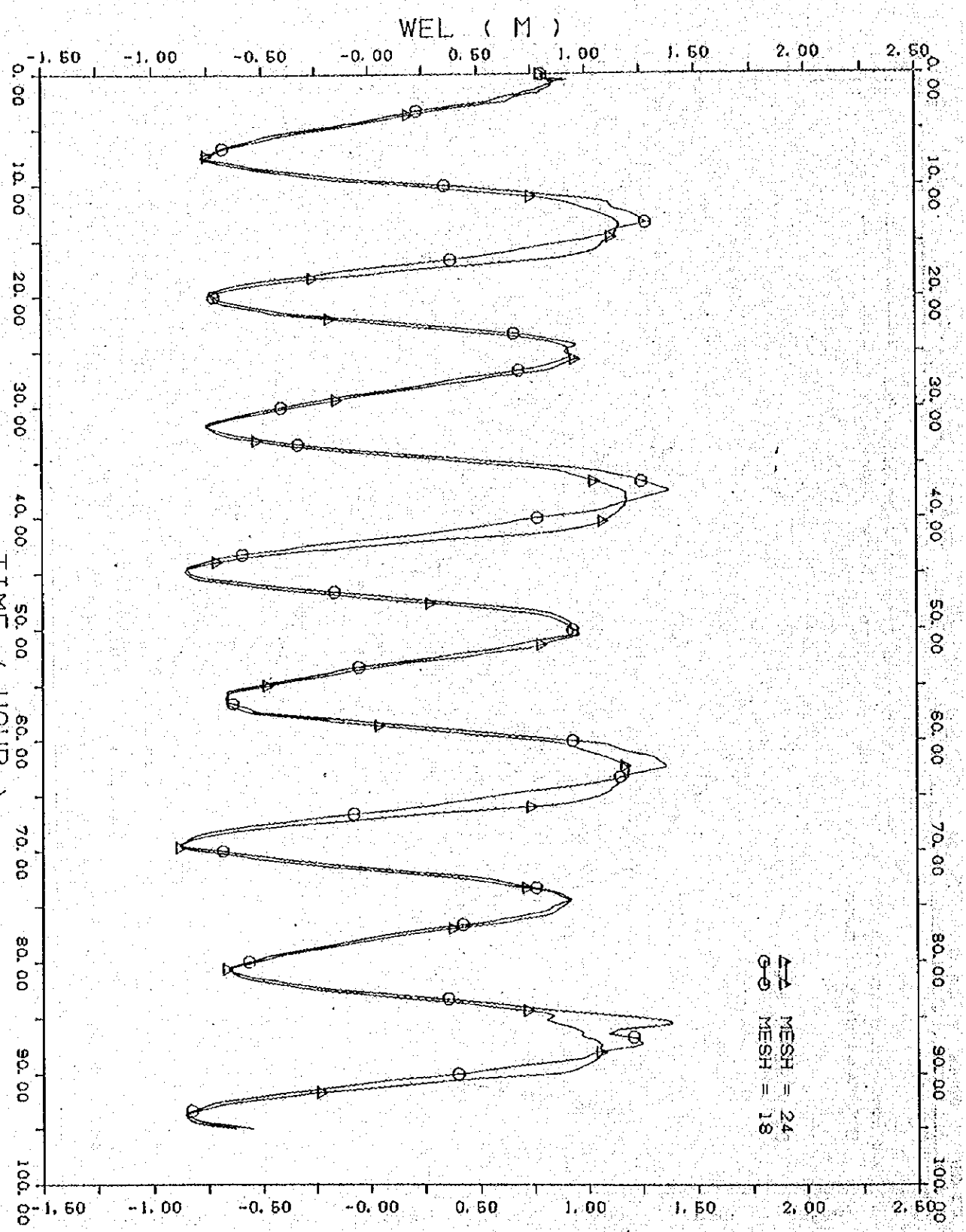

Fig.1-7 Fluctuation of water level at Mesh 18 and Mesh 24

DATA (XYP33.D01) 17 OCT
OINI = 10.0 RN = 0.020 RNG = 0.030

PRAI * CASE B-3 * NOV. 05,'88 PRAID.001
DOWN STREAM BOUNDALY TIDE TABLE (14/3/84 - 17/3/84)
INUN. AREA 8KM (26-40) 0.M AT 0.8 M. 660.M AT 1.0 M

XYPLOT33 15/10/88

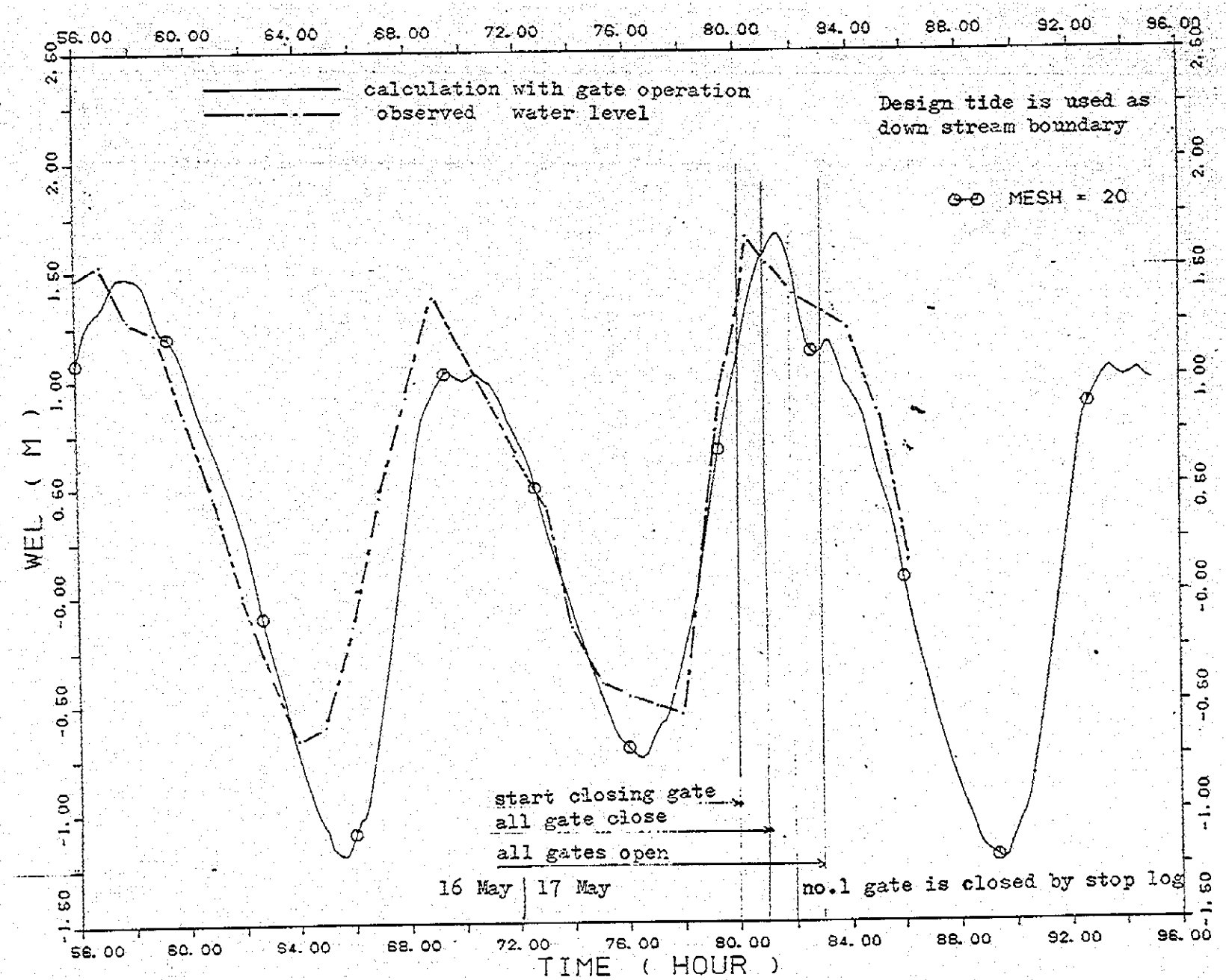

Fig.1-8 Fluctuation of water level at downstream of the Barrge, Mesh 20

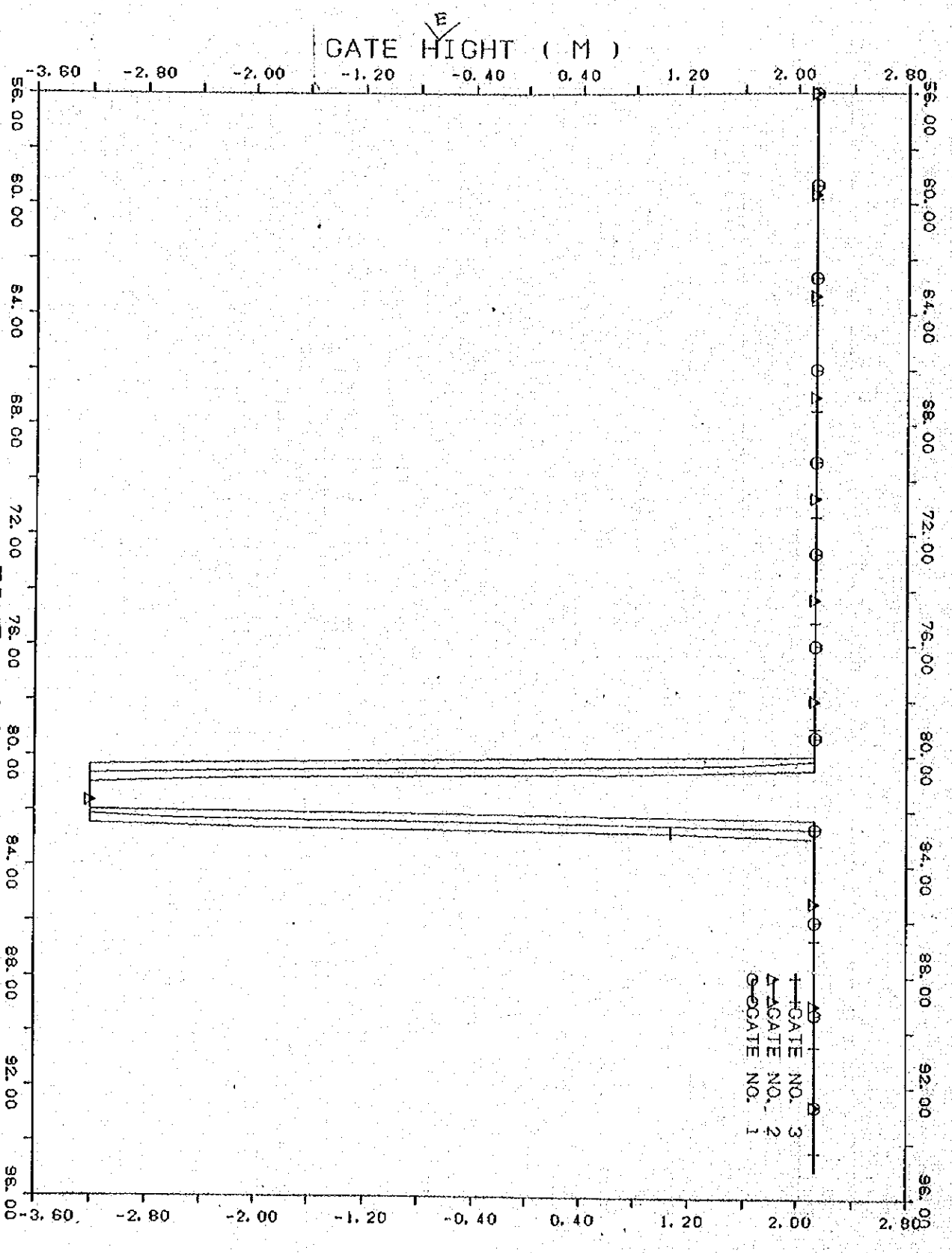

DATA (XYP3.D81)
QINI = 10.0 RN = 0.020 RNC = 0.030 17 OCT

PRA1 * CASE B-4 * NOV. 04,'88 PRA1D.D02
DOWN STREAM BOUNDALY TIDE TABLE (31/7/88)
INUN. AREA 8KM (26-40) 0.M AT 0.6 M. 550.M AT 1.0 M

XYPLOT33 15/10/88

Fig.1-9 Opening height of gates

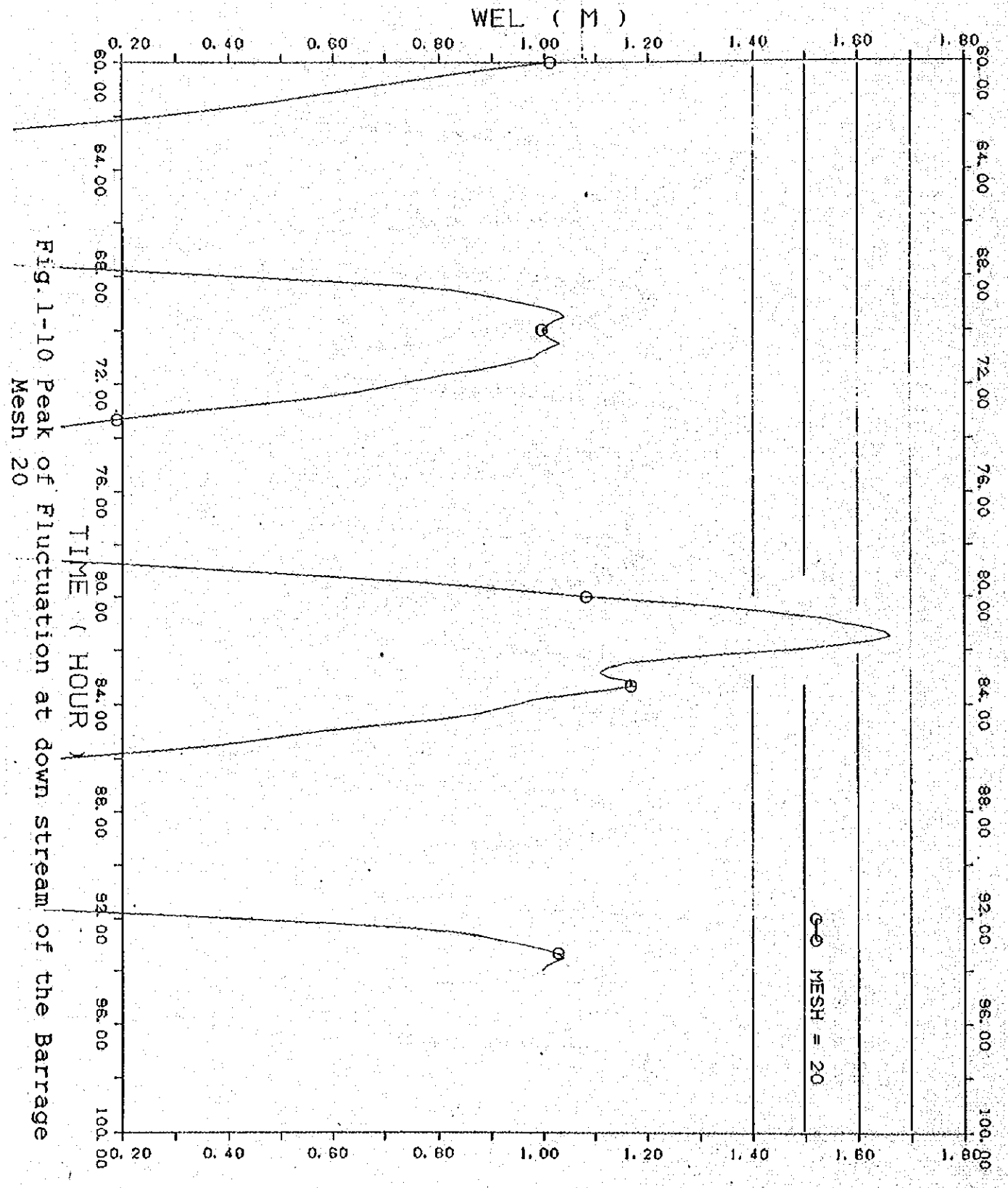

Fig. 1-10 Peak of Fluctuation at down stream of the Barrage Mesh 20

DATA (XYP33. D05) 5 NOV
QINI = 10. 0 RN = 0. 020 RND = 0. 030

PRAI * CASE B-4 * NOV. 04, '88 PRAID. D02
DOWN STREAM BOUNDALY TIDE TABLE (31/7/88)
INUN. AREA 8KM (26-40) 0. M AT 0. 8 M. 550. M AT 1. 0 M

XYPLOT33 15/10/88

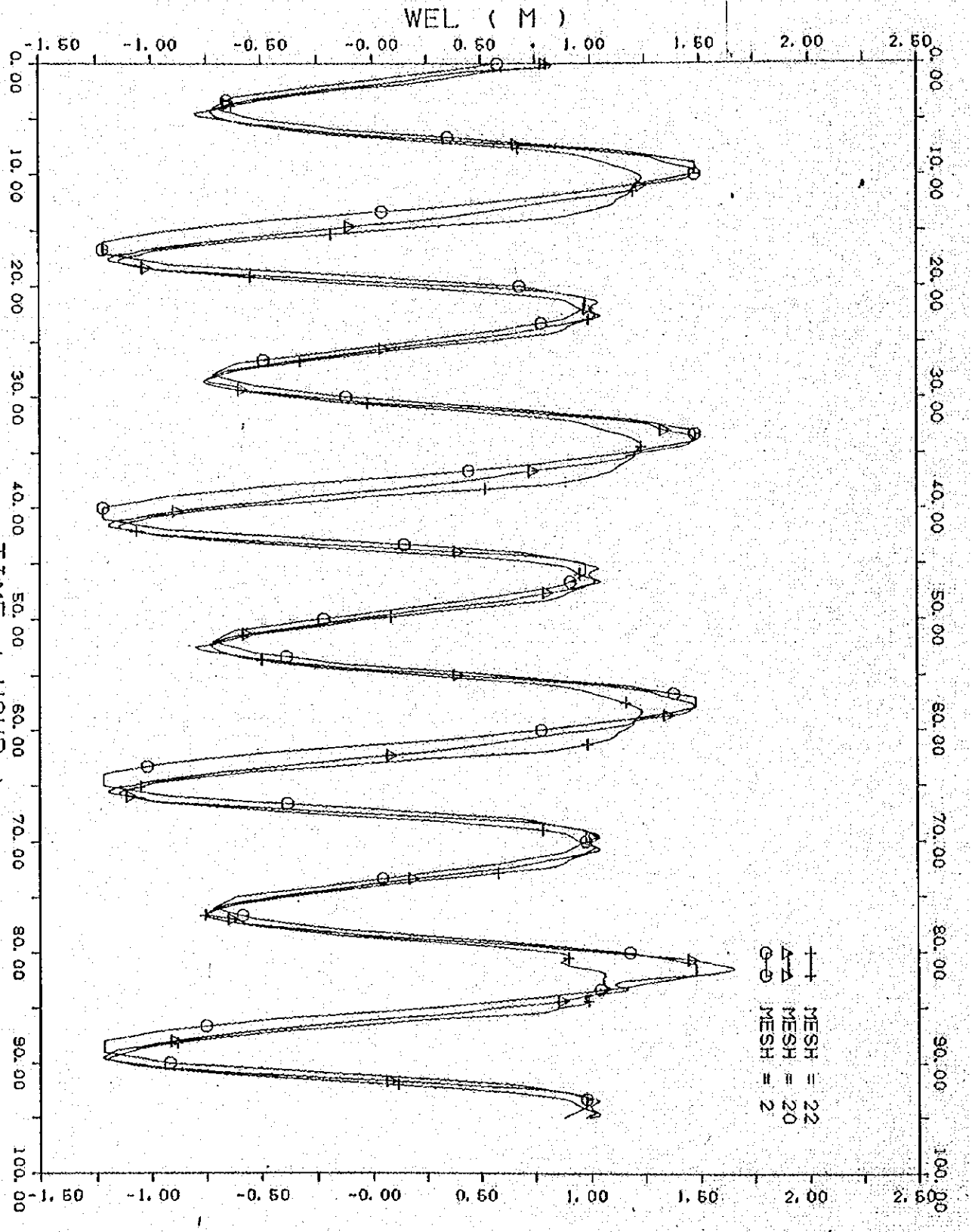

Fig.1-11 Fluctuation of water level at downstream, Mesh 20 and upstream, Mesh 22 of the Barrage

Fig.1-12 Fluctuation of water level at Mesh 18 and Mesh 24

Fig.1-13 Fluctuation of water level at downstream of the Barrge, Mesh 20

Fig.1-14 Opening height of gates

Fig.1-15 Peak of Fluctuation at down stream of the Barrage
Mesh 20

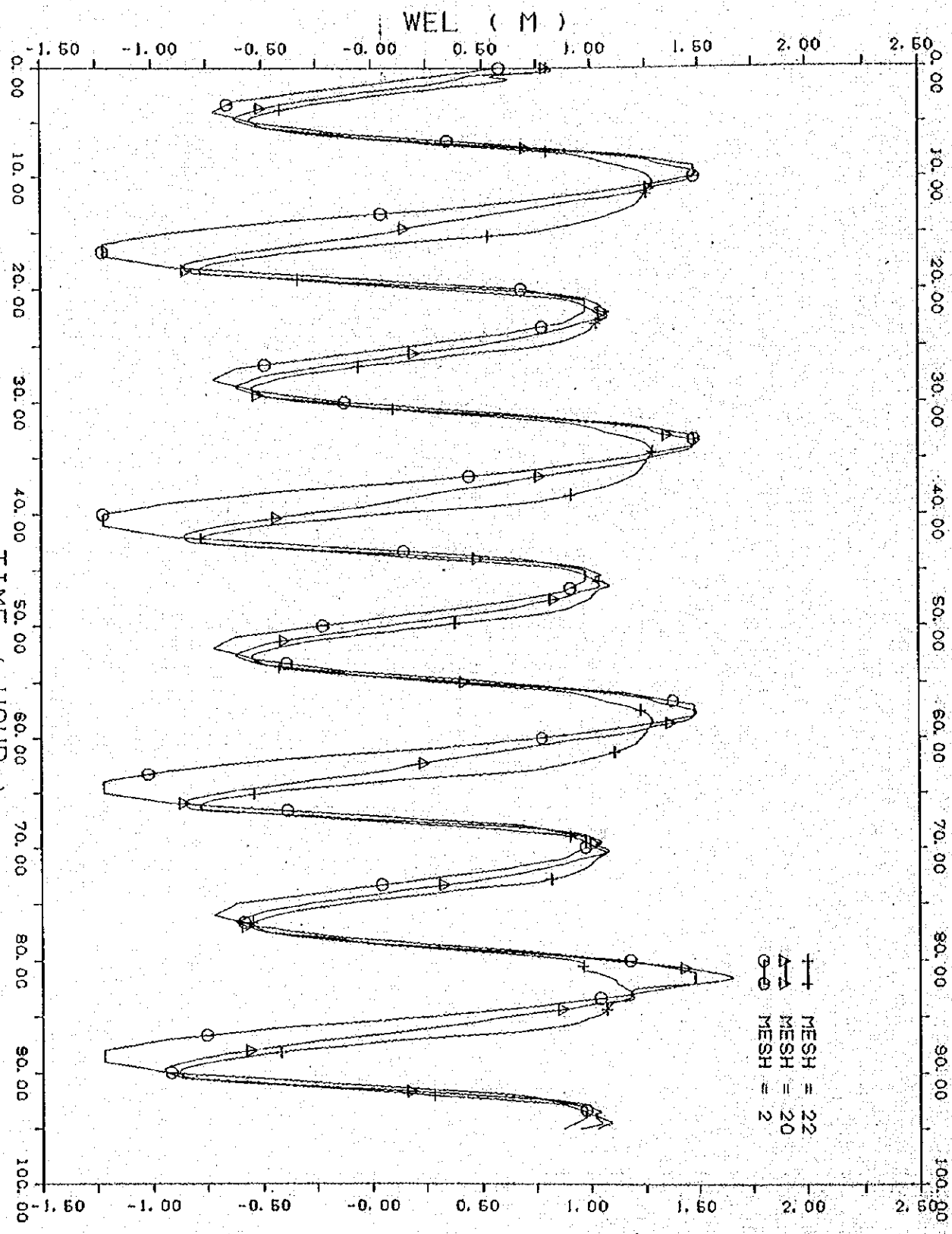

Fig. 1-16 Fluctuation of water level at downstream, Mesh 20 and upstream, Mesh 22 of the Barrage

DATA (XYP33.D10) WEL OF PRAI RIVER 17 OCT
QINI = 100.0 RN = 0.020 RNO = 0.030

PRAI * CASE B-5 * NOV. 04,'88 PRAID.D02
DOWN STREAM BOUNDALY TIDE TABLE (31/7/88)
INUN. AREA 8KM (26-40) 0.M AT 0.8 M. 550.M AT 1.0 M

XYPLOT33 16/10/88

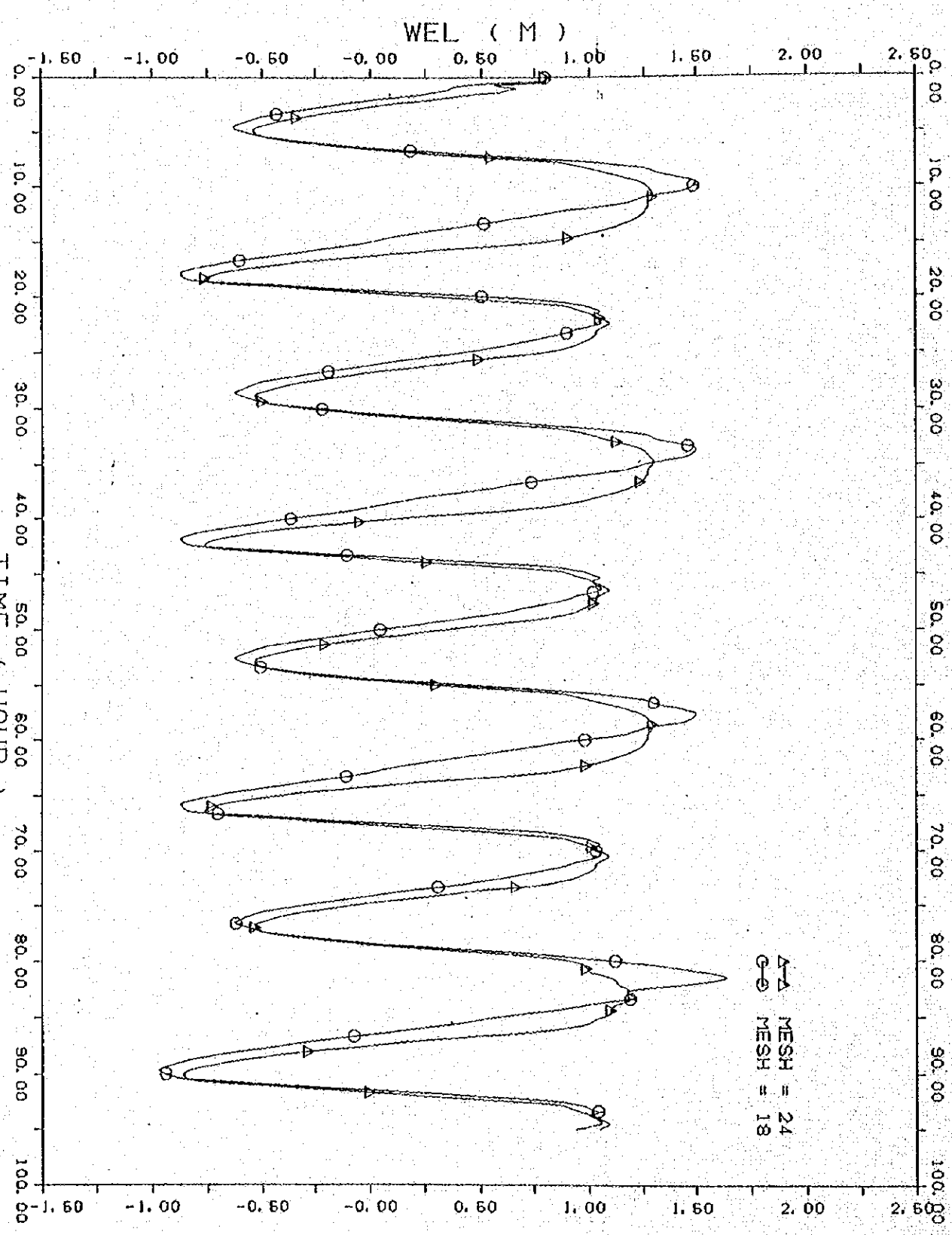

DATA (XYP33.D01)
QINI = 100.0 RN = 0.020 RNG = 0.030

17 OCT

PRAI * CASE B-5 * NOV. 04,'88 PRAID.D02
DOWN STREAM BOUNDALY TIDE TABLE (31/7/88)
INUN. AREA 8KM (26-40) 0.M AT 0.8 M. 550.M AT 1.0 M

XYPLOT33 16/10/88

Fig.1-17 Fluctuation of water level at Mesh 18 and Mesh 24

CASE-2

Fig.2-1 Fluctuation of water level at downstream, Mesh 20 and upstream, Mesh 22 of the Barrage

Fig.2-2 Fluctuation of water level at Mesh 18 and upstream, Mesh 24

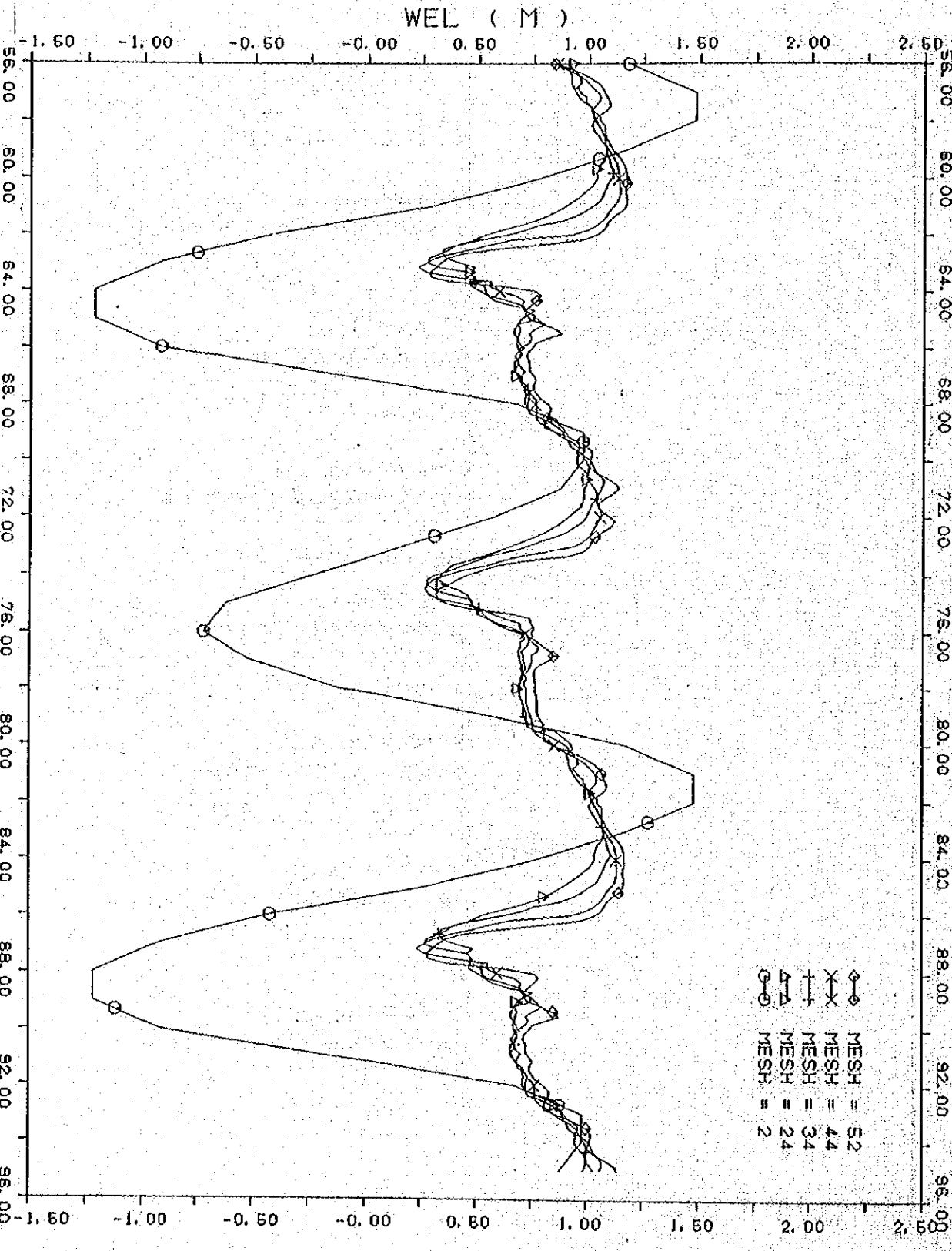

DATA (XYP33.DII) WEL OF PRAI RIVER 17 OCT
QINI = 100.0 RN = 0.020 RNO = 0.030

PRAI ** CASE H-1 ** NOV. 07,'88 PRAI3D.D03
DOWN STREAM BOUNDALY DESIGN TIDE (BASED ON 31 JULY '88)
INUN. AREA 8KM (26-40) 0.M AT 0.8 M. 550.M AT 1.0 M

XYPLOT33 15/10/88

Fig.2-3 Fluctuation of water level at Mesh 24, Mesh 34, Mesh 44 and Mesh 52

Fig.2-4 Discharge passed through gates

Fig.2-5 Opening height of gates

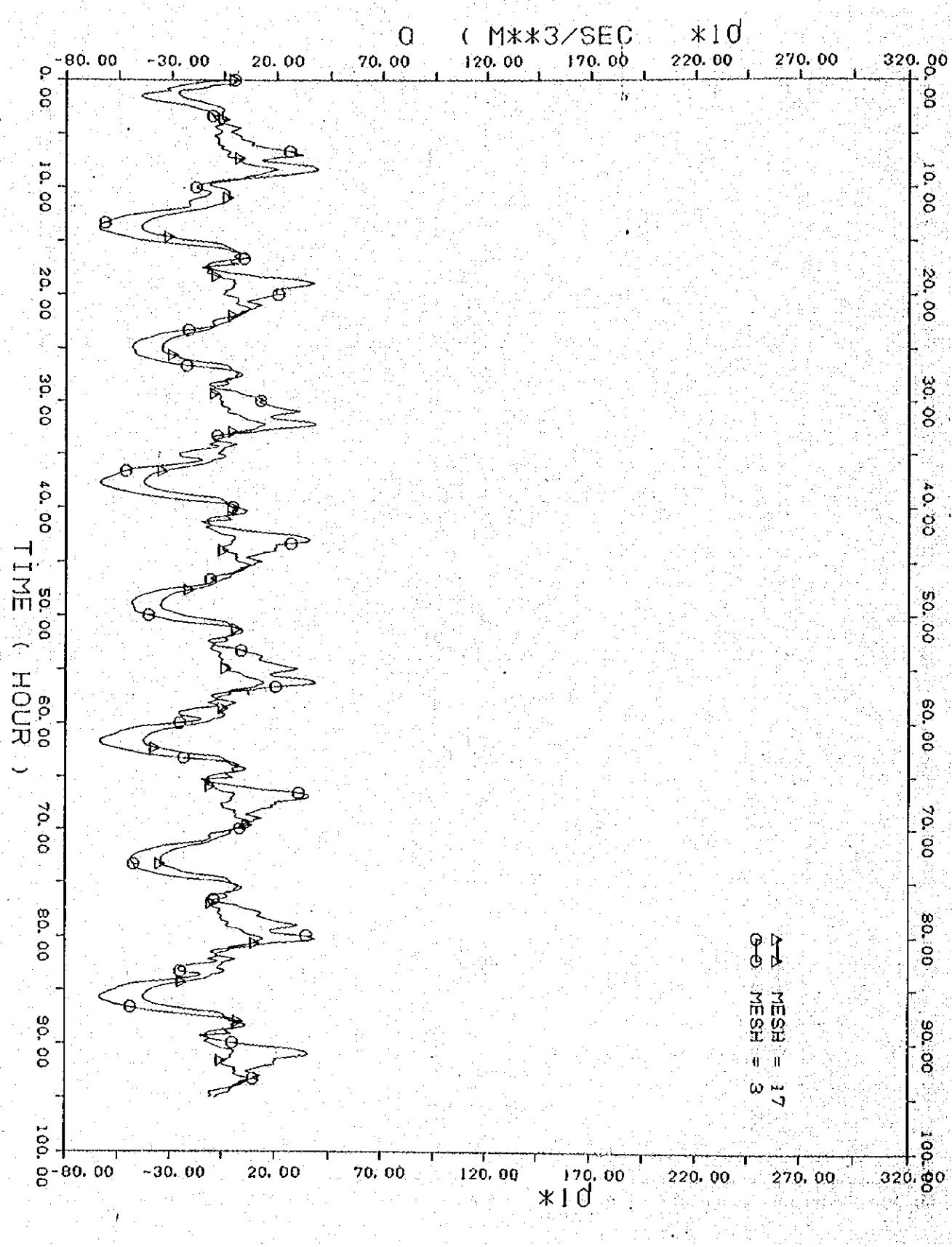

DATA (XYP33.D64) DISCHARGE 31 NOV
QINI = 100.0 RN = 0.020 RNO = 0.030

PRA1 ** CASE H-1 ** NOV. 07,'88 PRA13D.D03
DOWN STREAM BOUNDALY DESIGN TIDE (BASED ON 31 JULY '88)
INUN. AREA 8KM (26-40) 0.M AT 0.8 M. 650.M AT 1.0 M

'XYPLOT33 15/10/88

Fig.2-6 Discharge at Mesh 3 and Mesh 17

Fig.2-7 Discharge at Mesh 23 and Mesh 43

CASE-3

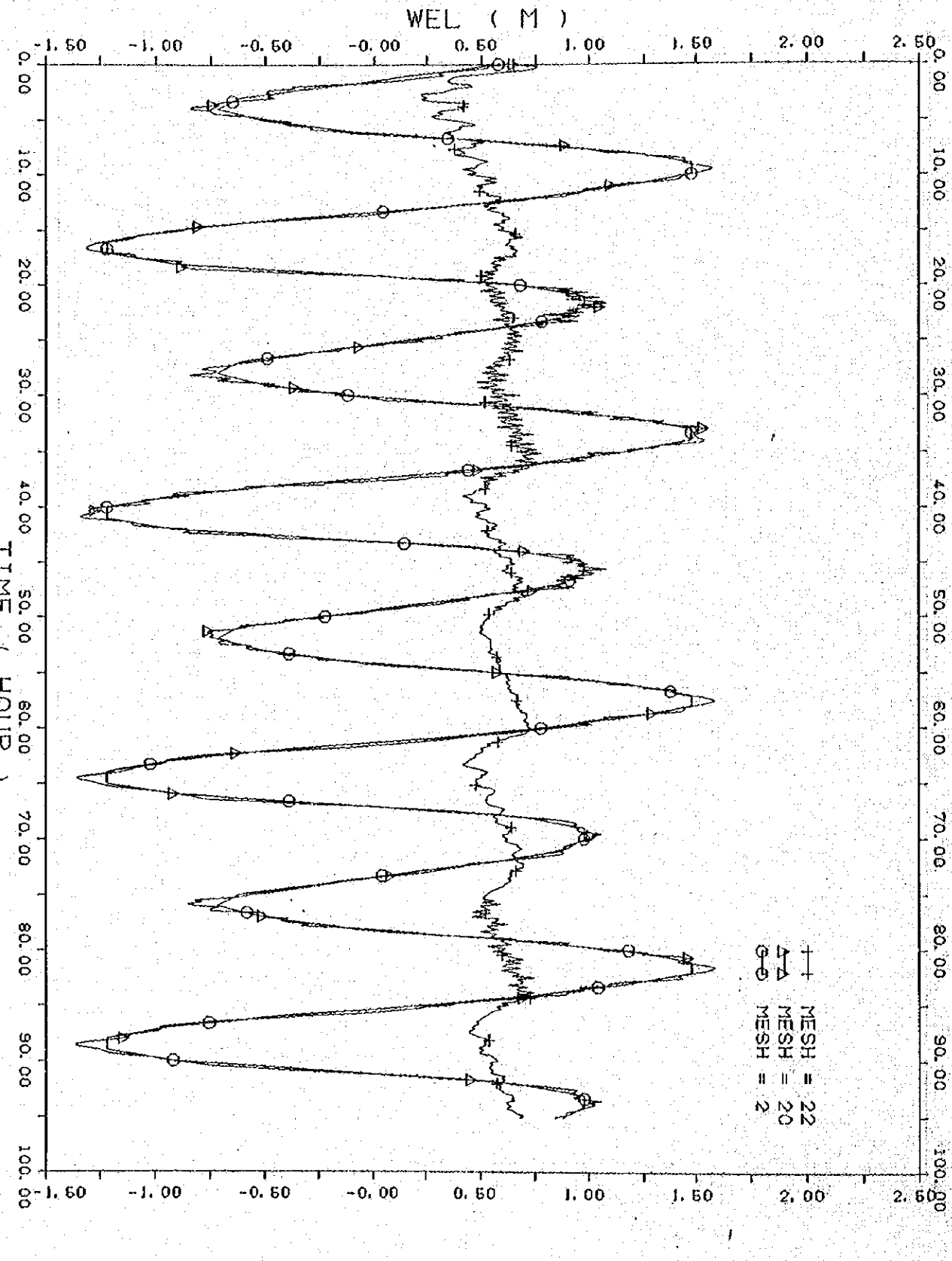

Fig. 3-1 Fluctuation of water level at downstream, Mesh 20 and upstream, Mesh 22 of the Barrage

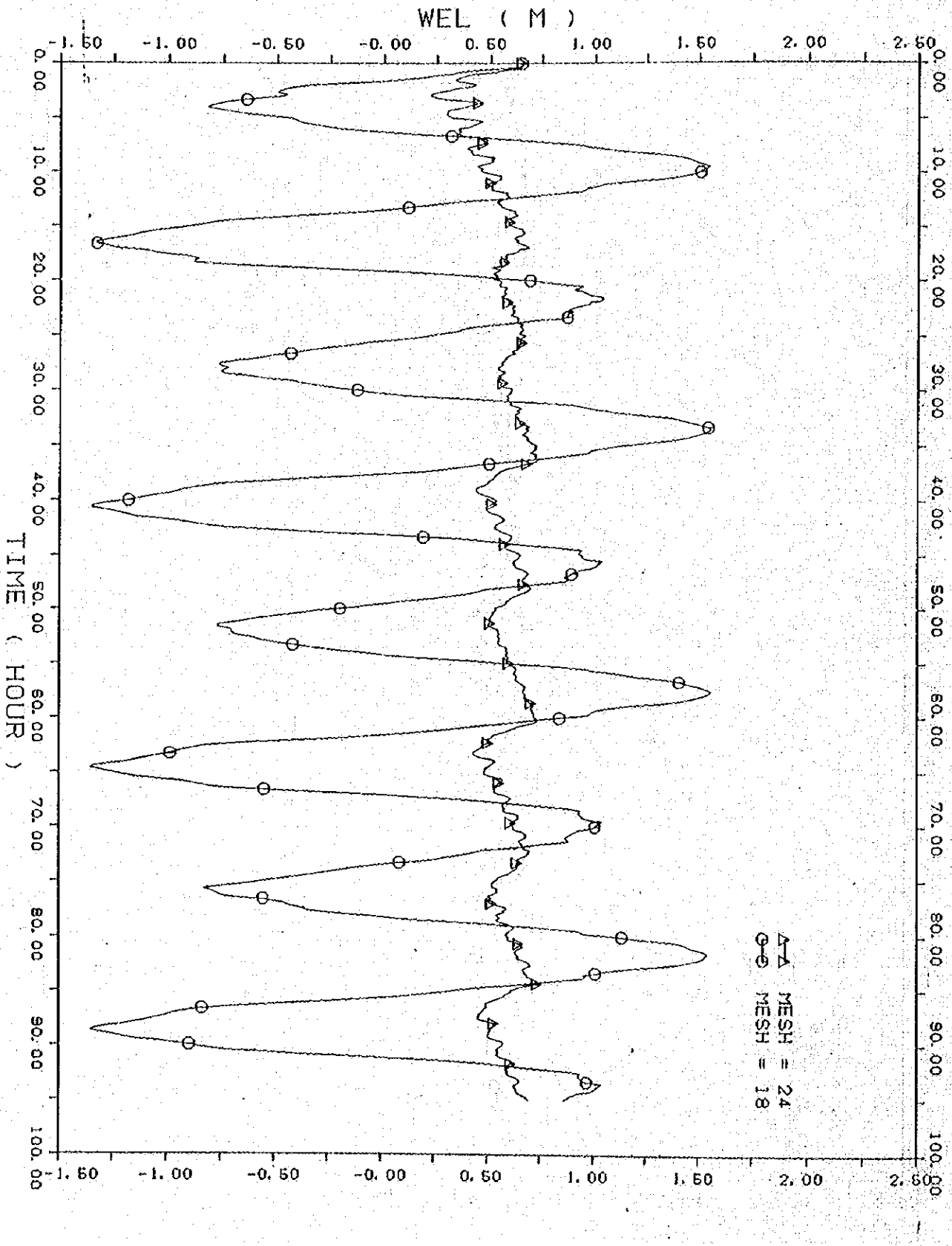

DATA (XYP33.D01)
QINI = 10.0 RN = 0.020 RNG = 0.030

17 OCT

PRAI ** CASE F-1 ** NOV. 03,'88 PRAI3D.D01
DOWN STREAM BOUNDALY DESIGN TIDE (BASED ON 31 JULY '88)
INUN. AREA 8KM (26-40) 0.M AT 0.8 M. 550.M AT 1.0 M

XYPLOT33 15/10/88

Fig.3-2 Fluctuation of water level at Mesh 18 and Mesh 24

Fig.3-3 Fluctuation of water level at Mesh 24, Mesh 34, Mesh 44 and Mesh 52

Fig.3-4 Discharge passed through gates

Fig.3-5 Opening height of gates

Fig.3-6 Fluctuation of water level at downstream, Mesh 20 and upstream, Mesh 22 of the Barrage

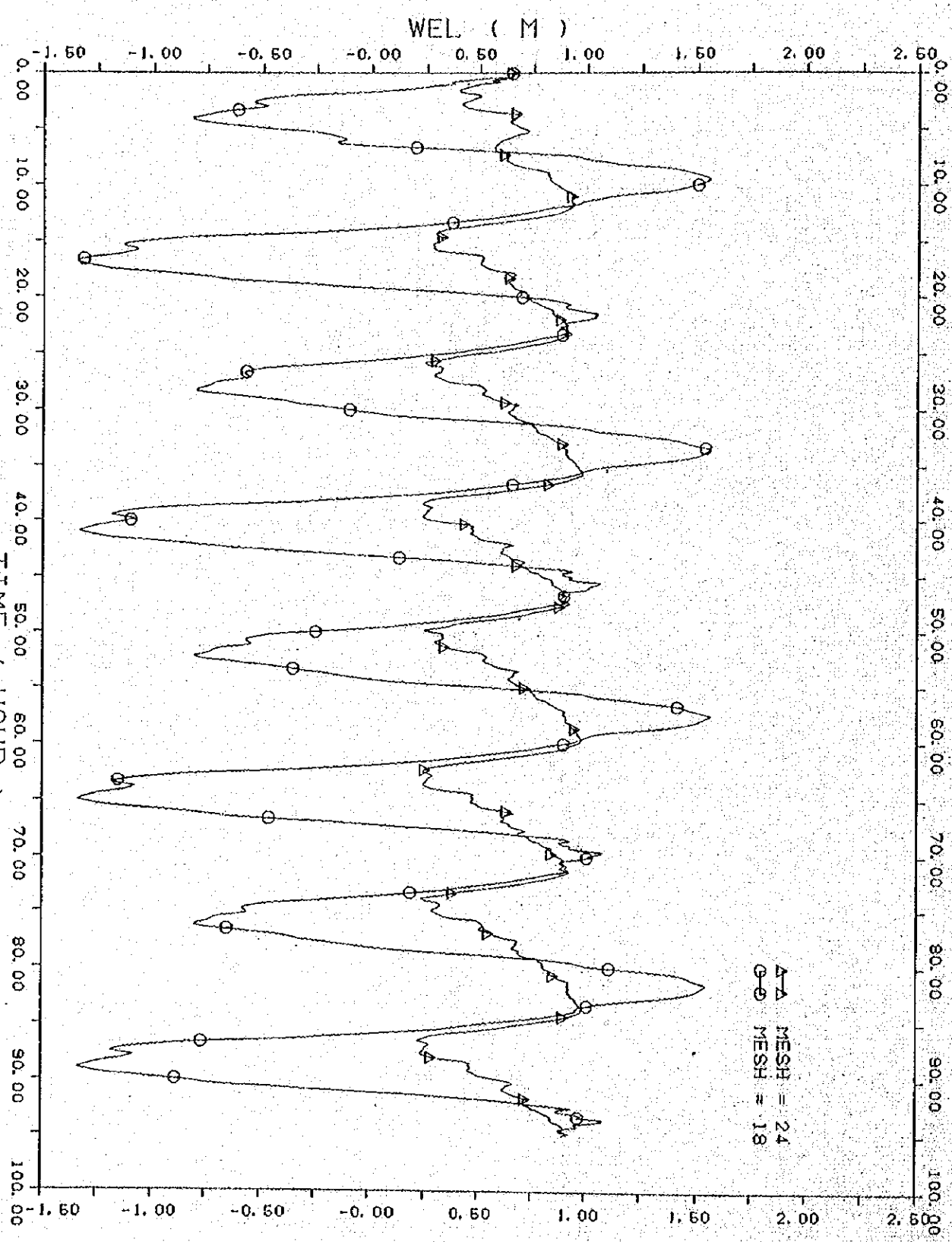

DATA (XYP33.D01)
QINI = 50.0 RN = 0.020 RNG = 0.030 17 OCT

PRAI ** CASE F-2 ** NOV. 03,'88 PRAI3D.D03
DOWN STREAM BOUNDALY DESIGN TIDE (BASED ON 31 JULY '88)
INUN. AREA 8KM (26-40) 0.M AT 0.8 M. 550.M AT 1.0 M

XYPLOT33 15/10/88

Fig.3-7 Fluctuation of water level at Mesh 18 and Mesh 24

Fig.3-8 Fluctuation of water level at Mesh 24, Mesh 34, Mesh 44 and Mesh 52

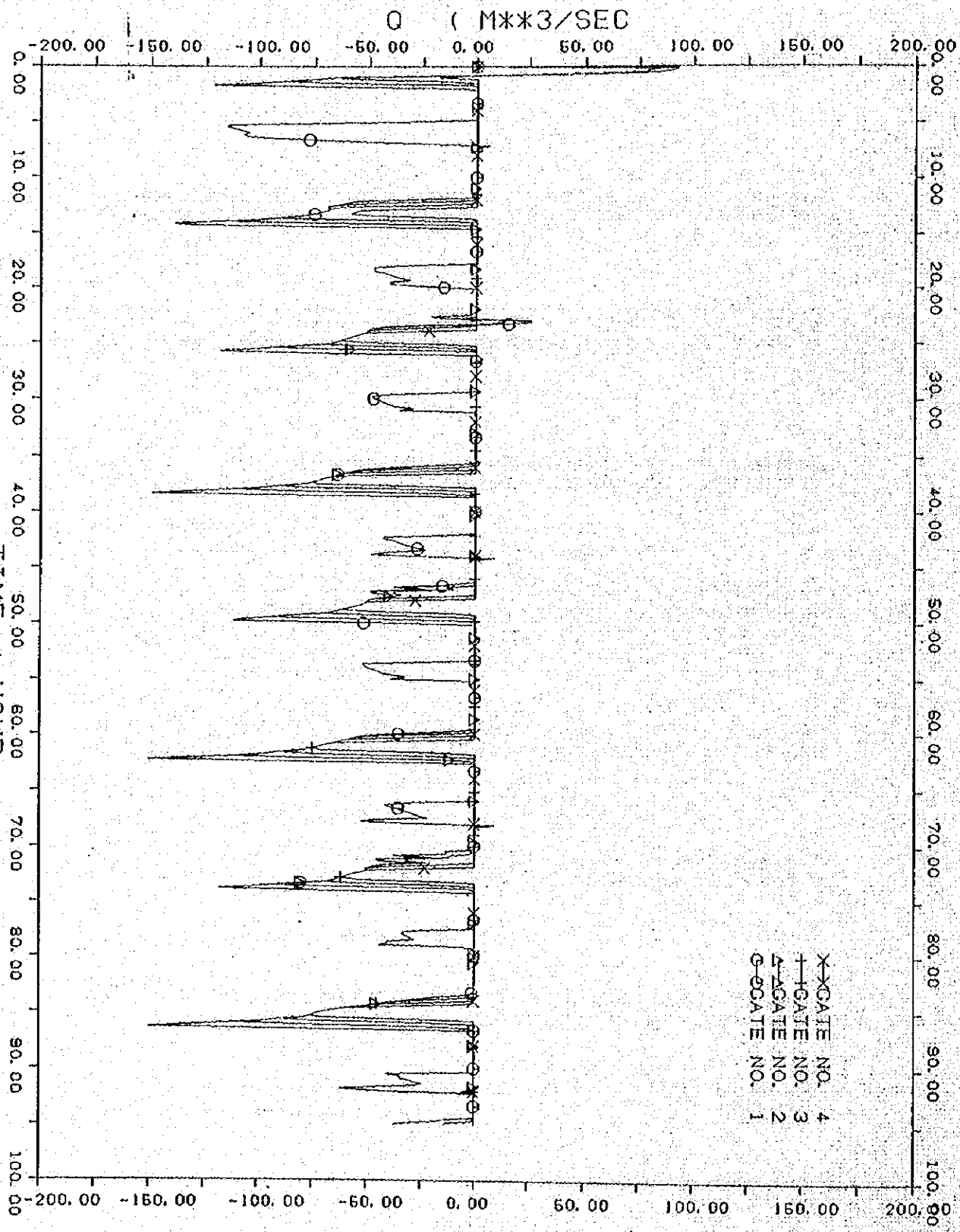

Fig. 3-9 Discharge passed through gates

DATA (XYP3.D61) DISCHARGE OF GATE 17 OCT
QINI = 50.0 RN = 0.020 RNG = 0.030

PRAI ** CASE F-2 ** NOV. 03,'88 PRAI3D.D03
DOWN STREAM BOUNDALY DESIGN TIDE (BASED ON 31 JULY '88)
INUN. AREA 8KM (26-40) 0.M AT 0.8 M. 550.M AT 1.0 M

XYPLOT33 15/10/88

Fig.3-10 Opening height of gates

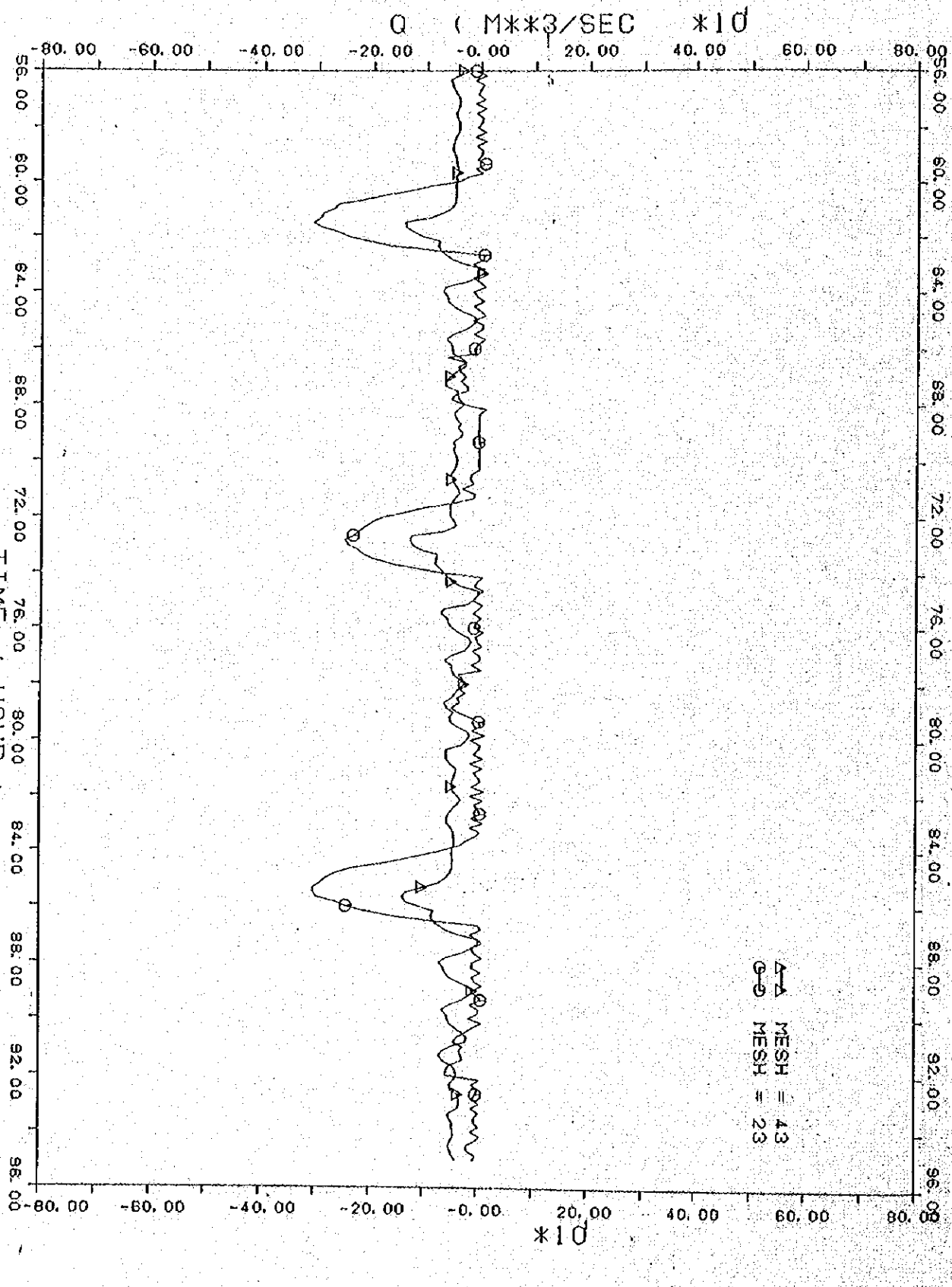

Fig.3-11 Discharge at Mesh 23 and Mesh 43

Fig.3-12 Fluctuation of water level at downstream, Mesh 20 and upstream, Mesh 22 of the Barrage

Fig.3-13 Discharge passed through gates

Fig.3-14 Opening height of gates

Fig.3-15 Discharge at Mesh 23 and Mesh 43

CASE-4

Fig. 4-1 Fluctuation of water level at downstream, Mesh 20 and upstream, Mesh 22 of the Barrage

Fig.4-2 Fluctuation of water level at Mesh 18 and Mesh 24

Fig. 4-3 Fluctuation of water level at Mesh 24, Mesh 34, Mesh 44 and Mesh 52

Fig.4-4 Discharge passed through gates

Fig. 4-5 Opening height of gates

Fig. 4-6 Discharge at Mesh 3, Mesh 17 and Mesh 53

Fig. 4-7 Discharge at Mesh 23 and Mesh 43

CASE-5

Fig.5-1 Fluctuation of water level at downstream, Mesh 20 and upstream, Mesh 22 of the Barrage

Fig.5-2 Fluctuation of water level at Mesh 18 and Mesh 24

Fig.5-3 Fluctuation of water level at Mesh 24, Mesh 34, Mesh 44 and Mesh 52

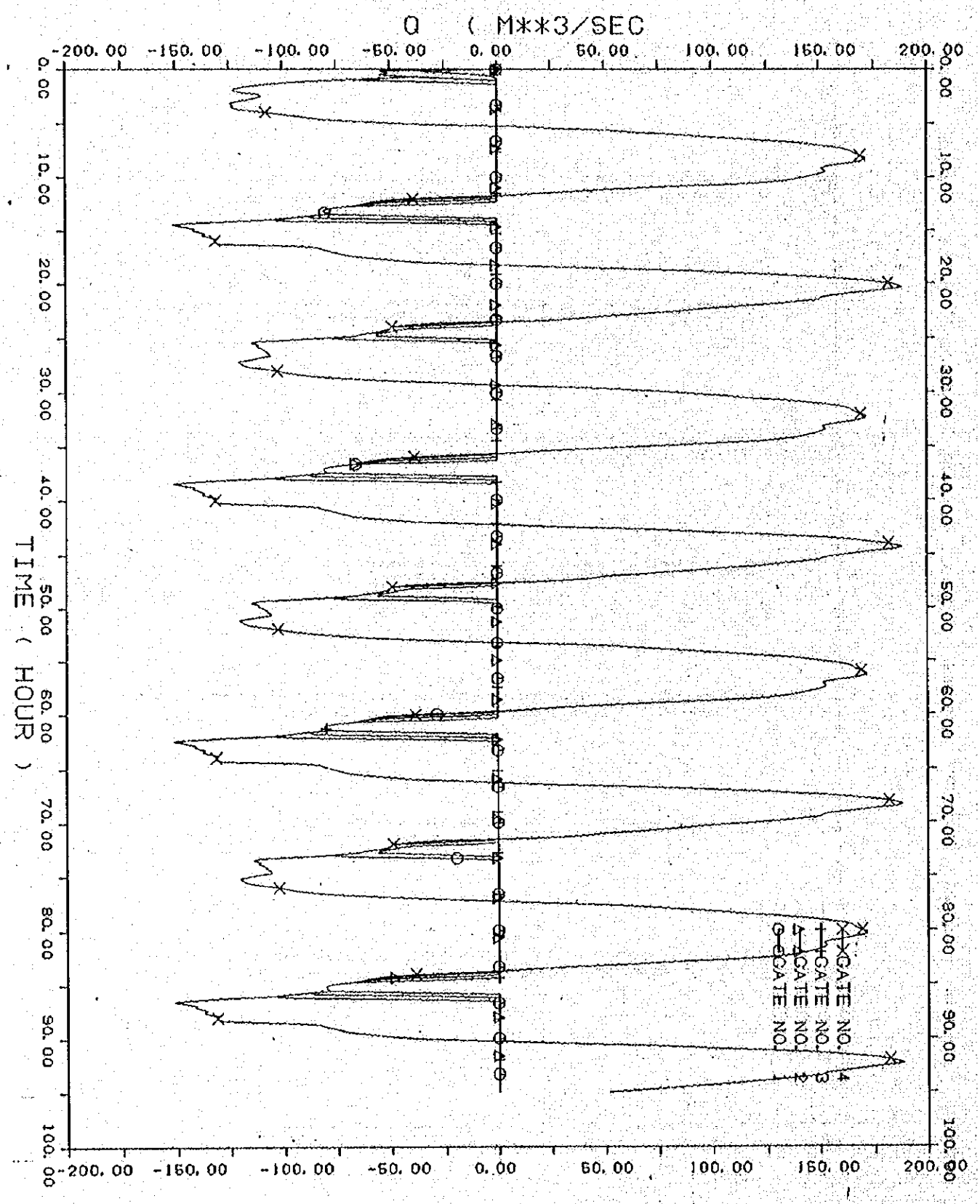

Fig.5-4 Discharge passed through gates

DATA (XYP3.D61) DISCHARGE OF GATE 17 OCT
QINI = 10.0 RN = 0.020 RNG = 0.030

PRA1 ** CASE G-1 ** NOV. 07,'88 PRA13D.D03
DOWN STREAM BOUNDALY DESIGN TIDE (BASED ON 31 JULY '88)
INUN. AREA 8KM (26-40) 0.M AT 0.8 M. 550.M AT 1.0 M

XYPLOT33 15/10/88

Fig.5-5 Opening height of gates

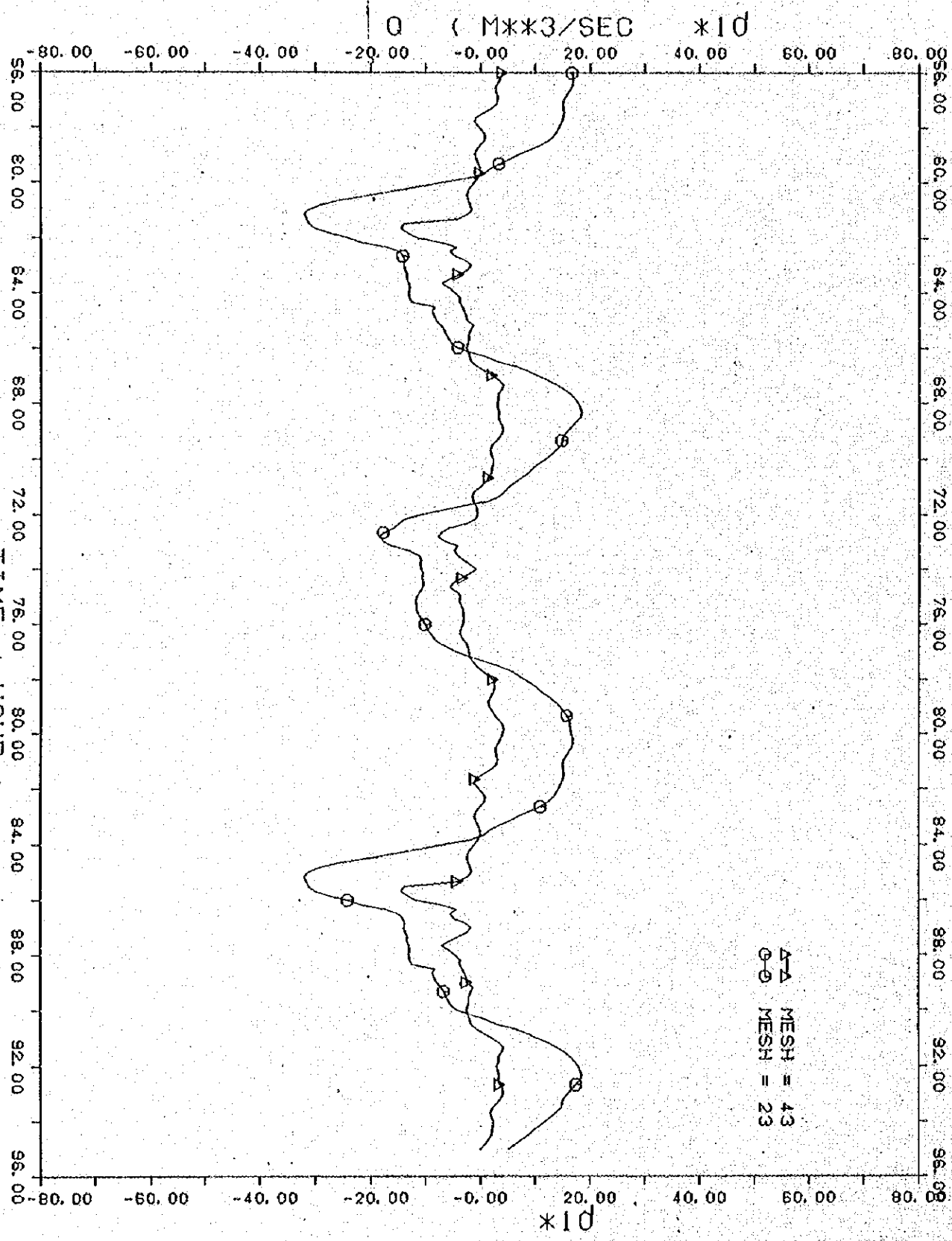

Fig.5-6 Discharge at Mesh 23 and Mesh 43

DATA (XYP33.D63) DISCHARGE 28 OCT
OINI = 10.0 RN = 0.020 RNO = 0.030

PRAI ** CASE C-1 ** NOV. 07,'88 PRA13D.D03
DOWN STREAM BOUNDALY DESIGN TIDE (BASED ON 31 JULY '88)
INUN. AREA 8KM (26-40) 0.M AT 0.8 M. 550.M AT 1.0 M

XYPLOT33 15/10/88

FLOOD ROUTING

Fig.6-1 Fluctuation of water level at downstream, Mesh 20 and upstream, Mesh 22 of the Barrage

Fig.6-2 Fluctuation of water level at Mesh 18 and Mesh 24

Fig.6-3 Fluctuation of water level at Mesh 24, Mesh 34, Mesh 44 and Mesh 52

Fig.6-4 Discharge passed through gates

Fig.6-5 Opening height of gates

Fig.6-6 Discharge at Mesh 3, Mesh 17 and Mesh 53

Fig.6-7 Discharge at Mesh 23 and Mesh 43

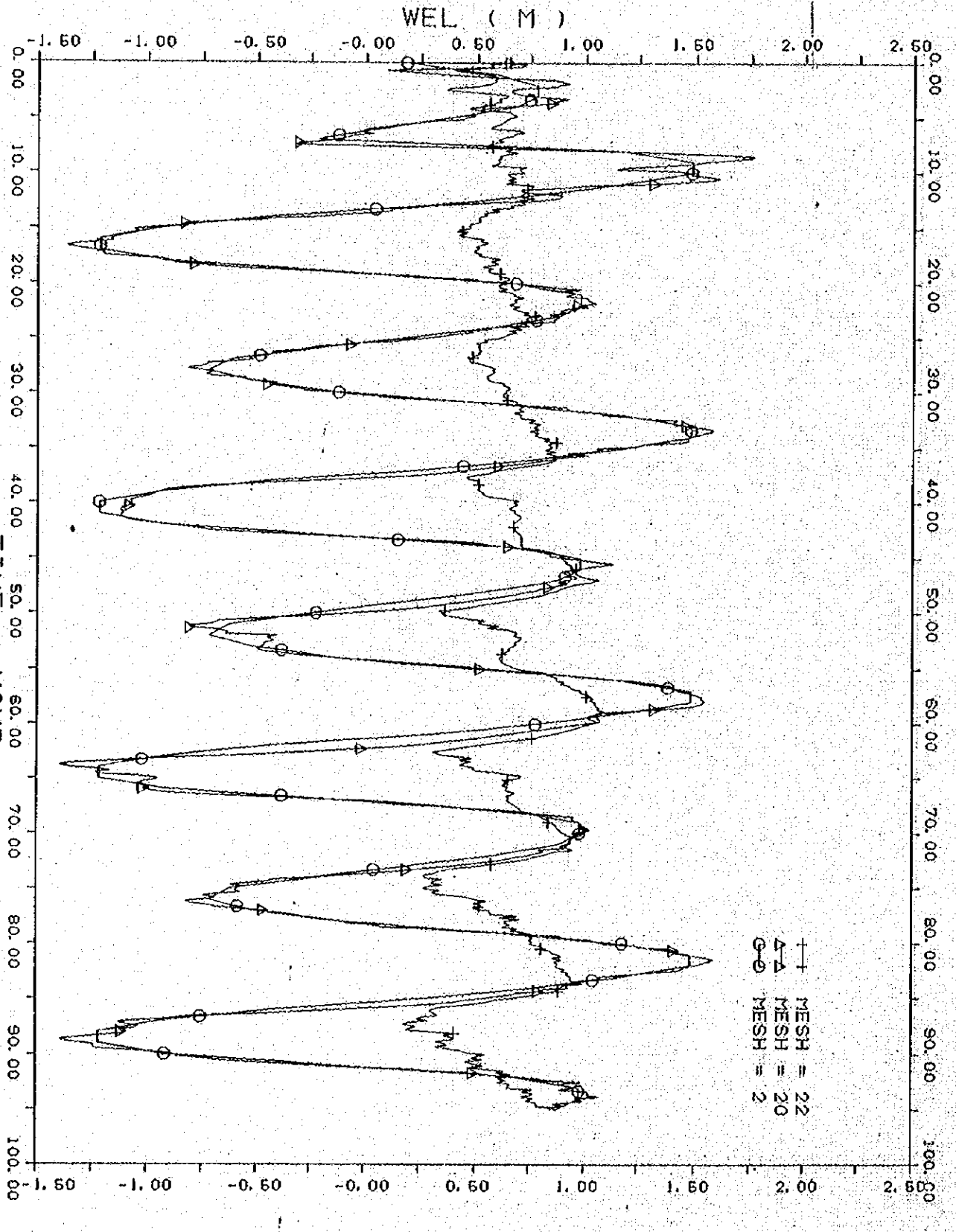

Fig. 6-8 Fluctuation of water level at downstream, Mesh 20 and upstream, Mesh 22 of the Barrage

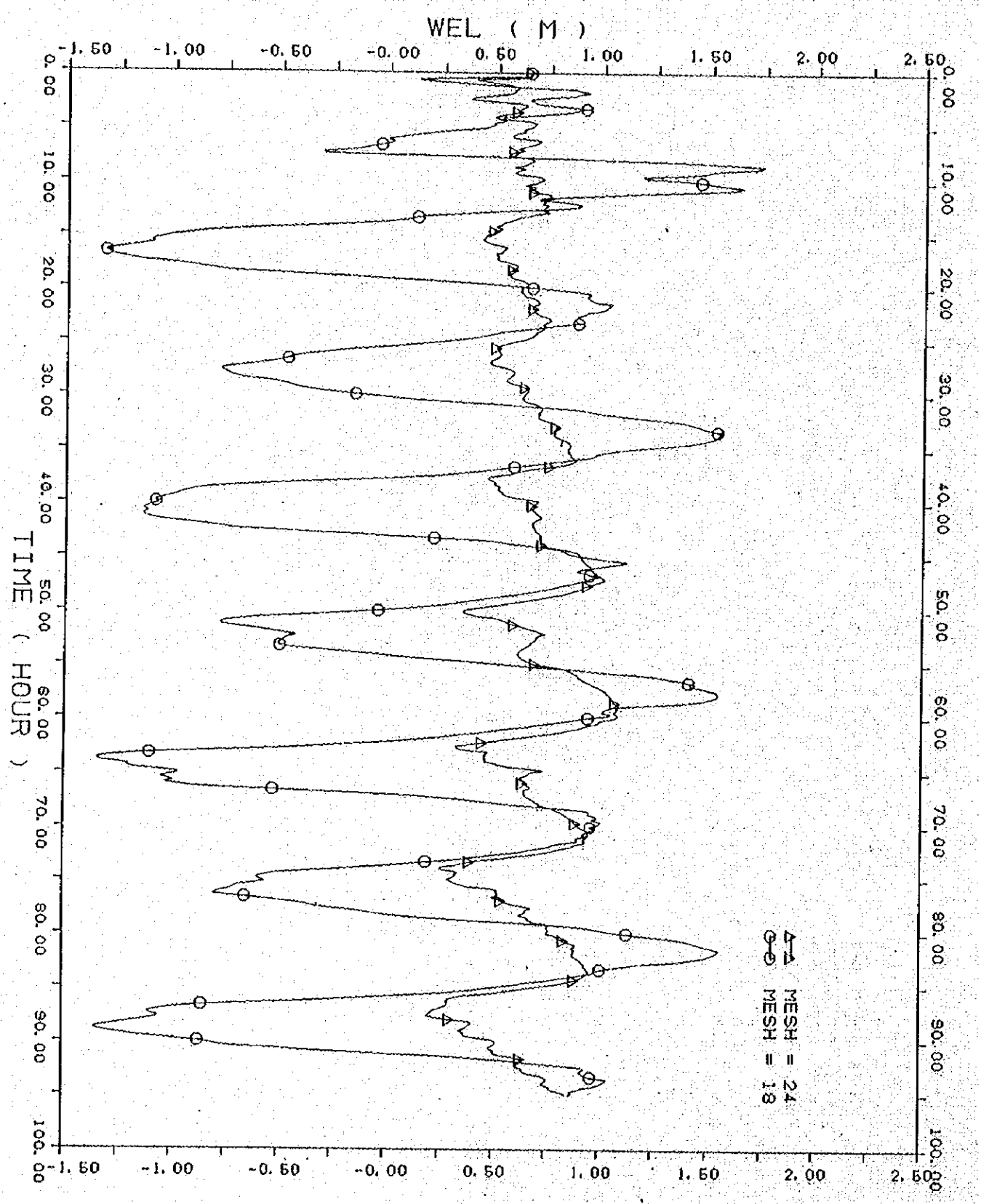

DATA (XYP33.D01)
QINI = 13.5 RN = 0.020 RNO = 0.030 17 OCT

PRAI ** CASE J-2 ** NOV. 12,'88 PRA13D.D31
DOWN STREAM BOUNDALY DESION TIDE (BASED ON 31 JULY '88)
INUN. AREA 8KM (26-40) 0.M AT 0.8 M. 650.M AT 1.0 M

'XYPLOT33 15/10/88

Fig.6-9 Fluctuation of water level at Mesh 18 and Mesh 24

Fig.6-10 Fluctuation of water level at Mesh 24, Mesh 34, Mesh 44 and Mesh 52

Fig.6-11 Discharge passed through gates

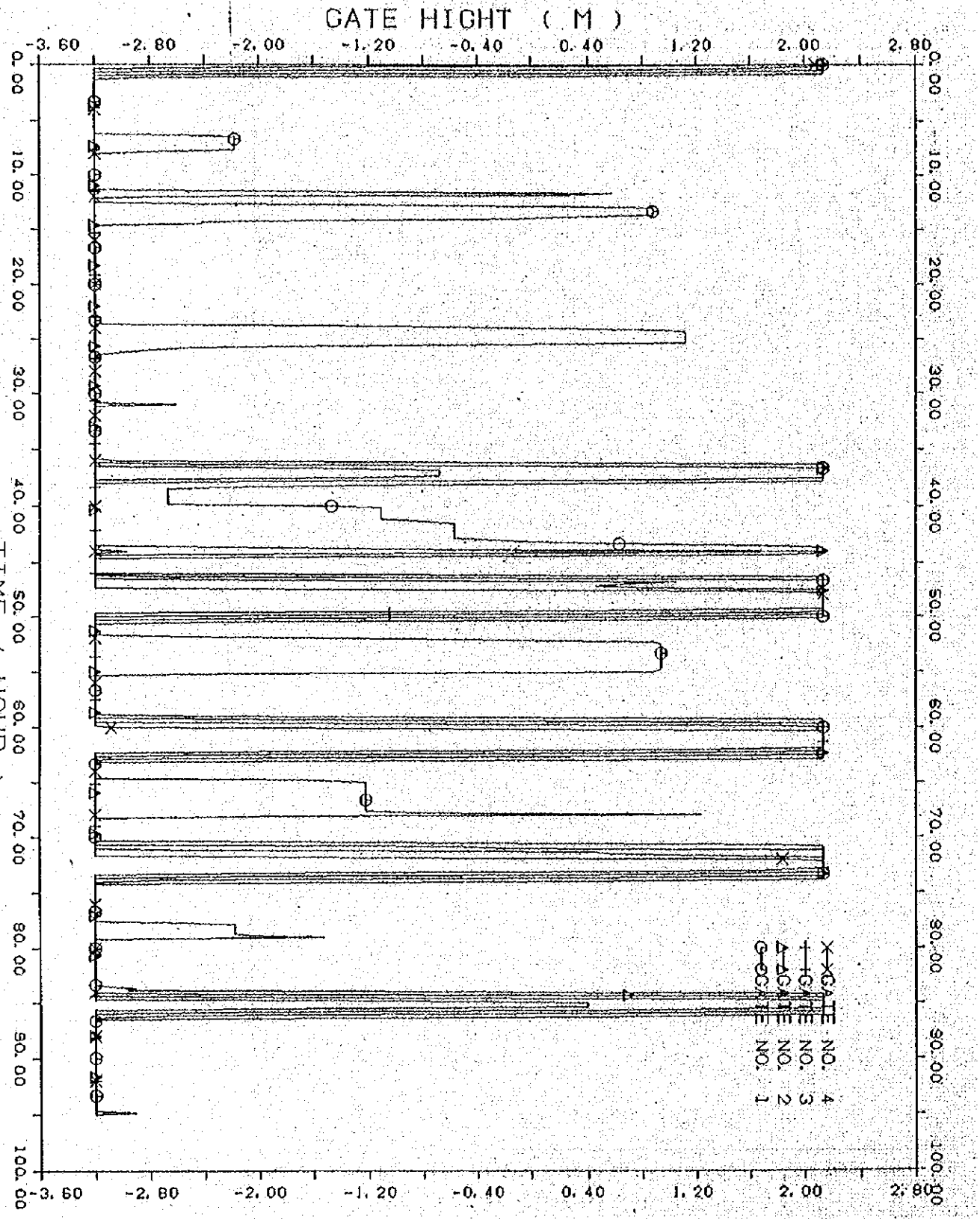

DATA (XYP3. DB2) 17 OCT
QINI = 13.5 RN = 0.020 RNO = 0.030

PRA1 ** CASE J-2 ** NOV. 12,' 88 PRA13D. D31
DOWN STREAM BOUNDALY DESIGN TIDE (BASED ON 31 JULY' 88)
INUN. AREA 8KM (26-40) 0.M AT 0.8 M. 550.M AT 1.0 M

XYPLOT33 15/10/88

Fig. 6-12 Opening height of gates

Fig.6-13 Discharge at Mesh 3, Mesh 17 and Mesh 53

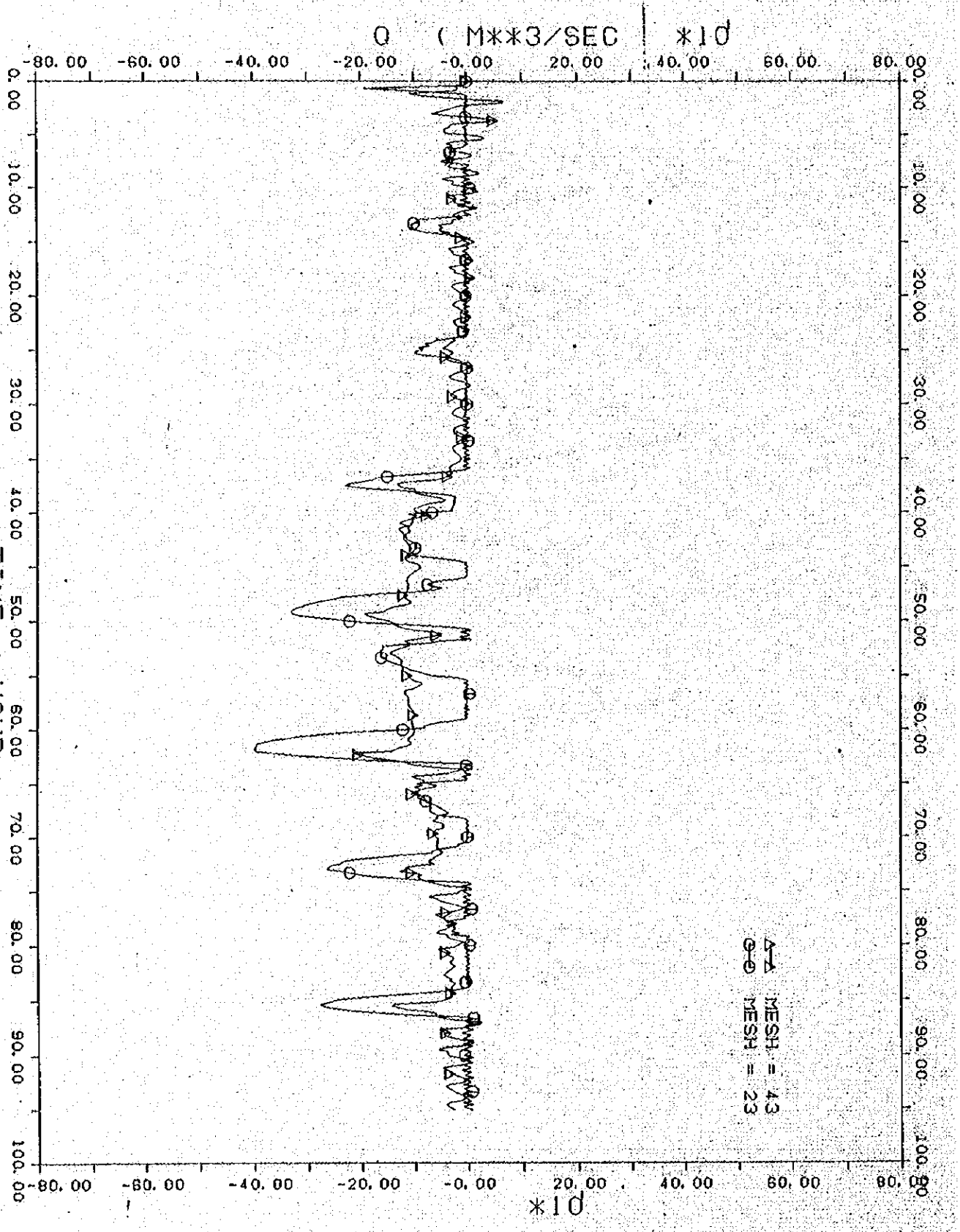

Fig.6-14 Discharge at Mesh 23 and Mesh 43

DATA (XYP33.D63) DISCHARGE 28 OCT
QINI = 13.5 RN = 0.020 RNO = 0.030

PRAI ** CASE J-2 ** NOV. 12,'88 PRAI3D.D31
DOWN STREAM BOUNDALY DESIGN TIDE (BASED ON 31 JULY '86)
INUN. AREA 8KM (26-40) 0.M AT 0.8 M. 550.M AT 1.0 M

XYPLOT33 15/10/88

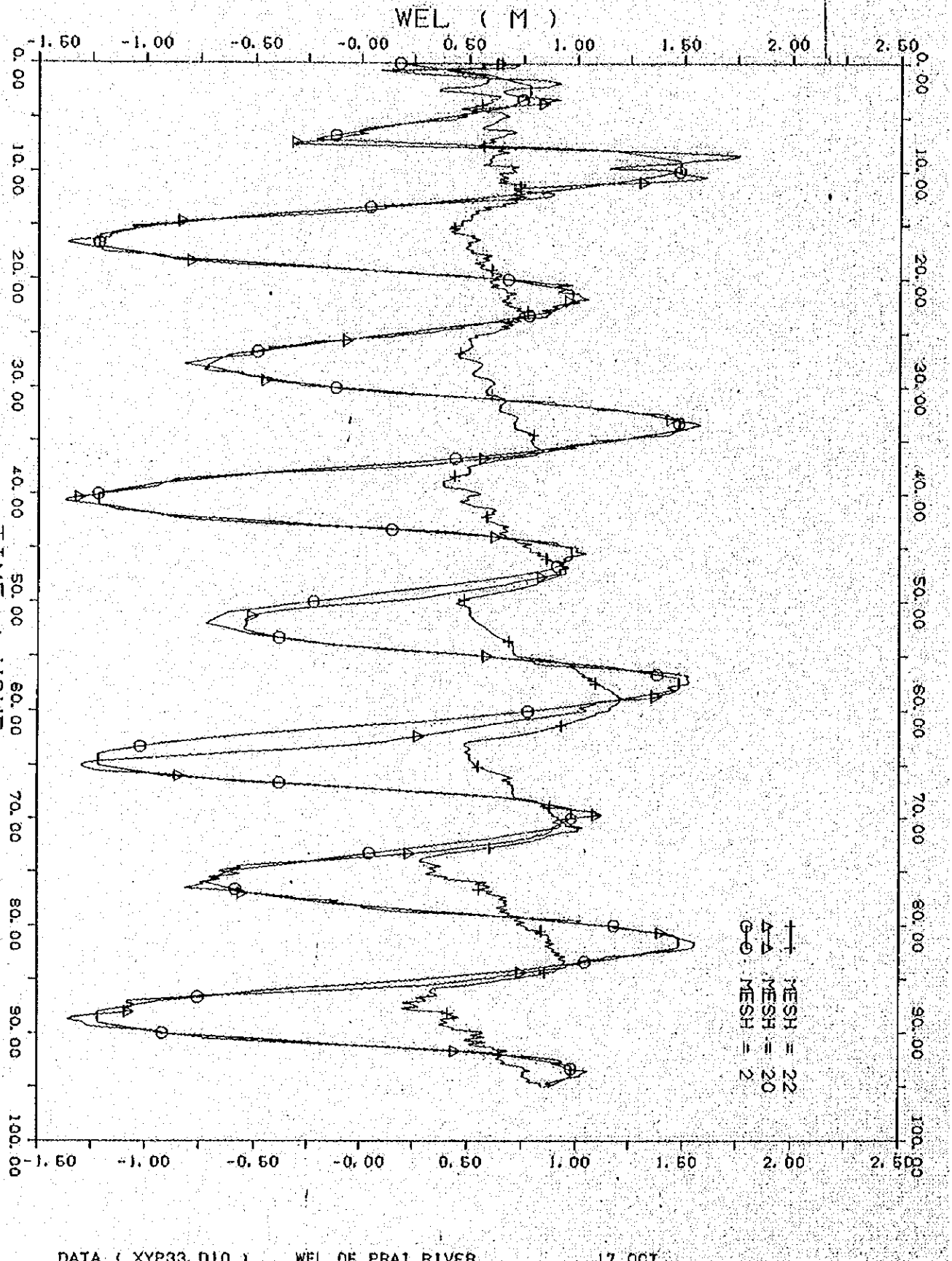

DATA (XYP33.D10) WEL OF PRAI RIVER 17 OCT
QINI = 13.5 RN = 0.020 RNO = 0.030

PRAI ** CASE J-3 ** NOV. 12,'88 PRAI3D.D32
DOWN STREAM BOUNDALY DESIGN TIDE (BASED ON 31 JULY,'88)
INUN. AREA 8KM (26-40) 0.M AT 0.8 M. 550.M AT 1.0 M

XYPLOT33 15/10/88

Fig. 6-15 Fluctuation of water level at downstream, Mesh 20 and upstream, Mesh 22 of the Barrage

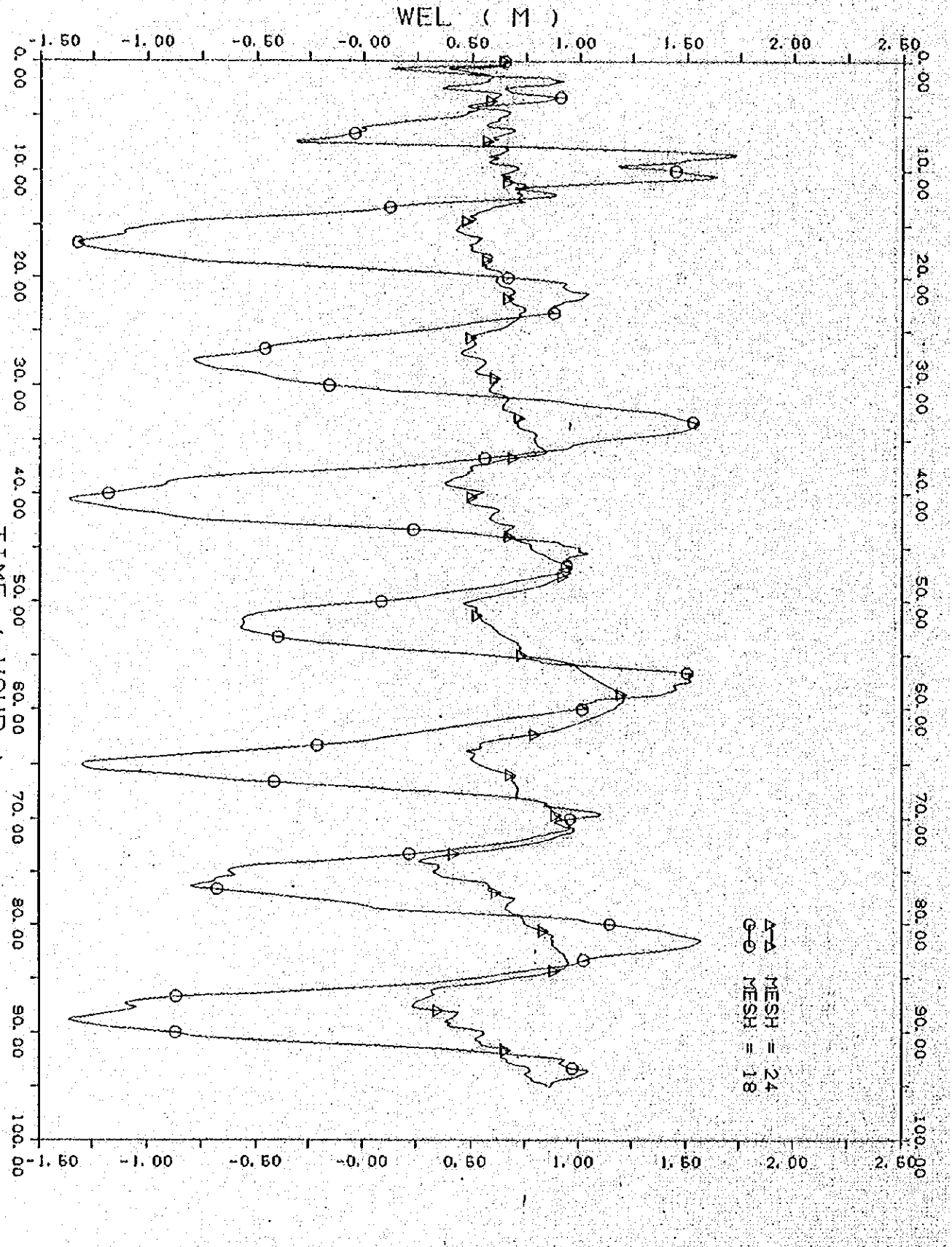

Fig.6-16 Fluctuation of water level at Mesh 18 and Mesh 24

DATA (XYP33.D01) 17 OCT
QINI = 13.5 RN = 0.020 RNO = 0.030

PRA1 ** CASE J-3 ** NOV. 12, '88 PRA13D/D32
DOWN STREAM BOUNDALY DESIGN TIDE (BASED ON 31 JULY '88)
INUN. AREA 8KM (26-40) 0.M AT 0.8 M. 660.M AT 1.0 M

XYPLOT33 15/10/88

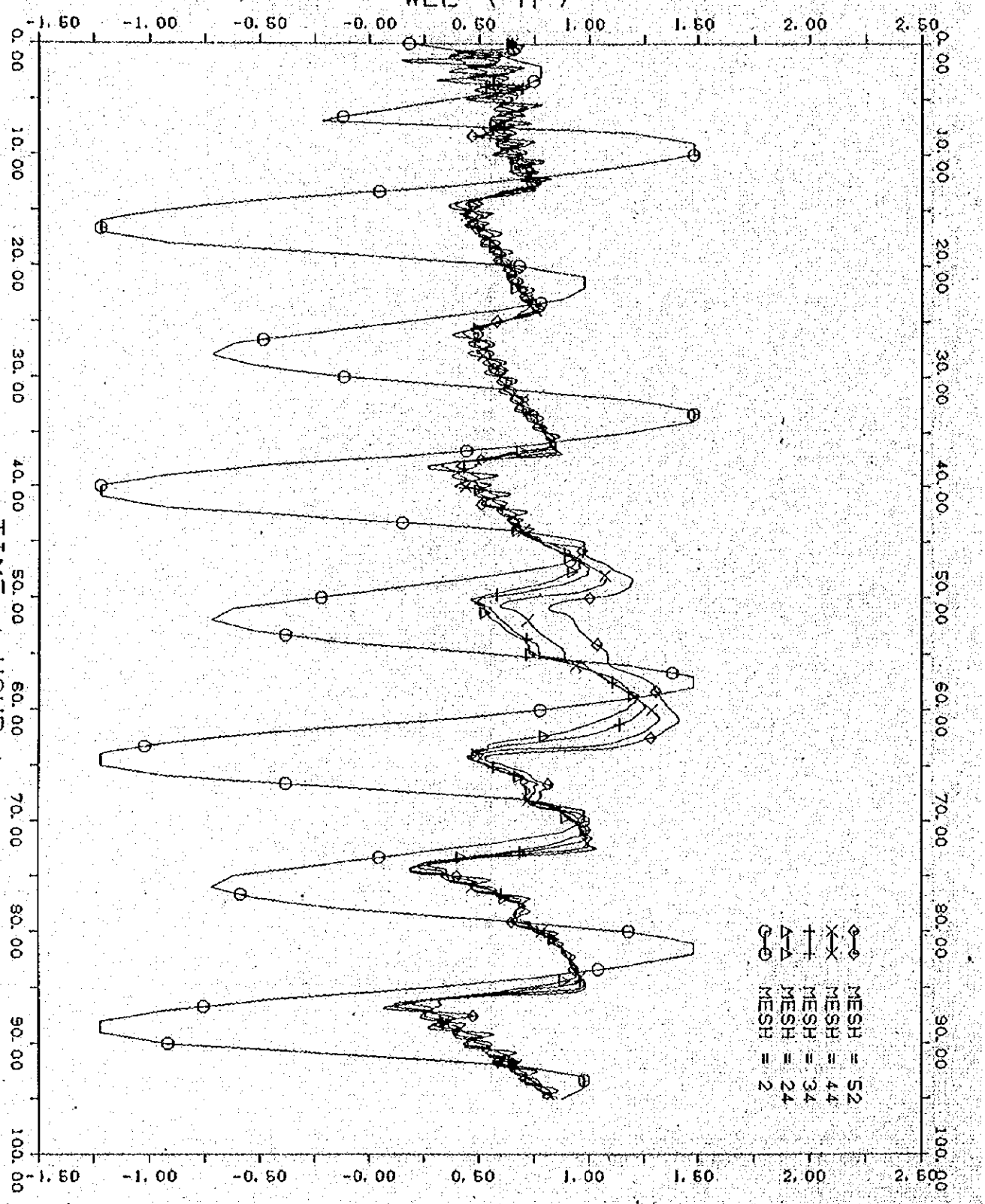

DATA (XYP33.D11) WEL OF PRAI RIVER 17 OCT
QIN1 = 13.5 RN = 0.020 RNO = 0.030

PRAI ** CASE J-3 ** NOV. 12,'88 PRAI3D.D32
DOWN STREAM BOUNDALY DESIGN TIDE (BASED ON 31 JULY '88)
INUN. AREA 8KM (26-40) 0.M AT 0.8 M. 550.M AT 1.0 M

XYPLOT33 15/10/88

Fig. 6-17 Fluctuation of water level at Mesh 24, Mesh 34, Mesh 44 and Mesh 52

Fig.6-18 Discharge passed through gates

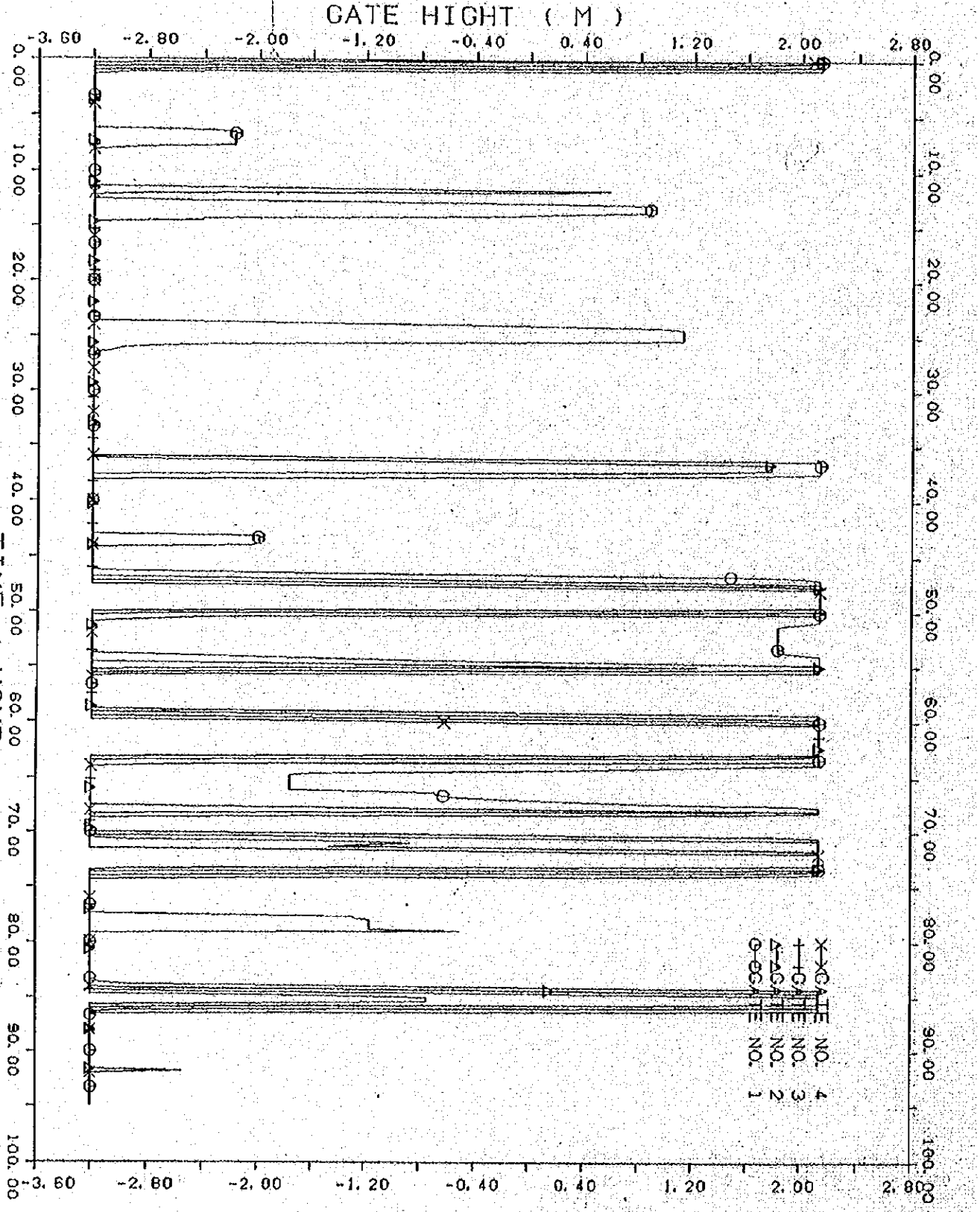

DATA (XYP3.DB2) 17 OCT
QINI = 13.5 RN = 0.020 RNO = 0.030

PRAI ** CASE J-3 ** NOV. 12,'88 PRAI3D.D32
DOWN STREAM BOUNDALY DESIGN TIDE (BASED ON 31 JULY,'88)
INUN. AREA 8KM (26-40) 0.M AT 0.8 M. 550.M AT 1.0 M

XYPLOT33 15/10/88

Fig. 6-19 Opening height of gates

Fig.6-20 Discharge at Mesh 3, Mesh 17 and Mesh 53

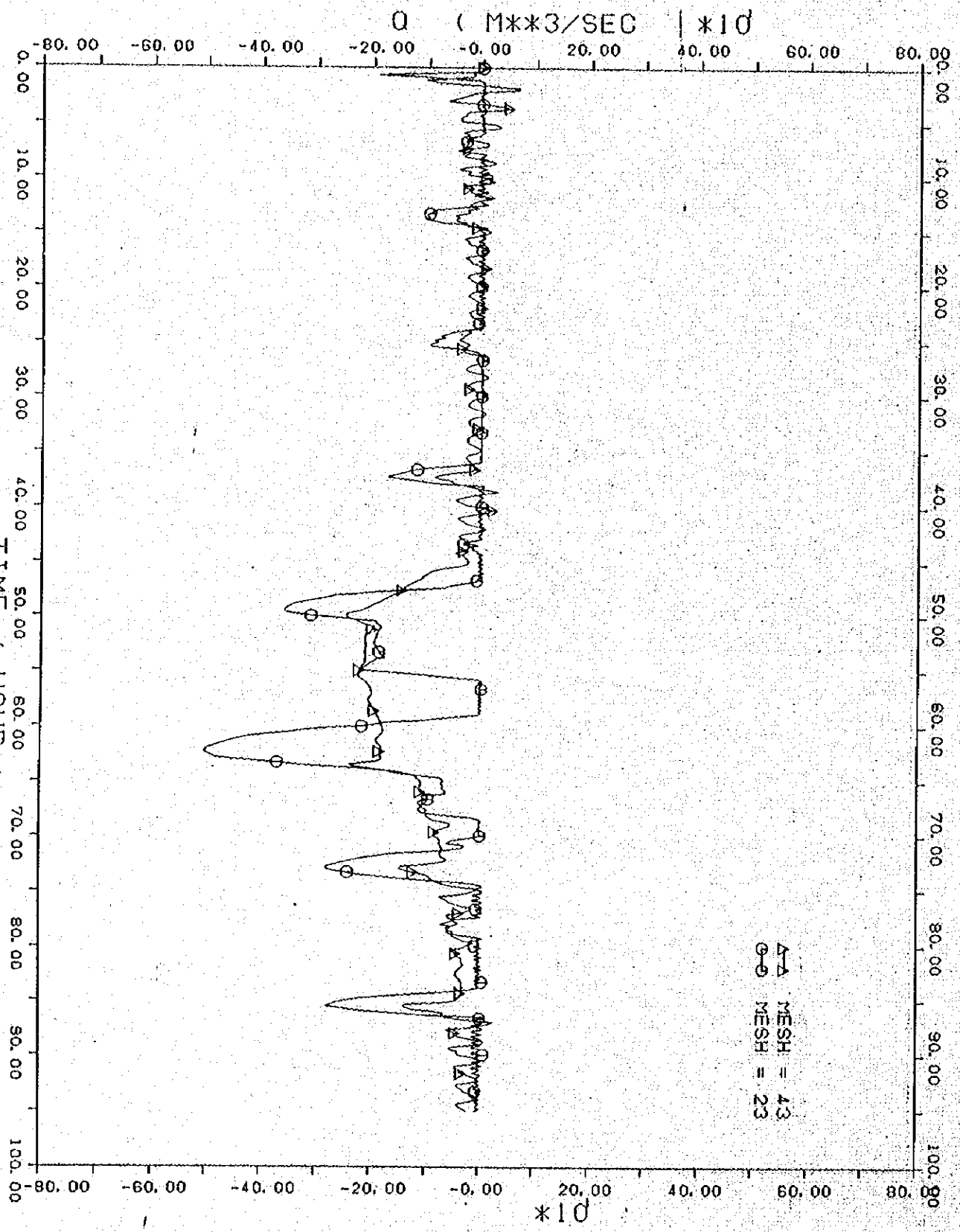

DATA (XYP33.D63) DISCHARGE 28 OCT
QINI = 13.5 RN = 0.020 RNO = 0.030

PRAI ** CASE J-3 ** NOV. 12,'88 PRA13D.D32
DOWN STREAM BOUNDALY DESIGN TIDE (BASED ON 31 JULY '88)
INUN. AREA 8KM (26-40) 0.M AT 0.8 M. 650.M AT 1.0 M

XYPLOT33 15/10/88

Fig.6-21 Discharge at Mesh 23 and Mesh 43

Fig. 6-22 Fluctuation of water level at downstream, Mesh 20 and upstream, Mesh 22 of the Barrage

Fig. 6-23 Fluctuation of water level at Mesh 18 and Mesh 24

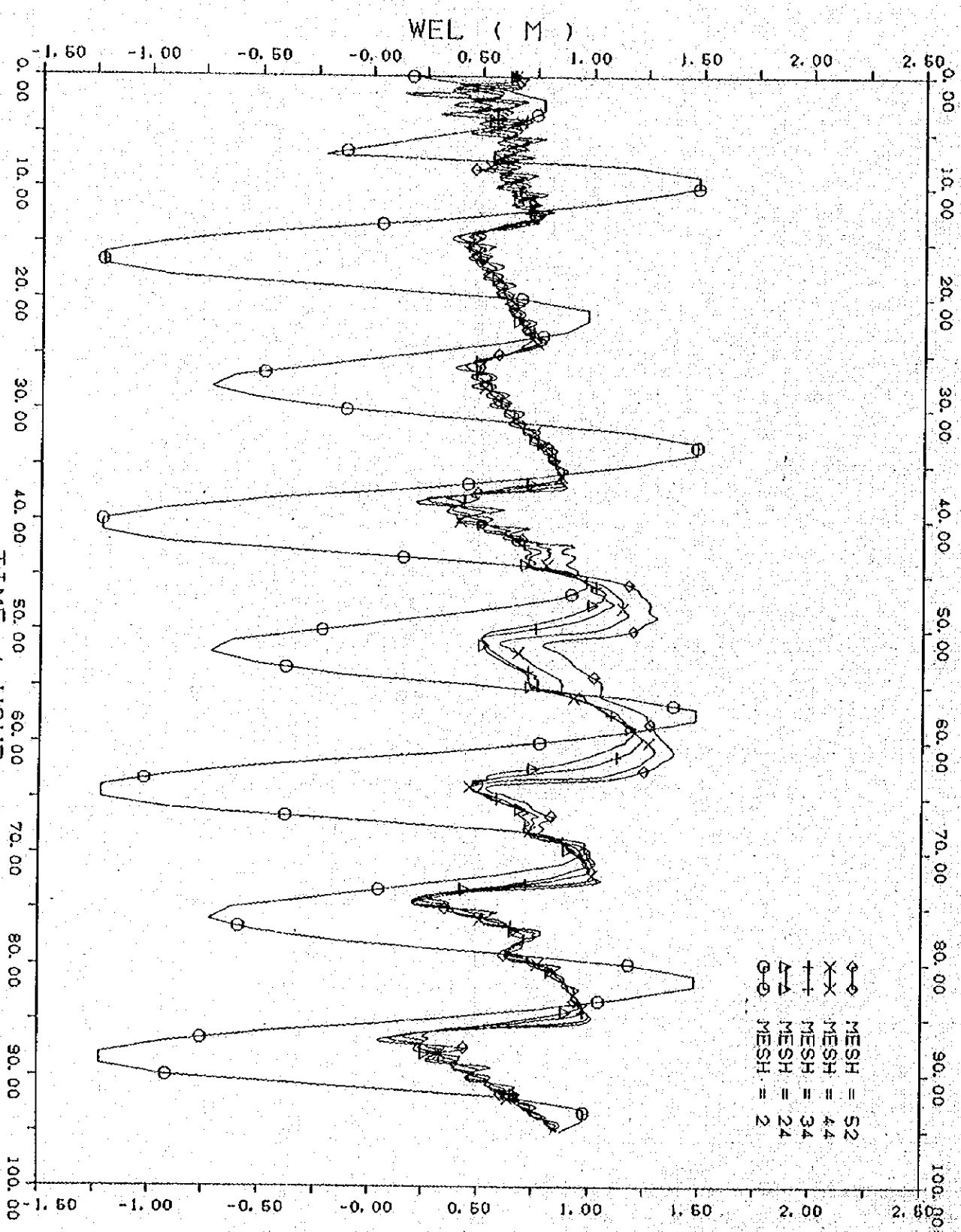

Fig. 6-24 Fluctuation of water level at Mesh 24, Mesh 34, Mesh 44 and Mesh 52

DATA (XYP33.D11) WEL OF PRAI RIVER 17 OCT
QINI = 13.5 RN = 0.020 RNC = 0.030

PRAI ** CASE J-4 ** NOV. 12,'88 PRAI3D.D33
DOWN STREAM BOUNDALY DESIGN TIDE (BASED ON 3) JULY '88)
INUN. AREA 8KM (26-40) 0.M AT 0.8 M. 550.M AT 1.0 M

XYPLOT33 15/10/88

Fig.6-25 Discharge passed through gates

Fig.6-26 Opening height of gates

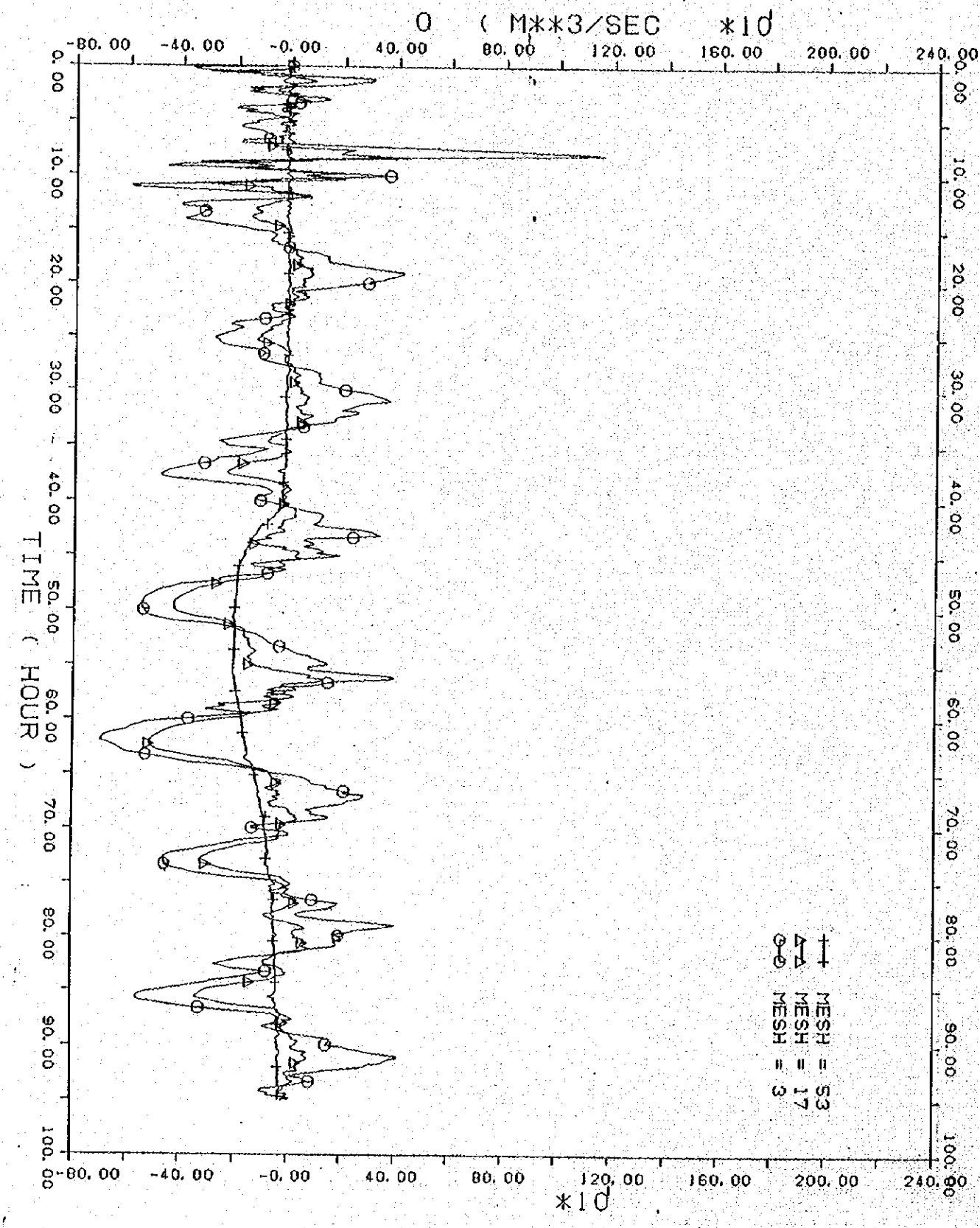

DATA (XYP33. D64) DISCHARGE 31 NOV
QINI = 13.5 RN = 0.020 RNO = 0.030

PRAI ** CASE J-4 ** NOV. 12, '88 PRAI3D. D33
DOWN STREAM BOUNDALY DESIGN TIDE (BASED ON 31 JULY '88)
INUN. AREA 8KM (26-40) 0.M AT 0.8 M. 560.M AT 1.0 M

XYPLOT33 15/10/88

Fig.6-27 Discharge at Mesh 3, Mesh 17 and Mesh 53

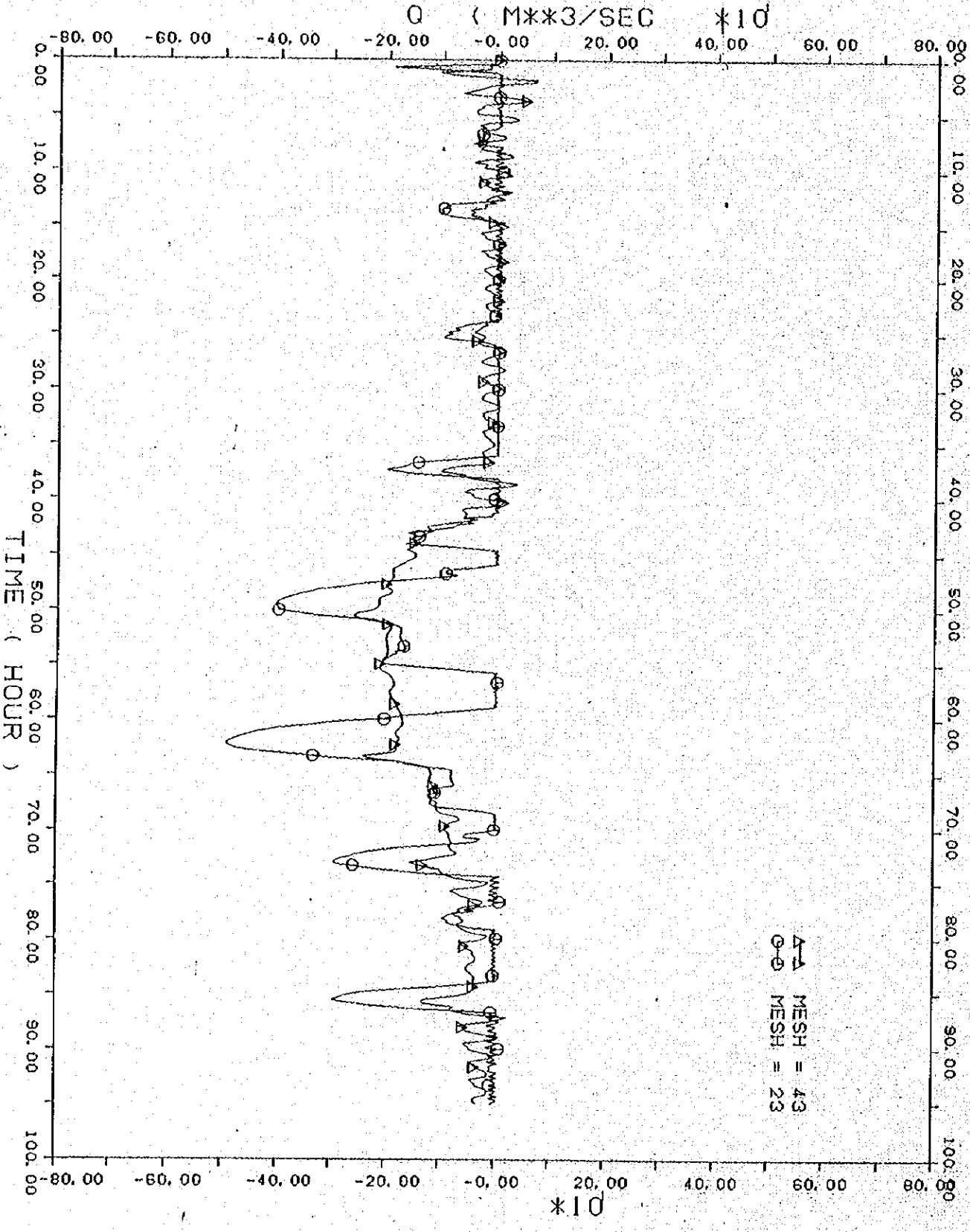

DATA (XYP33.D63) DISCHARGE 28 OCT
QINI = 13.5 RN = 0.020 RNO = 0.030

PRAI ** CASE J-4 ** NOV. 12,'88 PRAI3D.D33
DOWN STREAM BOUNDALY DESIGN TIDE (BASED ON 31 JULY '88)
JNUN. AREA 8KM (26-40) 0.M AT 0.8 M. 650.M AT 1.0 M

XYPLOT33 16/10/88

Fig. 6-28 Discharge at Mesh 23 and Mesh 43

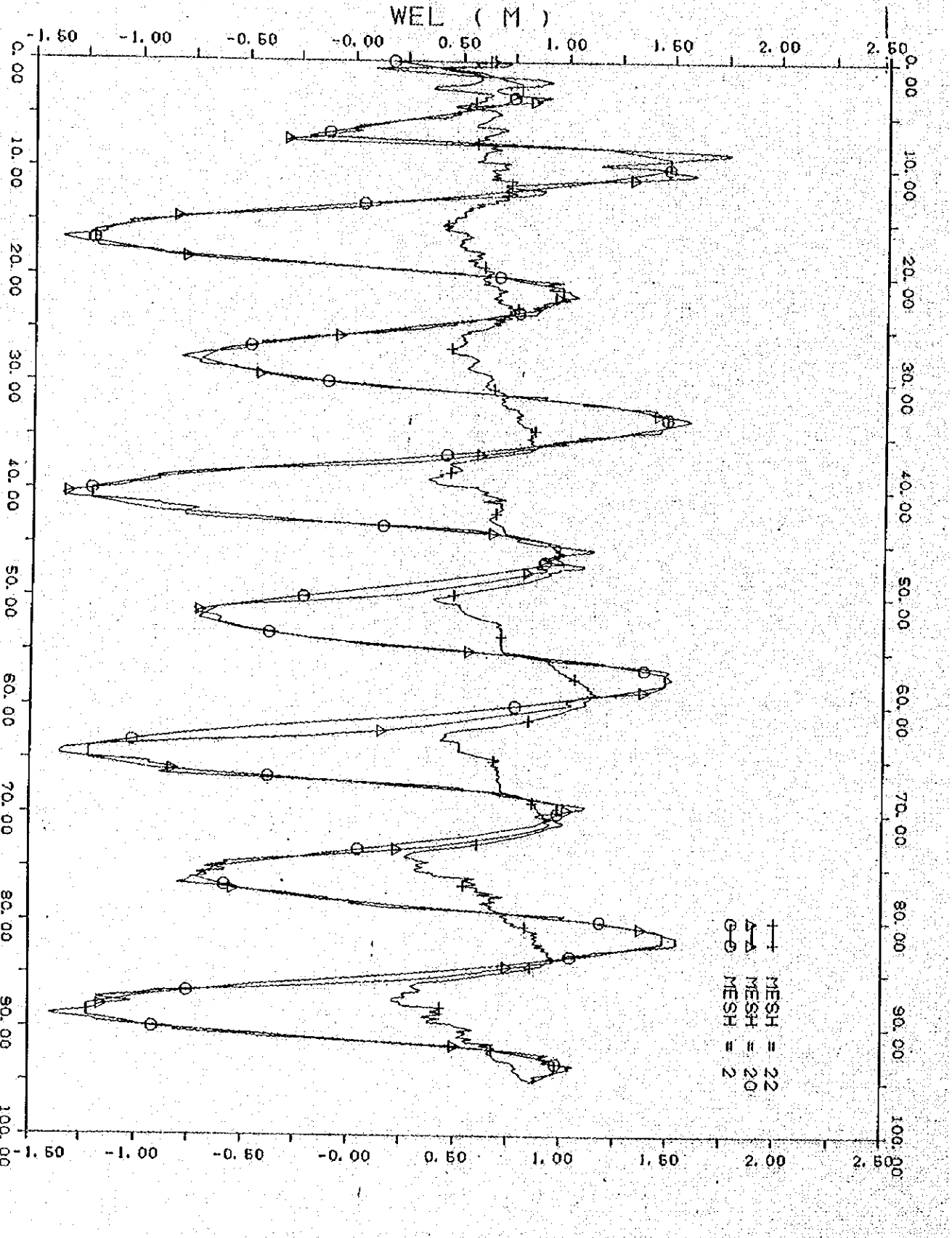

Fig. 6-29 Fluctuation of water level at downstream, Mesh 20 and upstream, Mesh 22 of the Barrage

DATA (XYP33.D10) WEL OF PRAI RIVER 17 OCT
QINI = 13.5 RN = 0.020 RNG = 0.030

PRAI ** CASE J-6 ** NOV. 12, '88 PRAI3D.D34
DOWN STREAM BOUNDALY DESIGN TIDE (BASED ON 31 JULY '88)
INUN. AREA 8KM (26-40) 0.M AT 0.8 M. 550.M AT 1.0 M

XYPLOT33 15/10/88

Fig.6-30 Fluctuation of water level at Mesh 18 and Mesh 24

Fig. 6-31 Fluctuation of water level at Mesh 24, Mesh 34, Mesh 44 and Mesh 52

Fig.6-32 Discharge passed through gates

Fig.6-33 Opening height of gates

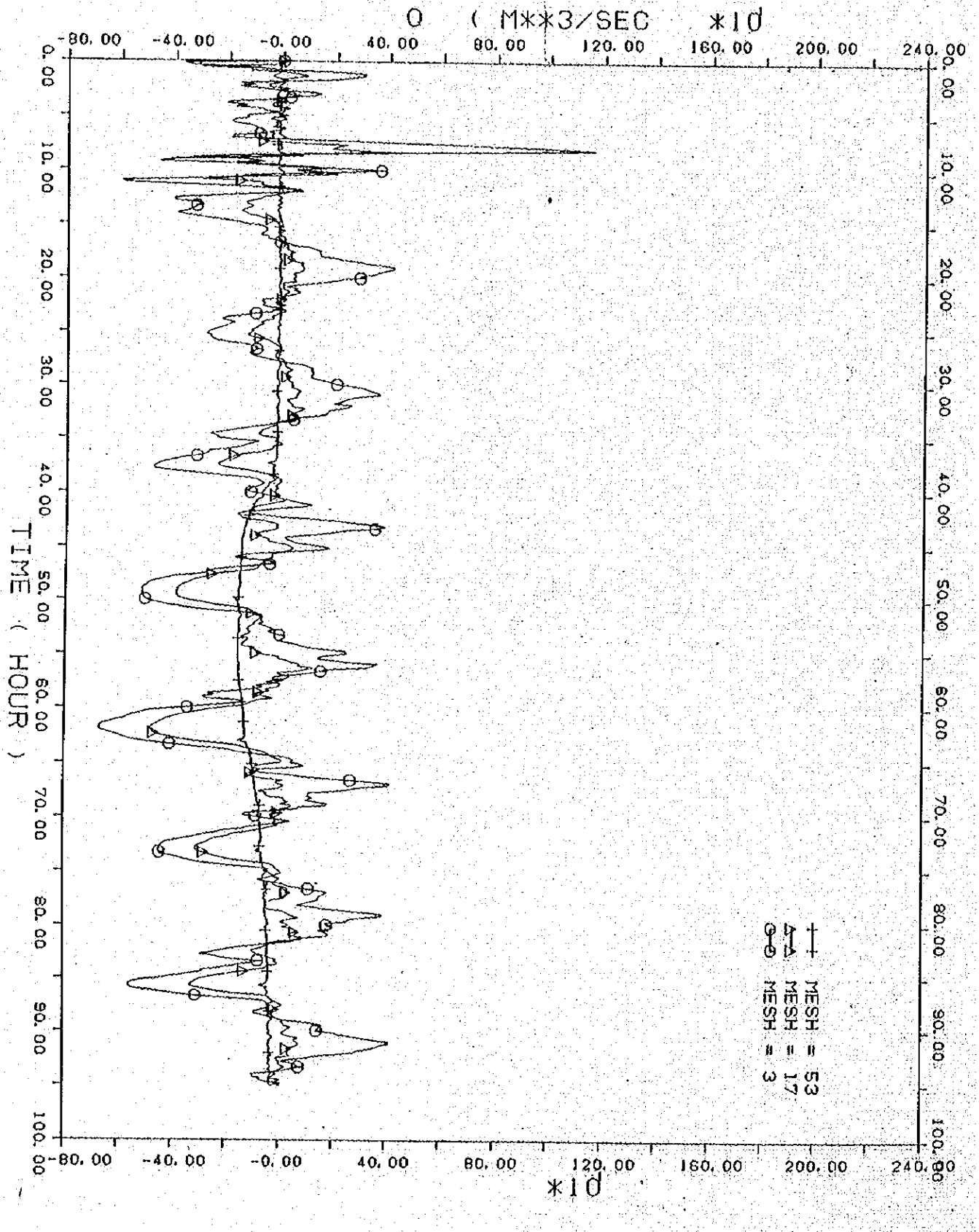

Fig. 6-34 Discharge at Mesh 3, Mesh 17 and Mesh 53

DATA (XYP33. D64) DISCHARGE 31 NOV
QINI = 13.5 RN = 0.020 RNO = 0.030

PRAI ** CASE J-5 ** NOV. 12,' 88 PRAI3D. D34
DOWN STREAM BOUNDALY DESION TIDE (BASED ON 31 JULY ' 88)
INUN. AREA 8KM (26-40) 0.M AT 0.8 M. 660.M AT 1.0 M

XYPLOT33 15/10/88

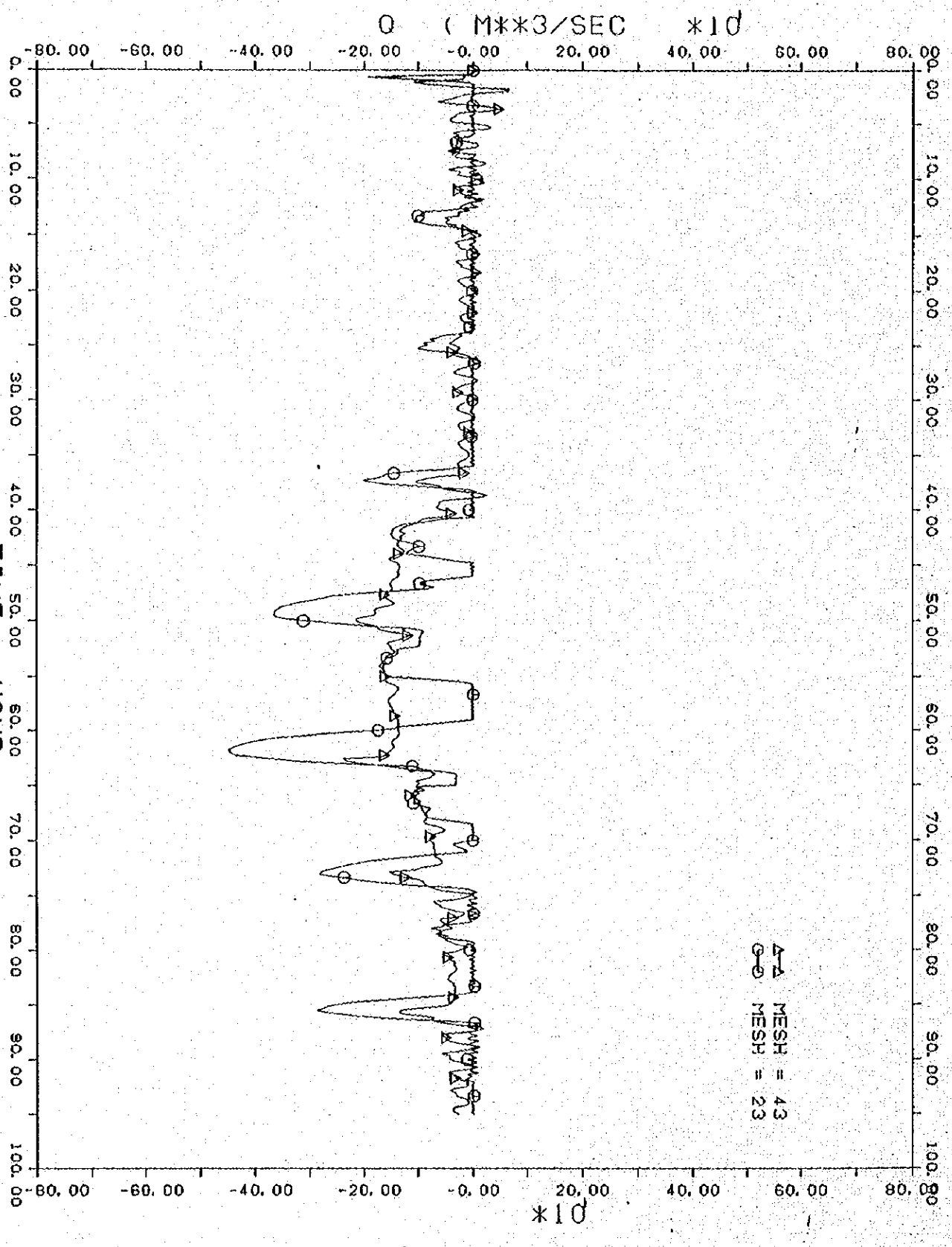

Fig.6-35 Discharge at Mesh 23 and Mesh 43

DATA (XYP33.D63) DISCHARGE 28 OCT
GINI = 13.5 RN = 0.020 RNG = 0.030

PRAI ** CASE J-6 ** NOV. 12,'88 PRA13D.D34
DOWN STREAM BOUNDALY DESIGN TIDE (BASED ON 31 JULY '68)
INUN. AREA 8KM (26-40) 0.M AT 0.8 M. 550.M AT 1.0 M

XYPLOT33 15/10/88